No. 12 June 1983 Nicosia Cyprus

Review

THE HIGHER TECHNICAL INSTITUTE

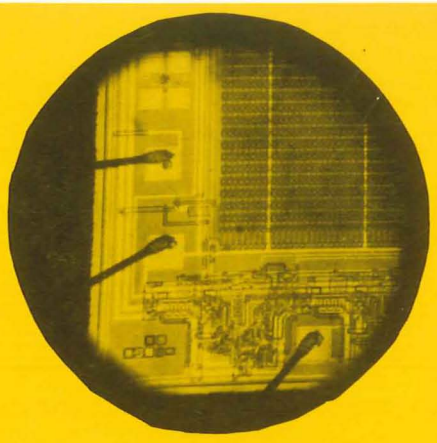

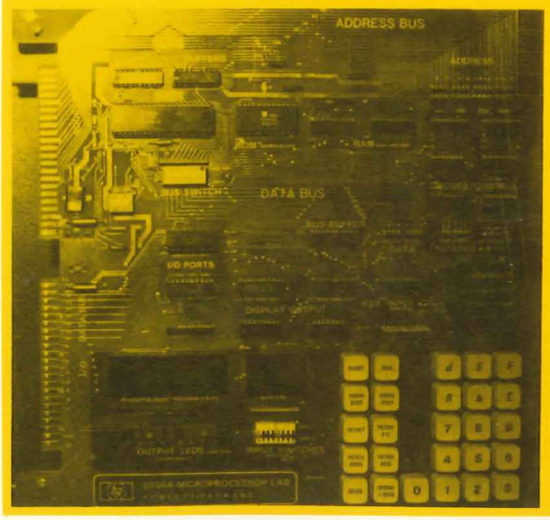

Review

No. 12

June 1983

Nicosia

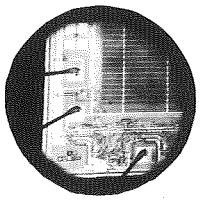

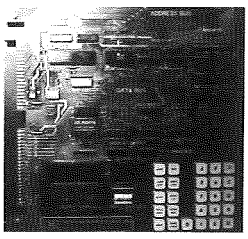

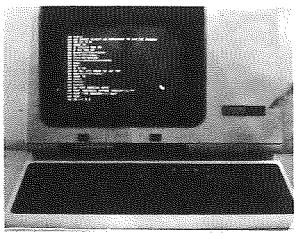

Cover Photographs by I. Aggeli.

H. T. I. Review is published by the Public Information Office in cooperation with the Higher Technical Institute, Nicosia. It accepts articles which promote and further new developments and knowledge in technology, especially with reference to Industries of Cyprus. Requests for further copies of the magazine and for information concerning the published articles should be made to Chief Editor H.T.I. Review, Higher Technical Institute, P.O.BOx 2423 - Nicosia.

CONTENTS

The Higher Technical Institute (H T I) was established in 1968 as a Government of Cyprus project with assistance by the United Nations Special Fund (UNDP), the United Nations - Educational Scientific and Cultural Organisation (UNESCO), and the International Labour Office (ILO). Cyprus Government Executing Agency: The Ministry of Labour and Social insurance.

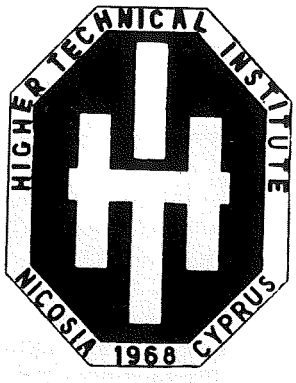

Review

No. 12 June 1983 Nicosia Cyprus

The Role of Technological Institutions as Agents for Development.

The Educational System tends by its nature to be a conservative system. Even if educational institutions are to follow change efforts to this end must be deliberate and persistent.

However, to follow change may not be all that would be required of an educational institution. Especially in the developing countries, their educational institutions would have to, even, become agents for change.

The Higher Technical Institute (H.T.I.) is one of those institutions of tertiary education level where mechanisms for change and adaptation have deliberately been built into its mode of operation. A standing instruction by the Board of Governors requires of it to engage in a full review of its objectives and policies and its educational system every five years.

As a result of this directive, the H.T.I. has had a number of such reviews since its establishment in 1968. The latest one was approved by the Board of Governors at its meeting in May 1983 to be fully implemented as from September next.

The, thus, revised objectives, policies curricula and syllabi aim among other things at a more extensive involvement of the students in the educational and training process, at introducing cultural electives subjects and at aligning the activities of the H.T.I. with the targets of the 4th Emergency Plan of Economic Development (1982 - 1986) prepared by Government.

Emphasis in the new syllabi of training is given, among other items, in topics relating to new and high technology, to energy, to product design and to quality control. Priority will also be given to applied research projects, to materials and product testing and to requests for mechanization and automation of small scale industrial production processes.

The articles in this issue reflect to the extent possible, some aspects of this new emphasis in the objectives of the H.T.I.

Editorial Committee

THE IMPORTANCE OF CALIBRATION IN QUALITY CONTROL

By S. Vassiliou
Quality Control Officer,
Cyprus Organization for Standards and Control of Quality (CYS)

It used to be the practice, and in some places it still is, for persons to be employed in the railway industry for the purpose of checking that the wheels of locomotives and carriages are free from cracks which may endanger the train. Those checks are carried out by tapping the wheels with a hardened steel hammer whilst the train is at the station. A sound wheel would ring loud and clear, and a cracked wheel would give a dull note, upon which the carriage would be removed from the train, taken to the maintenance workshop, and the offending wheel replaced.

A story is being said of a certain "wheel tapper" who had been scrapping wheels all day, because his hammer was cracked and nobody had noticed it up to the time the cracked hammer was checked on a sleigh bell.

This example and many other similar give a good indication of costs and inconveniences which can arise when the calibration of equipment is neglected. For the sake of checking a hammer, trains are diverted, schedules wrecked, passengers delayed, and carriages taken out of service. In short, the costs of ineffective equipment far out weigh the costs of calibration.

Where can calibration assist? The answer is any where a measurement is taken, or a test conducted. For example, consider the production of a plastic article. If the temperature of the plastic is not correctly controlled, the plastic may be too hot in which case it will not flow properly. The result is scrap production, wasted material, manhours and machine hours. If the fault remains unobserved, damage and breakdowns may occur at a later time. Obviously, the temperature controling device must be regularly checked.

But why do instruments give varying results? The answer is two-fold; Firstly all instruments will give slightly different results each time they are used. If the instrument has been chosen correctly these variations will be small in comparison to the measured value. Secondly all measuring instruments are subjected to vibration, temperature changes, corrosion, wear and tear due to the passing of time. All these factors contribute to a gradual deterioration of the instrument accuracy. It is this insidious creeping inaccuracy which causes problems, if an intrument ceases to function, or is wildly inaccurate, it is at least obvious, but what happens when it just gives less and less accurate results. Imagine the feelings of a manufacturer who has just rejected and scrapped a batch of pressure valves, only to discover that his test pressure gauge is reading 5% too high. Even worse, what happens if the instrument doesn't 'fall safe', if for example the wheel tappers hammer developed a fault which allowed it to ring a crasked wheel?

The remedy of course is to check all testing instruments at regular intervals. Every instrument should be checked before use to ensure that it is functioning well. In many cases, such a check is relatively simple, a small weight on a balance pan, zero reading on a micrometer will all indicate a functioning device. Such checks are valuable but are not enough in themselves. A micrometer which is accurate at zero reading may not be so at 10 mm, similarly a pressure gauge which measures an accurate static head may not be reliable in other conditions.

Calibration provides the answer. Basically, the instrument in question is either compared with an instrument of known accuracy, or is given known inputs, at several points along its measurement range. As a result of this, the instrument is either adjusted or provided with a statement as to its inaccuracies in the form of a table or graph.

This does not mean that every instrument in the works has to be sent away for calibration every week or even every year. It is normal practice, for either a spare instrument to be maintained as a factory standard, against which other similar instruments can be compared, or for a series of known measurements to be given to the instrument for comparison.

Thus for the purposes of calibrating a weighing machine or balance, a series of known weights can be maintained. For pressure gauges a master gauge, itself calibrated, can be used.

This still leaves the problem of calibrating the weights and master gauges. Normally, this would be done by a national calibration laboratory.

The following guide gives an indication of the frequency with which checking and calibration should take place.

1) Functional check.
   Should be performed before each use.

2) Comparison with factory master.
   Should be conducted at between 2 weeks and 12 weeks intervals dependent upon conditions.

3) Calibration of factory master.
   6 months interval maximum.

It is important that items 2 and 3 above are fully recorded and documented. In this way, a measure of deterioration can be made, and decisions taken as to when to replace or renovate an instrument. To do this, an inventory of all instruments, test equipment and associated accessories is required, with systematic records of the calibration of each item. Bearing in mind the objective of maintaining factory master devices in good condition, they should be kept in a protected environment, as free as possible from climatic variations, unnecessary handling as far as possible and being used by one person only who is responsible for the calibration of equipment.

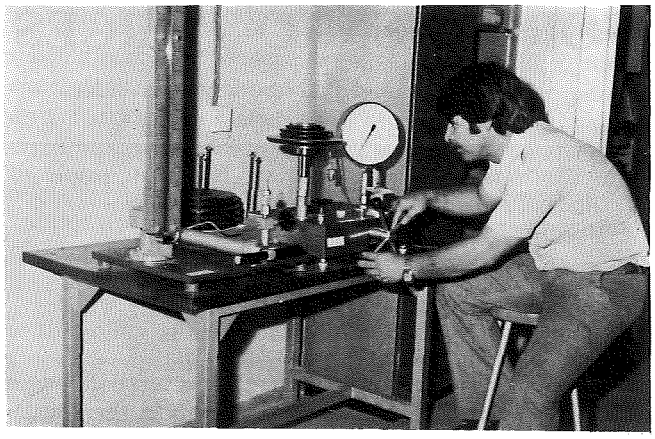

Calibration of Pressure Gauge using the Dead Weight Pressure Tester, at H.T.I.

The Cyprus Organization for Standards and Control of Quality (CYS) realizing the importance of calibration, from the very beginning of its existence, established in cooperation with the H.T.I. a calibration laboratory at H.T.I. This laboratory offers a service to the local industry by providing authenticated calibration, at a nominal fee, and issuing certificates to provide an assurance of the correctness of the calibration of the instrument that has been checked. Parameters that can be calibrated at the above calibration laboratory are Temperature, Pressure, Viscosity, Length, Angle, Electrical Characteristics etc.

For more information on this subject interested persons may contact either CYS or H.T.I., telephone No. 40-3441 and 40-3358 respectively.

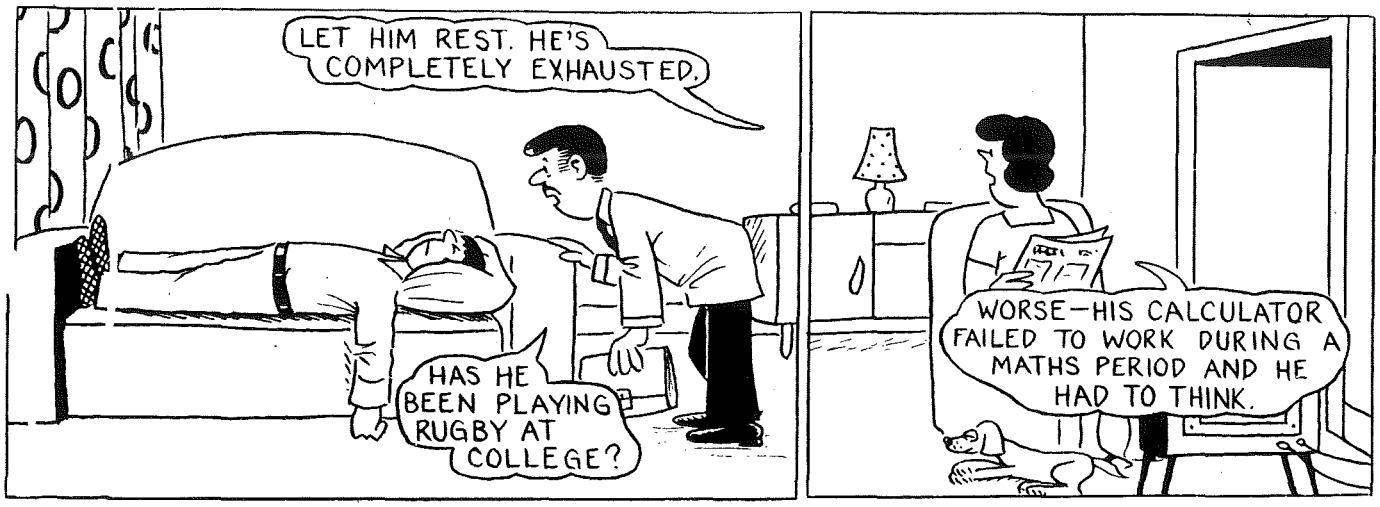

The Kingdom of God on earth is the love of all people, of all nations.

Tolstoi

The more I learn the more I discover my ignorance.

Kartesios

Bear malice for no one ; give help to the needy.
Be strict with yourself and linient to others.

Kong-Tse

ANALYSING STRUCTURES FOR SEISMIC FORCES

By Herodotos Stavrides,
Senior Lecturer H.T.I.

NOTATION

α = Distribution coefficient (Refer to Fig. 2).

β = Coefficient of rigidity decrease due to plastic shear deformations.

δBn = Wall deformation due to bending at n^{th} storey.

δRn = Wall deformation at n^{th} storey due to rotation of foundation.

δsn = Wall deformation due to shear at n^{th} storey.

δn = Total wall deformation at n^{th} storey ($\delta n = \delta Bn + \delta Rn + \delta sn$)

$\Delta bn = \sum_{i=1}^{n-1} \frac{Mi}{Kwi} + \frac{1}{2}\frac{Mn}{Kwn}$

k = shape factor for shear stress distribution.

Examples:

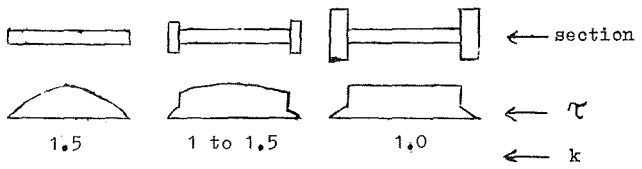

Aw = Cross sectional area of wall.

D = Individual column rigidity.

D_F = Total storey rigidity of frame.

Dw = $\frac{Qn}{h_n}$ = wall rigidity to lateral movements representing the force which gives unit desplacement δ.

E = Young's Modulus of Elasticity of concrete.

G = Shear Modulus of Elasticity of concrete (E/G Ratio taken as 2.3).

Ic = Second moment of area of column cross section.

Iw = Second moment of area of wall cross section.

K = Standard rigidity coefficient (arbitrarily selected).

$\bar{K}$ = Refer to Fig. 2.

Kb = Beam stiffness.

Kc = Column stiffness = $\frac{Ic}{h_n K}$

Kw = Wall stiffness = $\frac{Iw}{h_n}$

Mi = wall bending moment in the centre of storey i.

Mwn = wall cumulative moment at n^{th} storey.

Q = column shear.

QFn = frame n^{th} storey shear.

Qn = storey shear.

Qwn = wall n^{th} storey shear.

y = coefficient for height of inflexion point in columns (taken from standard tables).

h_n = storey height.

Other symbols are explained in the text.

1. Introduction

Earthquakes often cause severe structural damages the collapse of buildings, and they leave in their wake many casualties. Observations of the performance of buildings during earthquakes show that structures which are properly designed are capable of withstanding very severe ground motions without significant damage. It has by now been established that, especially in the case of reinforced concrete structures, aseismic construction can be accomplished at very little added expense. Emphasis must be given to the detailing especially at the connections. As long as there is a good follow-up from design to construction even a severe earthquake can cause minimum damage without any loss in lives.

Cyprus lies in an earthquake zone but we have not experienced any significant tremors severe enough to cause either extensive structural damage, or loss of lives on a mass scale. However the fact remains that Cyprus lies in a sensitive area and we should be applying to our designs and constructions the minimum requirements necessary, to ensure that in the event of an earthquake we are not faced with a catastrophy.

The fact that we have not had any severe earthquakes in recent times should not make us complacent and forget the fact that we do lie in a sensitive earthquake zone. As an example I give here the case of Jugoslavia. The last earthquake in this Balkan country before the twentieth century, was in the medieval ages. However since the first major and catastrophic earthquake of this century that of Skopjie in 1963, there have been a series of major earthquakes throughout the country. Jugoslavia was therefore a classic example of a country lying in a seismically sensitive area without having the "earthquake conscience". However since the Skopjie earthquake the Jugoslavians adopted this conscience and the following earthquakes throughout the country from 1963 to date, were much less catastrophic, even though they were as severe as that at Skopjie. It must be said here however that the Skopjie earthquake was of the shock type, as the hypocentre was exactly under the city itself.

One of the major problems in the analysis of structures for earthquake resistance is to establish the relative proportions of the seismic forces which are taken by the beams the columns and the structural walls. The latter are better known as "shear walls". However this is a mis-nomen since the behaviour of these walls is more in bending rather than shear. The method of equivalent seismic forces acting in the horizontal direction at the height of the floors is most commonly used in the aseismic analysis of high structures.

For the purpose of determination of the equivalent seismic forces, it is necessary to find out the dynamic characteristics of the structure. These are the periods and forms of vibration which are functions of distribution and rigidity as well as structural masses.

1.1. Frame structures

Pure frame structures consist of columns and beams which are firmly connected between them.

Careful construction and attention to detail especially at the joints of beams to columns, make the pure frame a very favourable system for aseismic behaviour. However the strength of the constituent members of the frame is not very high due to their limited proportions.

1.2. Frames of walls with openings

To achieve a system of several times higher rigidity, the space between windows may be used to enlarge the proportions of columns and the parapets are used to increase the depth of the beams. Contrary to any possible initial reaction such a system is an economical and rational solution for high seismicity areas.

1.3. Structural walls

Shear walls or structural walls made in reinforced concrete have high resistance to both shear and bending and are very effective bearing members.

Buildings consisting of several floors have decreased rigidity in the upper storeys due to the accumulation of bending deformations in the lower storeys. In the case of high buildings therefore, structural walls may be applied in combination with frames which have almost constant rigidity along the height of the building.

When deciding which structural system to employ in a building, it is necessary to establish the way in which the lateral seismic forces in the different storeys is transferred to these different systems and what percentage of this seismic force is going to be received by each system. This percentage will influence the bending moments and shear forces in these elements and hence the final sizing and amount of reinforcement. The distribution of the transverse seismic forces is performed according to the rigidity of each structural system.

2. Seismic Forces - Dynamic Characteristics

The dynamic characteristics of a structure may be determined by using what are known as Stodola and Holzer methods. The Stodola method is used for the first mode of vibration of the structure, and the Holzer method for the second and third. These methods are based on known floor masses and rigidities. The determination of the dynamic characteristics of the structure, as well as the evaluation of the seismic forces are beyond the scope of this paper; however a brief explanation is given below on the determination of the dynamic characteristics. For the evaluation of seismic forces any aseismic code may be used.

Assuming that the principal vibration mode shape is known, the seismic force amplitude values can be determined as follows:

$$Si = mi.\ Ai\ wr^2 \qquad (1)$$

where mi = mass of i^{th} floor

Ai = Displacement amplitude

wr = Circular frequency of r^{th} vibration mode, which is constant for the mode considered.

The total force acting at the i^{th} floor is obtained as a sum, that is:-

$$Qi = wr^2\ \bar{Q}i \qquad (2)$$

where $$\bar{Q}i = \sum_{j=i}^{n} mj\ \ Aj \qquad (2a)$$

The relative displacement of the i^{th} floor Δi is obtained by dividing the Qi expression by the corresponding floor rigidity Ki

i.e.:

$$\Delta i = \frac{Qi}{ki} \qquad (3)$$

or $$\Delta i = wr^2\ \frac{Qi}{ki} \qquad (3a)$$

or $$\Delta i = wr^2\ \Delta i \qquad (3b)$$

$$\bar{\Delta}i = \frac{\bar{Q}i}{Ki} \qquad (3c)$$

Now, the amplitude of the total displacement of the i^{th} floor is btained as a sum of expression (3c) i.e.:.

$$Ai = \sum_{\kappa=1}^{i} \Delta K = W_r^2 \sum_{k=1}^{i} \Delta K \qquad (4)$$

or $$Ai = W_r^2\ \bar{A}i \qquad (4a)$$

where: $$\bar{A}i = \sum_{\kappa=1}^{i} \Delta K = \sum_{k=1}^{i} \frac{Q\bar{k}}{K\kappa} \qquad (4\beta)$$

The circular frequency wr can be determined from expression (5), i.e.:

$$W_r^2 = \frac{Ai}{\bar{A}i} \qquad (5)$$

and w_r must be constant for all floors. If, after the first cycle of calculations, this is not the case, i.e. w_r is not constant for all floors, then the calculation must be repeated with new amplitude values, obtained if the amplitude of all floors Ai is divided by the amplitude of the first floor Ai. More cycles may be necessary until all the w_r values are approximately equal. In other words with a small number of cycles the correct solution for w_r i.e. W_1 is obtained, while the value of A_1 can be used to determine the Si coefficients which in turn enable the determination of the seismic forces.

Stodola's method is a dynamic analysis method which should be used for structures above five storeys in height. For structures up to five storeys the seismic force distribution may be obtained by using the simplified expression given below:

$$Si = S \frac{mi.\ Hi}{\sum_{i=1}^{n} mi.\ Hi}$$

where: S = total horizontal seismic force

Hi = Height of i^{th} floor from the upper edge of the foundation

and mi = weight of i^{th} floor.

3. Muto's Method

3.1. *Aseismic walls*

Both experimental and actual experience on the behaviour of buildings during a cyclic excitation or an earthquake, shows that a uniform grid of frames and symmetrical distribution of walls or cores (staircases or lift shafts) contribute to the structural resistance of the building.

The analysis of structural walls for horizontal seismic forces is considerably complicated. The reason for this is that deformations along the height of such walls are not equal. A practical method for the analysis of buildings with structural walls is the D-method. In this method the wall deformations under horizontal forces are divided into:

1. Shear deformations (δs)
2. Bending deformations (δ_B)
3. Deformations due to rotation of the wall at its base (δ_R)

The detailed explanation and derivation of the expression for these deformations are beyond the scope of this paper. However these expressions are given herein for a better understanding of the example given.

The horizontal displacement at the top of a structural reinforced concrete wall is expressed as the sum of shear and bending deformations δs and δ_B as well deformations due to foundation rotation δ_R

$$\text{i.e. } \delta w_n = \delta_{sn} + \delta B_n + \delta R_n \qquad (7)$$

Where: δs_n expressed in the common unit $\frac{h^2 n}{12.E.K.}$

$$\delta s_n = \frac{K.Qn.hn}{\beta G.Aw\ n} \cdot \left[\frac{12.E.K.}{h^2 n}\right] = (\Delta s) \quad \left(\frac{27.6K}{h_n}\right) \qquad (8)$$

Note $\frac{E}{G}$ taken as 2.3

$$\text{And } \Delta s = \frac{k.Qn}{Aw.n} \qquad (8a)$$

Note: β taken as unity

$$\delta B_n = 4\,\Delta B_n \frac{3}{h_n} \qquad (9)$$

$$\text{where: } \Delta Bn = \sum_{i=1}^{n-1} \frac{Mi}{Kwi} + {}^1/_2 \frac{Mn}{Kwn} \qquad (9a)$$

$$\text{and } \delta R_n = \Theta h_n \frac{12EK}{h_n^2} = \frac{12EK.\Theta}{h_n} \qquad (10)$$

3.2 *D-Values*

Using the method proposed by Kiyoshi Muto (Japan) the regidities can be expressed in terms of the D values. These depend on the rigidity of columns and the relative rigidity of beams with respect to the columns as well as the position of the column in the frame.

Generally:

$D = a.Kc$

where: Kc = Column Rigidity $= \frac{Ic}{Kh_n}$

Ic = 2nd M.O.A. of cross section of column

h_n = storey height

K = Arbitrary coefficient (selected as unity as well)

$\alpha < 1$ factor (refer to Fig. 2 below)

Muto's method is an approximate one but is based on systematic theoretical and experimental investigations.

The basic characteristics of this method are the following:

(a) the determination of the coefficients of horizontal shear force distribution (D-values) and

(b) the determination of the inflexion points on the column.

4. Analysis of a structure for Seismic Loading

The structure to be analysed is shown in Fig. 1. In the elevation of the structure lateral forces are shown at all floor levels. These forces have been chosen arbitrarily but their final distribution will depend on such factors as anticipated earthquake magnitude and dynamic characteristics of the structure.

Firstly the values of all member stiffnesses i.e. Kc, Kb and Kw at all storey levels are evaluated. From these $\bar{K}$ is found by using the exressions shown in Fig. 2. The D values for the frame can therefore be evaluated and these are also included in Fig. 2. The total sum per storey of the D value is indicated as ΣD, in Fig. 2. (The Kw values are shown in Table 1).

The rest of the procedure in the analysis is presented in Table 1. Explanations on this table are given below.

First the wall area Aw and wall stiffness Kw at the various levels is evaluated (columns 2 and 3). Column 4 shows the arbitrarily chosen lateral forces and in column 5 the ratio Qn/Aw_n is included. In column 6 the ratio $\frac{27.6 \times 1.2}{h_n}$ is tabulated.

This ratio comes from $\frac{12\,K\,E}{G\,h_n}$ (The shape factor for the shear distribution is taken as 1.2 and the ratio E/G as 2.3).

In column 7 the value of the shear deformations in the wall are tabulated (i,e, column 5 values multiplied by those of column 6 — expression (8). In column 8 the

product Qn h_n is given from which the values of the cumulative wall moments are obtained as shown in column 9. Columns 10 and 11 are constructed to aid the evaluation of the quantity $4\Delta B_n$ shown in column 12.

Note that the arrows shown in columns 9, 10, 11 and 12 are included to assist the reader in following the construction of columns 10 and 12. The ratios $3/h_n$ appear in column 13 which when multiplied by the $4\Delta B_n$ values of column 12 give the values of the wall deformations due to bending (column 14 — expression 9). In column 15 the wall deformations due to the rotation are included. These are evaluated using expression 10. The total deformations δn which are made up of shear, bending and rotation deformations are tabulated in column 16. The relative wall rigidities or D values are given in column 17. In column 18 the D values for the frame for each storey are indicated and the total sum of the D values per storey are tabulated in column 19. From columns 4, 17, 18 and 19 the values of storey shear for both the frames and the structural walls are evaluated using the appropriate expressions as shown in columns 20 and 21. This completes one cycle of calculations. Columns 22 to 35 represent the second cycle by employing now instead of the original Qn values, the values of Q taken by the wall, i.e. using the values obtained in column 21. The procedure is stopped when the values of δn, the total storey deformations of the new cycle are approximately equal to the δn of the preceding cycle. As it can be seen, the values of δn in the third cycle (columns 36 to 51) are very close to the values of δn in the second cycle and hence the third cycle was considered to be sufficient without having to go to a fourth cycle.

The final bending moment diagram for the wall is shown in Fig. 3. (The values plotted are those in column 51 of Table 1).

Fig. 4 shows the column shears for the frame which are distributed to all columns according to their D values i.e.:

$$Q = Q_{Fn}\frac{D}{\Sigma D}$$

In Fig. 4 the y values are also included for all columns. Values of y may be taken from standard tables. These y values are the percentage distance of the column height taken from the bottom of the column to the point of inflexion.

Now, the product Qh is equal to the summation of the moments at the top and bottom of the column i.e.

$$Qh = Mt + Mb$$

Hence with the point of inflexion known it may be easily found that:

$$Mt = M\,(1-y)$$

and $$Mb = M.y$$

where Mt = Moment at the top of column

Mb = Moment at the bottom of column.

These moments in all the columns of the pure frame are shown in the bending moment diagram in Fig. 5. In Fig. 5 the beam moments are also included and they are found simply by distributing the column moments at every joint, to the beams on either side of the joint i.e.

$$M_{BL} = \frac{K_{bl}}{K_{bl} + K_{bR}}\,(M_{bn+1} + Mt_n)$$

where K_{bl} = stiffness of beam left of joint

K_{bR} = stiffness of beam right of joint

M_{bn+1} = Moment at the bottom of column in storey n+1

Mt_n=Moment at the top of column in storey n.

From the beam moments the beam shears can easily be found. these are also included in Fig. 5.

5. General Comments and Conclusions

Some useful observations may be made based on the results of the analysis but nevertheless having a more general application.

When the ratio between the beam and the column rigidity is high the inflexion point in the column is approximately at the middle of the storey height and hence the bending moments are the same at the upper and the lower ends of the columns. This is the case of the columns in the second storey where the inflexion point in the columns occurs at the mid-height exactly (i.e. y=0.5). On the contrary when the ratio between the beam and column rigidity is low, the inflexion point moves up and down or it may even be outside the storey. Thus the inflexion point in the case of the fifth storey columns moves downwards. Hence y=0.3 for the column on the right and y=0.35 for the central and the column on the left hand side of the frame.

When the rigidity of the upper and the lower beams is different, the inflexion point moves towards the beams with the lower rigidity. Moreover, when the height of a neighbouring storey is bigger, the inflexion point moves towards the higher storey as is the case of the inflexion points in the second storey columns which are closer to the first storey rather than the third storey.

Low relative rigidities of beams with respect to the columns are not desirable. The higher the relative beam rigidity to the column rigidity the higher the likelyhood of the inflexion point in the column to occur at the mid-height of the column. Fig. 6a shows a typical case of high beam to column rigidity and Fig. 6b a typical case of low beam to column rigidity. In the case of low relative rigidity of beams to columns more reinforcement is needed in the columns and this is not ideal for earthquake design.

Very high reinforcement concentrations in the columns will render them brittle and as such they will suffer heavy damage during an earthquake. From past experience on earthquakes it has been concluded that the degree of structural damage is related to the post-elastic deformation capacity of the non-linear plastic hinges as well as to the behaviour of both structural and non-structural elements. The structure fails due to failure of plastic hinges and zones, that means when the transmitted energy exceeds the capacity of energy absorption and dissipation of the structure.

In the case of thin and high cantilever walls the resistance of the upper storeys is very small. In actual buildings, cantilever walls do not exist as such. Walls supposedly of the cantilever type are surrounded by frames in both directions decreasing the level of deformations of these walls. Taking into account the interaction effect between walls and frames the bending moment diagram in the wall is more like the bending moment of a frame, i.e. more like what is shown in Fig. 7 than what was derived in the example above and shown in Fig. 3.

A further point on walls is the following: In evaluating I values of frame sections — beams and columns — the total cross-sectional area is taken ignoring reinforcement and cracking. However in structural (shear) walls which are more rigid than frames, in the area where plastic hinges are expected, the I value may be taken as half its actual value. This area of plastic hinges, for earthquake purposes, may be assumed to be the region in the lower floors equal (in height) to the width of the wall.

In conclusion the importance of good construction is stressed again. No matter how sophisticated the analysis and the design of a structure is, if the construction does not conform to certain standards the good work performed in the analysis and design will be wasted. Apart from the obvious point relating to poor construction, that is the use of inferior quality materials, there are are other pure construction points worth mentioning. Some of these having special importance relevant to aseismic construction are, the use of smaller spacing of links at the panel joints, good and generous anchorage lengths, proper tying of reinforcement especially of links and stirrups, and the use of adequate cover to all bars. An example of bad practice in Cyprus is the fact that although a closer spacing of links is required at the panel joints most often these are not used at all. One can only presume that the reason for this is the difficulty that the closer link spacing creates in properly compacting the concrete at the panel joints.

However, even though this can become a problem it is certainly not a valid reason for not using links there at all!

One can only wish that engineers in Cyprus acquire the "seismic" conscience and start applying the few basic principles governing aseismic design. It must be mentioned finally that there is currently an aseismic code being drafted in Cyprus. It is hoped that the work of the committee will soon be completed and Cyprus will have its own "much needed" aseismic regulations.

REFERENCES

1. M. HIROSAWA: "Past Experimental Results on R.C. Shear Walls and Analysis on Them". Building Research Institute, Report No. 6, Tokyo, March 1975.
2. A. CARDENAS & D. MAGURA: "Strength of High-Rise Shear Walls - Rectangular Cross Section". A.C.I. Publication SP-36, 1973.
3. T. TAKEDA, M.A. SOZEN & N.N. NIELSEN: "Reinforced Concrete Response to Simulated Earthquakes". A.S.C.E. Proceedings Vol. 96 No. ST12 Dec. 1970.
4. T. PAULAY & D.D. SPURR: "Frame Shear Wall Assemblies Subjected to Simulated Seismic Loading". VI WCEE, New Delhi, January 1977.

Table 1. Analysis - Procedure

n	1 hn(cm)	2 Aw (cm^2)	3 Kwx10^2 (cm^3)	4 Qn tons	5 Qn/Aw ton/cm^2	6 $\frac{27.6x1.2}{h_n}$	7 δsn (cm)	8 Qnh_nx10^3 ton.cm	9 Mw_nx10^3 ton.cm	10 2Mnx10^3 ton.cm	11 2Mn/Kw ton/cm^2	12 4ΔBn t/cm^2	13 $3/h_n$ cm^{-1}
5	350	90x10^2	18800	30	0.333	0.0946	0.0315	10.5	10.5	10.5	0.56 →	65.66	0.0086
4	350	90x10^2	18800	70	0.777	0.0946	0.0736	24.5	35.0	45.5	2.42 →	62.68	0.0086
3	350	90x10^2	18800	110	1.222	0.0946	0.1156	38.5	73.5	108.5	5.77 →	54.49	0.0086
2	350	120x10^2	26074	150	1.250	0.0946	0.1183	52.5	126.0	199.5	7.61 →	41.11	0.0086
1	450	120x10^2	20280	200	1.666	0.0736	0.1226	90.0	216.0	342.0	16.75 →	16.75	0.0067

14 δBn cm	15 δRn cm	16 δn total= δsn+δBn+δRn Cm	17 Dw=Qn/δn	18 DF	19 Σ D= DW+DF	20 $QF_n=DF\frac{Qn}{\Sigma D}$	21 $Qw_n=Dw\frac{Qn}{\Sigma D}$	22 Qw_n/Aw ton/cm^2	23 δs_n (cm)	24 $Qw_nh_nx10^3$ ton/cm	25 Mw_nx10^3 ton.cm	26 $2Mw_nx10^3$ ton.cm
0.56	0.80	1.39	21.58	11.12	32.70	10.20	19.80	0.22	0.02	6.93	6.93	6.93
0.54	0.80	1.41	49.65	11.12	60.77	12.80	57.20	0.64	0.06	20.02	26.95	33.88
0.47	0.80	1.39	79.14	11.12	90.26	13.50	96.50	1.07	0.10	33.78	60.73	87.68
0.35	0.80	1.27	118.11	12..88	130.99	14.70	135.30	1.13	0.11	47.36	108.10	168.82
0.11	0.62	0.87	235.29	22.31	257.60	17.30	182.70	1.52	0.11	82.22	190.31	298.40

27 $2M_n/Kw$ ton/cm^2	28 $4\Delta B_n$ ton/cm^2	29 δBn	30 δRn	31 δn total	32 DW	33 ΣD	34 QFn	35 QWn	36 Qw_n/Aw_n	37 δs_n	38 $Q_{w_n}h_nx10^3$	39 Mw_n $x10^3$
0.37	55.63	0.48	0.80	1.30	15.23	26.35	12.66	17.34	0.192	0.018	6.07	6.07
1.80	53.46	0.46	0.80	1.32	43.33	54.45	14.30	55.70	0.619	0.059	19.50	25.56
4.66	47.00	0.40	0.80	1.30	74.23	85.35	14.30	95.70	1.060	0.100	33.50	59.06
6.47	35.87	0.31	0.80	1.22	111.90	123.78	15.60	134.40	1.120	0.106	47.00	106.10
14.70	14.70	0.10	0.62	0.83	220.12	142.43	18.40	181.60	1.513	0.111	81.70	187.82

40 $2Mw_n$	41 $2Mw_n/Kw$	42 4ΔBn	43 $3/h_n$	44 δB_n	45 δR_n	46 δn total	47 DW	48 ΣD	49 Q_{F_n}	50 Qw_n	51 $Mw_n=Qw_nh_n$
6.07	0.323	54.343	0.0086	0.467	0.8	1.285	13.49	24.61	13.55	16.45	5.76
31.64	1.683	52.337	0.0086	0.450	0.8	1.309	42.55	53.67	14.50	55.50	25.19
84.63	4.500	46.154	0.0086	0.397	0.8	1.297	73.78	84.90	14.40	95.60	58.65
165.16	6.334	35.320	0.0086	0.304	0.8	1.210	111.10	123.98	15.58	134.42	105.70
293.92	14.493	14.493	0.0086	0.097	0.8	0.828	219.32	241.63	18.46	181.54	187.40

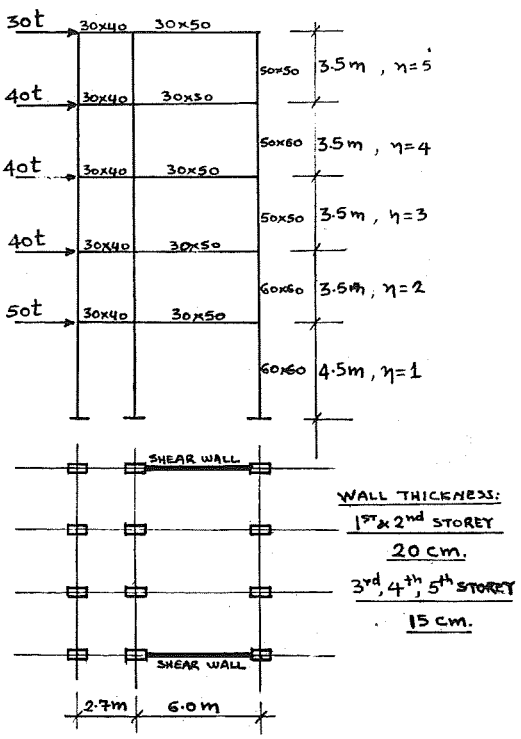

FIG. 1 ELEVATION & PLAN OF STRUCTURE.

FIG. 2. MEMBER STIFFNESSES AND D-VALUES.

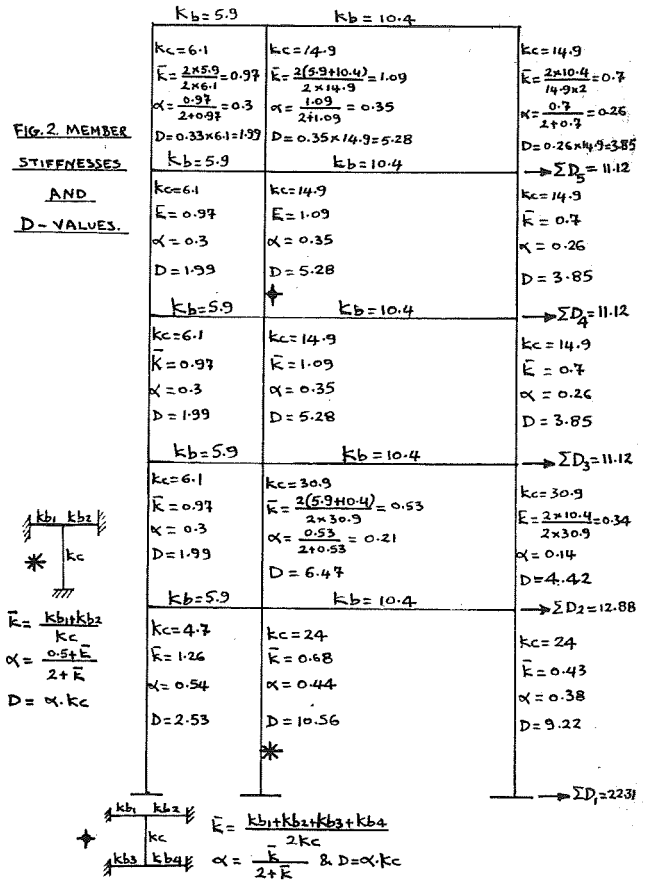

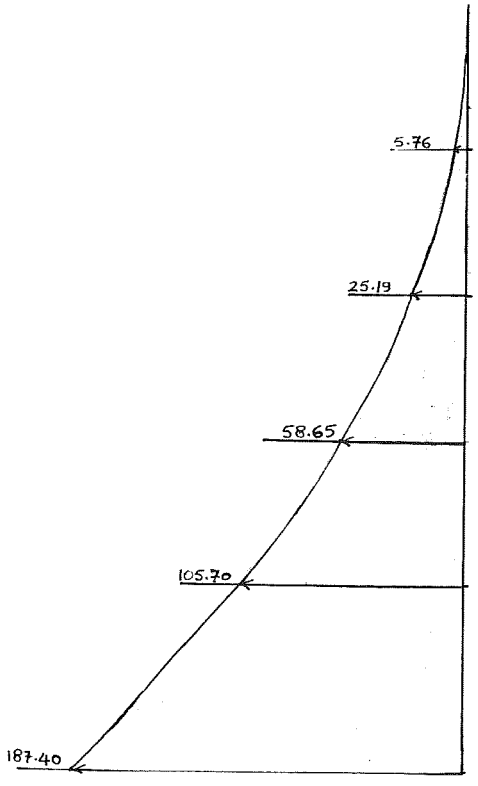

FIG. 3 B.M.D. OF STRUCTURAL WALL.

$Q = 2.42$ $Q_h = 8.47$ $y = 0.35$	$Q = \frac{5.28}{11.12} \times 13.55 = 6.43$ $Q_h = 22.5$ $y = 0.35$	$Q = \frac{3.85}{11.12} \times 13.55 = 4.69$ $Q_h = 16.40$ $y = 0.30$
$Q = 2.59$ $Q_h = 9.10$ $y = 0.40$	$Q = \frac{5.28}{11.12} \times 14.50 = 6.88$ $Q_h = 24.10$ $y = 0.40$	$Q = \frac{3.85}{11.12} \times 14.50 = 5.00$ $Q_h = 17.50$ $y = 0.40$
$Q = 2.58$ $Q_h = 9.10$ $y = 0.45$	$Q = \frac{5.28}{11.12} \times 14.40 = 6.84$ $Q_h = 23.94$ $y = 0.45$	$Q = \frac{3.85}{11.12} \times 14.40 = 4.99.$ $Q_h = 17.50$ $y = 0.45.$
$Q = 2.41$ $Q_h = 8.44$ $y = 0.50$	$Q = \frac{6.44}{12.88} \times 15.58 = 7.74$ $Q_h = 27.26$ $y = 0.50$	$Q = \frac{4.45}{12.88} \times 15.58 = 5.38.$ $Q_h = 18.83$ $y = 0.50$
$Q = 2.10$ $Q_h = 9.45$ $y = 0.62$	$Q = \frac{10.56}{22.31} \times 18.46 = 8.74$ $Q_h = 39.33$ $y = 0.70$	$Q = \frac{9.22}{22.31} \times 18.46 = 7.63$ $Q_h = 34.33$ $y = 0.75.$

FIG. 4. EVALUATION OF COLUMN SHEAR FORCES. ($Q = Q_{F_n} \cdot \frac{D_c}{\Sigma D_c}$)

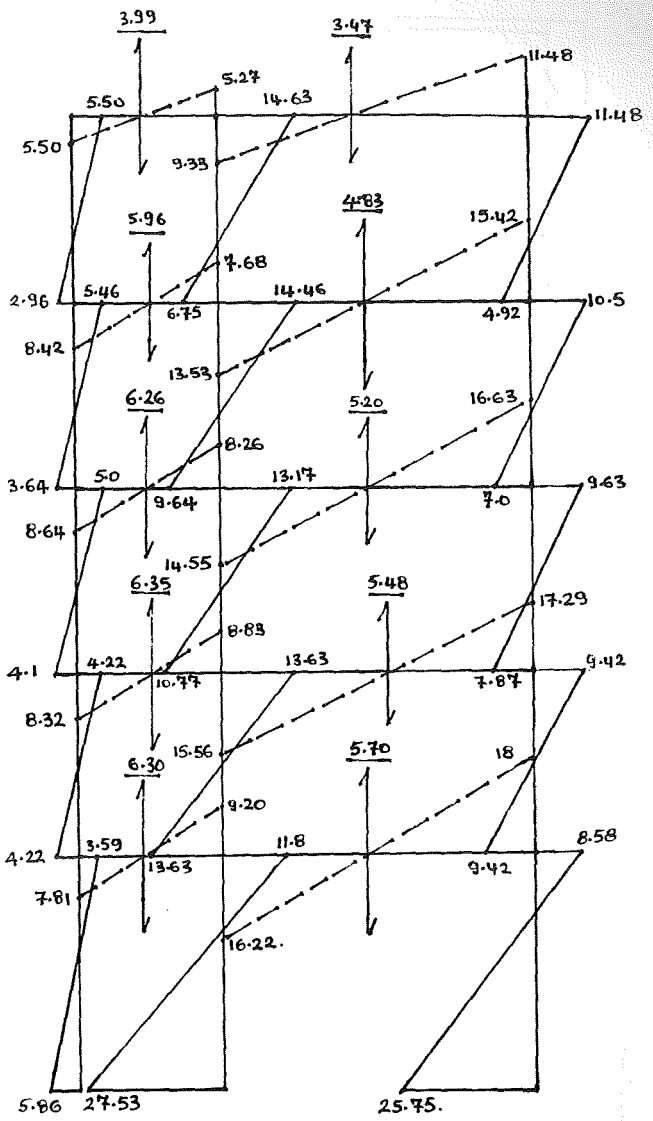

FIG. 5. B.M.D. OF FRAME. (UNITS t-m)

LEGEND: ——— ⇒ B.M. IN BEAMS

↕ ⇒ SHEAR IN BEAMS. (t)

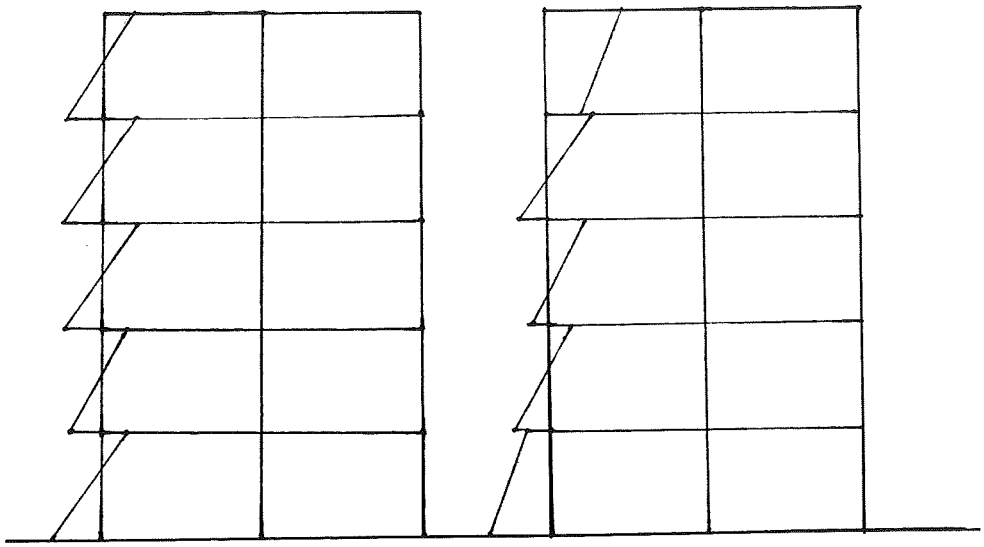

FIG. 6a

B.M.D FOR HIGH BEAM TO COLUMN RIGIDITY

FIG. 6b.

B.M.D. FOR LOW BEAM TO COLUMN RIGIDITY

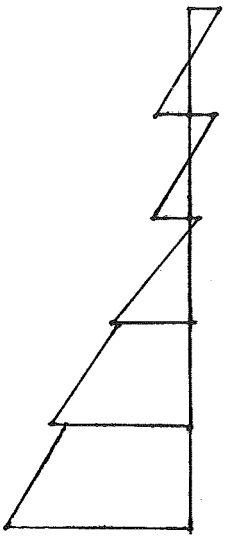

FIG. 7 B.M.D OF STRUCTURAL WALL TAKING INTO ACCOUNT THE INTERACTION EFFECT OF ADJOINING FRAMES.

OERLIKON

THE SYMBOL OF QUALITY

ELECTRODES

Manufacturers of the famous

OERLIKON electrodes

We can solve any problem in welding on mild steel or any other special steel

OERLIKON ELECTRODES LTD

P. O. Box 1458—Tel: 051-67133

Telex: 3016 OERLIKON CY.

Cables: OERLIKON

LIMASSOL—CYPRUS

ΣΕ ΤΙΜΕΣ ΕΥΚΑΙΡΙΑΣ

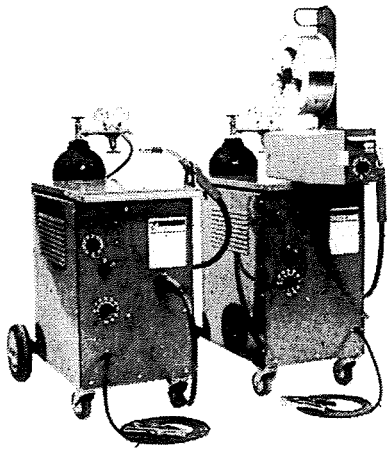

Διαθέτομεν μηχανὲς ἡμιαυτομάτου συγκολλήσεως CO_2 καὶ Ἀργὸν κατάλληλες διὰ Βιομηχανίες, ἰσιωτὲς αὐτοκινήτων καὶ γενικὲς συγκολλήσεις.

Ἐπίσης μηχανὲς κοπὴς εἰδικῶν μετάλλων ὅπως STAINLESS STEEL, Ἀλουμινίου κκπ. μὲ (PLAS MACUTTING).

Γιὰ περισσότερες πληροφορίες ἀποταθῆτε :

Α. ΕΠΙΦΑΝΙΟΥ

Ταχ. Κιβ. 1456 — Τηλ. 051-67133

ΛΕΜΕΣΟΣ

APPLICATION OF SYSTEMS ANALYSIS TO WATER RESOURCES PLANNING

By Chrysostomos Kambanellas,
Civil Engineer,
Water Development Department, Nicosia

The problems associated with managing land, water, air, and energy resources have never been simple. It often seems that the complexities of environmental management, which includes the control of pollution and allocation of resources are so intimidating that rational analysis is futile. This is partially because of the political nature of environmental decisions. However, a substantial source of complexity is the intricate physical interactions within environmental systems. Wastes are transported by water or air from one location to another with attendant chemical transformations. Land used for one purpose may limit other uses, and energy planning must consider a bewildering array of competing sources and consumers. It can be difficult to trace the impacts of pollution control and resource management decisions, and it often seems impossible to determine which of several alternatives best meet management objectives.

Fortunately, there is an analytical process that promises to reduce the complexities of environmental problems to manageable levels. Systems analysis has proved very useful in the resolution of complex management problems. Systems analysis has been applied recently with considerable success to environmental management.

Systems Analysis is, (i) the retional use of analysis to study and solve engineering and management problems, (ii) the application of the scientific method to operational problems, (iii) the practical application of economic principals.

In general the Systems Approach (a) takes into account all the relevant alternatives, (b) provides an orderly and systematic examination of alternatives, (c) sharpens the designer's awareness of his objectives by forcing him to make explicit statements about what they are and how they are to be measured, (d) seeks mechanisms for predicting the future demands on a system, which often are not observable in advance but must be determined from an interaction of social and economic factors, (e) establishes procedures for generating a large number of possible solutions and for determining efficient methods to search through them assembles optimization techniques which can pick out favorable alternatives, and (f) suggests strategies of decision-making which can be used to select among possible alternatives.

Systems analysis, at its core, consists of the application of classical microeconomic concepts to the problems to resource allocation. At its simplest, it could be a quantitative study of the possible ways to achieve certain goals or to use available resources. More technically, it generally involves the use of a number analytic tools, such as: Production functions to represent the combination of supplies, marginal analysis concepts and optimization techniques to determine preferable alternatives, utility and decision theory to define optimally desirable configurations, and sensitivy analysis to investigate the reliability of the conclusions. The use of sophisticated tools does not however constitute a systems analysis by itself. A good systems analysis is one that carefully identifies the important issues and alternatives and relates the several costs and benefits of each project in a way that is meaningful to the persons responsible for approving a program.

Systems analysis has five steps:

(1) Definition of objectives and constrains,
(2) Formulation of measures of effectiveness,
(3) Generation of alternatives,
(4) Evaluation of the alternative,
(5) Making a selection.

Linear Programming

Linear programming is one of the techniques of greatest potential value to those engaged in planning public works projects and demonstrates most of the key points of systems analysis. Linear programming requires that the objective function and all other equations in the mathematical model be linear. That is no term in any equation can contain more than one value and that variable must be to the first power. The three basic components of the linear programming are the objective function, the constraint equation and an iterative procedure for finding the optimum solution. Linear programming models are optimization models that can be solved by linear programming algorithms.

There are three methods of solution — the graphical method, the simplex method and the double description method.

Two dimentional (two variable) linear programming models can be solved by the graphical method as shown in the first question of the following example. For models having more than two variables and constraints or when the number or extreme points can be very large we can use the simplex method as shown in the second question of the following example.

The simplex method is an algebraic procedure used to examine extreme points efficiently. It selects the extreme points that are most likely to lead to an optimal solution.

The most commonly used algorithm is the simplex method. The simplex algorithm requires a basic feasible solution to start with. Such a starting point is not always easy to find and, in fact, none will exist if the constraints are inconsistent.

Example of application on Systems Analysis to Water Resources Planning

The island of Cyprus is situated in the eastern basin of the Mediterranean Sea in a semi-arid region. It's area is 3570 square miles and the population is about 640,000 inhabitants (80% Greeks and 18% Turks).

There are two mountains in Cyprus — Pentadaktylos with limestone and Troodos with igneous rocks. Between these mountains there is the main aquifer of Cyprus, the Morphou Aquifer.

The average annual precipitation in Cyprus is 489 mm. There was always a problem of enough water in Cyprus but from 1974 the water problem became worse.

In July 1974 the Turkish army occupied 40% of the island. The main water sources of Cyprus, Morphou aquifer and Pentadaktylos mountain, are now under the Turkish control.

As a result of the above, it appears an absolute necessity to develop agriculturally of the southern part of the island, especially the following three areas, Area 1, Area 2 and Area 3 because most of the refugees are living now in these areas. *(see fig. 1)*

Most of the precipitation of Cyprus occurs on Troodos mountain. In order to increase the irrigated land, it is necessary to store winter water and use it in the summer when there is a drought.

The S.C. Project consists of the construction of dams at Troodos area and with an aquiduct and/or pipelines it will irrigate Area 1, Area 2 and Area 3, as shown in figure 1.

Area 1 is the most agricultural productive area, and it has 30% of the refugees living there but it is further away from the Troodos mountain. The second most agricultural productive area is Area 2 with 20% of the refugees living there. At Area 3 there are 10% of the refugees and it is the nearest to Troodos mountain.

The water and the area to be developed are limited. The crop water requirement is determined from the curve of yield vs. applied water by maximizing farm income in dollars per acre *(figure 2)* as expressed in the relationship.

$$I = P_c Y - P_w Q - V_c Y - F_c$$

Where

P_c is the unit price received for the crop,

Y is the crop yield in units per acre,

P_w is the value of water in dollars per acre-foot,

Q is applied water in acre-feet per acre,

V_c is the variable cost of producing the crop in dollars per unit of crop yield, and

F_c is the fixed cost of crop production in dollars per acre.

Following are two of the most important questions that need to be answered.

1. What is the optimum combimation of land irrigation of Area 1 and Area 2 ?
2. What is the optimum combination of land irrigation of the three areas, i.e., Area 1, Area 2 and Area 3 ?

1) The first question is analyzed as follows: The available amount of water is Q acre-ft per year and the available area to be developed is X acres. It is found from the experiments that the net profit (or income) from Area 1 is $\$I_1$, per acre with the crop needs in water of V_1 acre-ft per year and from Area 2 the net profit is $\$I_2$ per acre with the crop's needs in water of V_2 acre-ft per year. What is the optimum combination of land irrigation of the above two areas that maximizes the farmer profits subject to a constraint of the amount of water?

Solution by Graphical Method

Let X_1 be the number of acres to be developed at Area 1 and X_2 be the number of acres to be developed at Area 2. X_1 and X_2 are the decision variables. Annual profits are $Z = I_1X_1 + I_2X_2$.

The objective function is Max. $Z = I_1X_1 + I_2X_2$ (1)

subject to $V_1X_1 + V_2X_2 \leqslant Q\ldots$ (2)

$X_1 + X_2 \leqslant X\ldots$ (3)

$X_1 \geqslant 0\ldots$ (4)

$X_2 \geqslant 0\ldots$ (5)

For the sake of demonstration:

Let $I_1 = 300$ dollars per acre
$I_2 = 200$ dollars per acre
$V_1 = 0.8$ acre-ft per year per acre
$V_2 = 0.5$ acre-ft per year per acre
$Q = 1300$ acre-ft per year
$X = 2000$ acres

Equation (1) becomes Max. $Z = 300X_1 + 200X_2\ldots$ (6)
S.T. $0.8X_1 + 0.5X_2 \leqslant 1300\ldots$ (7)
$X_1 + X_2 \leqslant 2000\ldots$ (8)
For (7) When $X_1 = 0$, $X_2 = 2600$ and
when $X_1 = 1625$, $X_2 = 0$
For (8) when $X_1 = 0$, $X_2 = 2000$ and
when $X_1 = 2000$, $X_2 = 0$
From $0.8X_1 + 0.5X_2 = 1300$, $X_1 = 1625 - 0.625X_2$
Substitute X_1 to $X_1 + X_2 = 2000$
Therefore $1625 - 0.625X_2 + X_2 = 2000$
$X_2 = 1000$ and $X_1 = 1000$

The feasible region for this problem is shown in figure 3.

Extreme point theorem: "The answer will be at a vertex." i.e. The answer in figure 3 will be at point C.

The conclusion of the above first question is that: The optimum combination of land irrigation must be Area 1 = Area 2 = 1000 acres for the maximum profit of 500,000 dollars.

2) The second question is analyzed as follows: The available amount of water is Q acre-ft per year from which the 2/3Q is decided to give to the Area 1 and Area 2. The available area to be developed is X acres. It is found from the experiments that the net profit from Area 1 is $\$I_1$ per acre with the crop's needs in water of V_1 acre-ft per year. From Area 2 the net profit is $\$I_2$

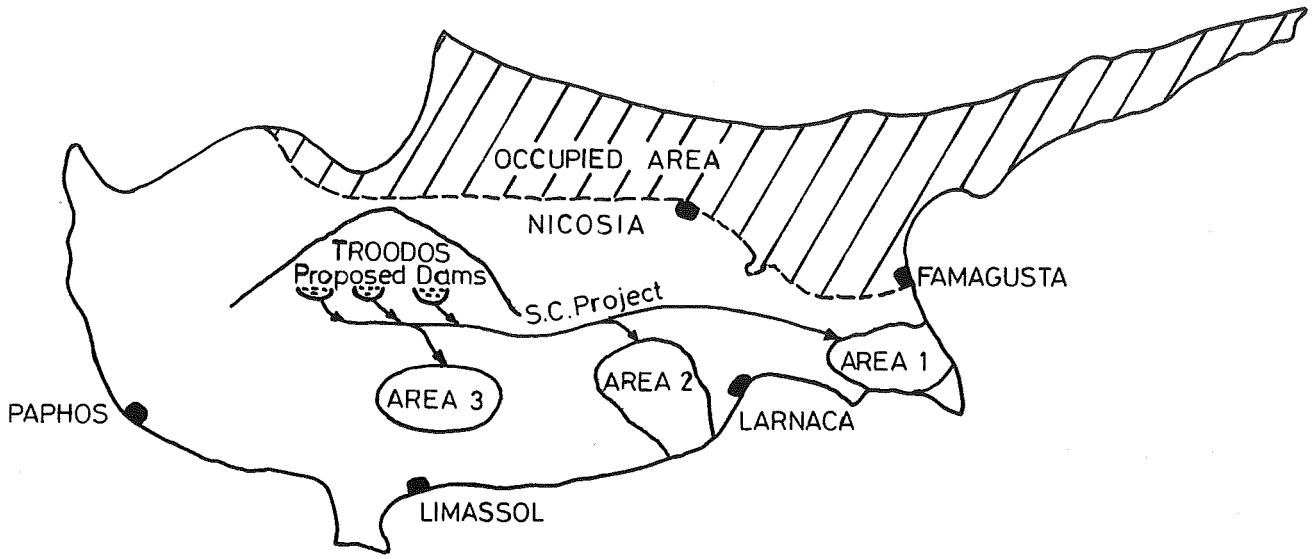

FIG.1 : CYPRUS

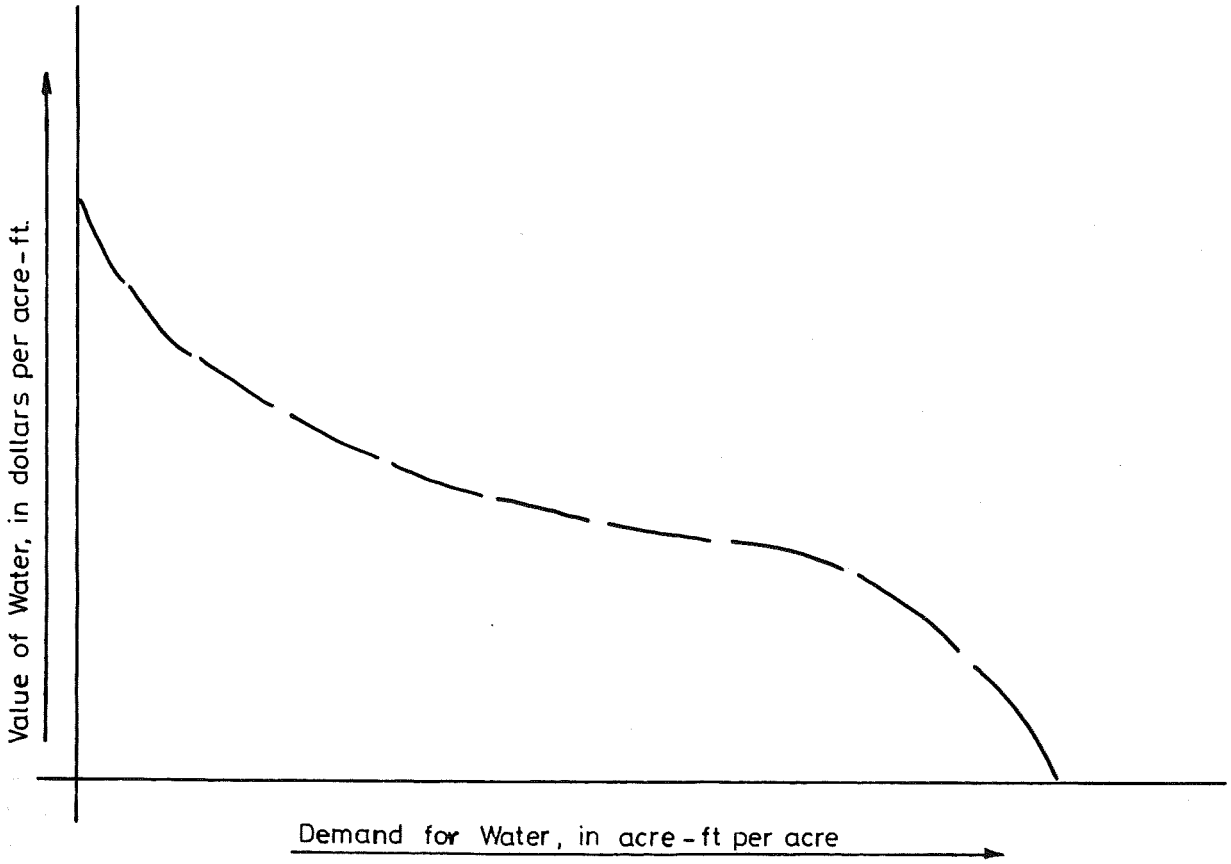

FIG.2 : DEMAND CURVE

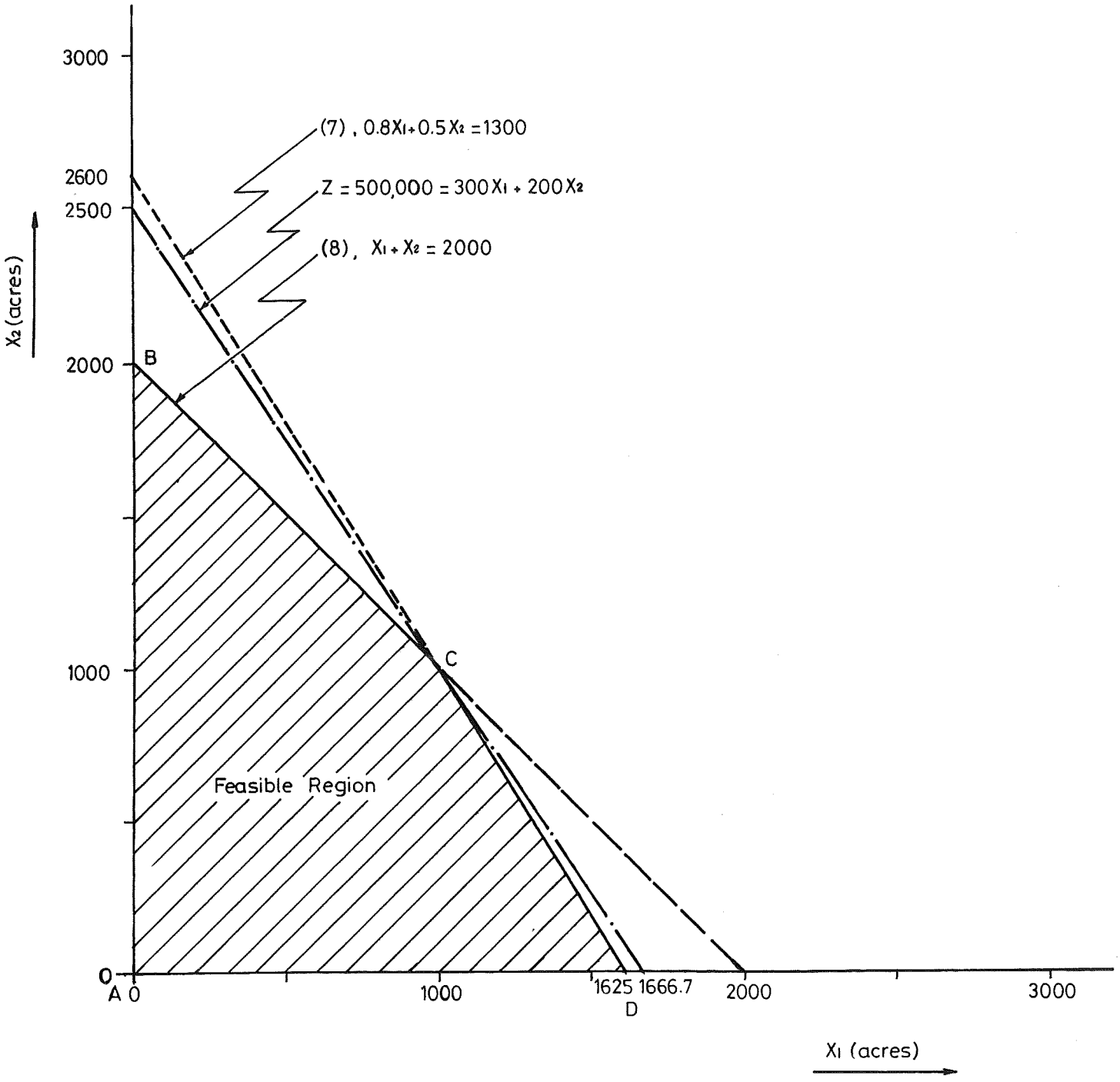

FIG. : 3

SET	X_1	X_2	$Z = 300X_1 + 200X_2$
A	0	0	0
B	0	2000	400,000
C	1000	1000	500,000 ← MAXIMUM
D	1650	0	487,500

per acre with the crop's needs in water of V_2 acre-ft per year, and from Area 3 the net profit is $\$I_3$ per acre with the crop's needs in water of V_3 acre-ft per year. What is the optimum combination of land irrigation of the above three areas that maximizes the farmer's profits subject to a constraint of the amount of water?

Solution by Simplex Method

Let X_1 be the number of acres to be developed at Area 1

X_2 be the number of acres to be developed at Area 2

X_3 be the number of acres to be developed at Area 3

X_1, X_2 and X_3 are the decision variables.

Annual profits are: $Z = I_1X_1 + I_2X_2 + I_3X_3$

The objective function is:

$$\text{Maximize } Z = I_1X_1 + I_2X_2 + I_3X_3 \quad (9)$$

$$\text{Subject to } X_1 + X_2 + X_3 \leqslant X\ldots \quad (10)$$

$$V_1X_1 + V_2X_2 + V_3X_3 \leqslant Q\ldots \quad (11)$$

$$V_1X_1 + V_2X_2 \leqslant 2/3Q\ldots \quad (12)$$

The Simplex method is based on the theory of simultaneous linear equations, so the first step is to rewrite all the constraints in the form of linear equations by adding the slack variables, "U", "V" and "W".

Therefore Max $Z = I_1X_1 + I_2X_2 + I_3X_3 + OU + OV + OW$

Subject to

$$X_1 + X_2 + X_3 + U = X$$
$$V_1X_1 + V_2X_2 + V_3X_3 + V = Q$$
$$V_1X_1 + V_2X_2 + W = 2/3\,Q$$

From the above first tableau is constructed

X_1	X_2	X_3	U	V	W	Z	RHS
1	1	1	0	0	0	0	X
V_1	V_2	V_3	0	1	0	0	Q
V_1	V_2	0	0	0	1	0	2/3 Q
$-I_1$	$-I_2$	$-I_3$	0	0	0	1	0

For sake of demonstration:

Let $I_1 = 300$ dollars per acre

$I_2 = 200$ dollars per acre

$I_3 = 150$ dollars per acre

$V_1 = 0.8$ acre-ft per year per acre

$V_2 = V_3 = 0.5$ acre-ft per year per acre

$Q = 1300$ acre-ft per year

$X = 2000$ acres.

The first tableau becomes as follows:

X_1	X_2	X_3	u	v	w	Z	RHS	Ratio RHS / COLUMN ELEMENT	BASIC VARIABLE	NON BASIC VARIABLE	Z
1	1	1	1	0	0	0	2000.0	INITIAL 2000	u=2000	$X_1=0$	
0.8	0.5	0.5	0	1	0	0	1300.0	TABLEAU 1625			
(0.8)	0.5	0	0	0	1	0	866.0	1083.3 ← MIN.	v=1300	$X_2=0$	0
-300	-200	-150	0	0	0	1	0	RHS ⩾ 0	w=866.7	$X_3=0$	
0	0.375	1	1	0	-1.25	0	916.6	916.6	$X_1=1083.4$	$X_2=0$	
0	0	(0.5)	0	1	-1.00	0	433.3	1st ITERATION 866.6 ← MIN.	u=916.6	$X_3=0$	325,012.5
1	0.675	0	0	0	1.25	0	1083.4	—			
0	-12.5	-150	0	0	375	1	325,012.5		v=433.3	w=0	
0	(0.375)	0	1	-2	0.75	0	50.0	133.4 ← MIN.	$X_1=1083.4$	$X_2=0$	
0	0	1	0	2	-2	0	866.6	2nd ITERATION —	$X_3=866.6$	v=0	455,002.5
1	0.625	0	0	0	1.25	0	1083.4	1733.4			
0	-12.5	0	0	300	75	1	455,002.5		u=50.0	w=0	
0	1	0	2.67	-5.33	2	0	133.4		$X_1=1000.0$	u=0	
0	0	1	0	2.0	-2	0	866.6	3rd ITERATION	$X_2=133.4$	v=0	456,670.0
1	0	0	-1.67	3.33	0	0	1000.0				
0	0	0	33.375	233.375	100	1	456,670.0		$X_3=866.6$	w=0	

NO NEGATIVES, ∴ STOP ! ↑ ANS.

∴ $Z = 456,670.0 - 0X_1 - 0X_2 - 0X_3 - 33.375u - 233.375v - 100w$

SHADOW PRICES : 33.375 u , 233.375 v, 100 w

ANSWERS : $X_1 = 1000.0$ acres

$X_2 = 133.4$ acres

$X_3 = 866.6$ acres

$Z = 456,670.0$ dollars

The conclusion of the above second question is: For the maximum profit of 456,670 dollars the optimum combination of land irrigation is Area 1 = 1000 acres, Area 2 = 133.4 acres and Area 3 = 866.6 acres, and if the total area X increases from 2000 to 2001 acres the profit Z increases from 456,670.0 to 456, 670.0 + 33.37 =456,703.37 dollars. If the amount of water Q increases from 1300 to 1301 acre-ft per year the profit Z increases from 456,670.0 to 456,670.0 +233.37 =456,903.37 dollars for the total area and 456,670.0 + 100 = 456,770.0 dollars for the Area 1 and Area 2.

REFERENCES

1) G. KENNETH YOUNG, "Systems Analysis Fundamentals".
2) H.M. WAGNER, "Principles of Operations Research".

The Wang Professional Computer

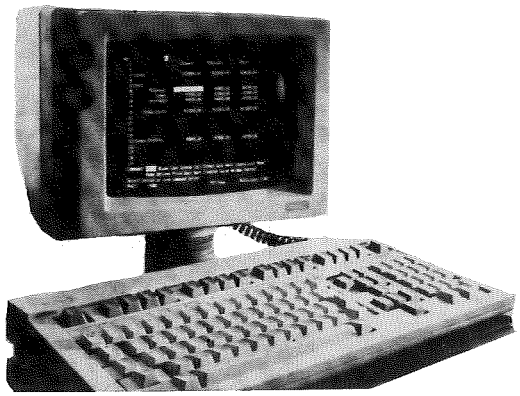

Special Introductory Offer

Are you serious about buying a personal computer for your office? Or do you want to play games?

We started building computers and word processing systems for the office when most computer companies were still building computers for the backroom. And ever since, Wang has been the leader in office automation.

Now we've put all that experience to work, with the introduction of the Wang Professional Computer — a computer so advanced in capability and design, it's like no other personal computer you've seen.

In data processing, the Wang Professional Computer is faster than any other personal computer we've tested.

Wang strengthened its office automation leadership position with the announcement of the Wang Professional Computer.

Designed for the new generation of personal computer users, the Wang Professional Computer has a variety of features including:

- A full 16-bit professional computing system which is one of the most powerful in the industry;
- the ability to function as a workstation on any Wang 2200, VS, OIS system, providing full office automation functionality; and
- more communications options than any other personal computer on the market today, including both industry standard and WangNet communications capabilities.

The Wang professional Computer has the Microsoft Disk Operating System (MS-DOS), offering users a wide selection of industry standard languages and applications, in addition to PC-Word Processing, a version of Wang's proven and popular word processing, and PC-Multiplan, an electronic spreadsheet tool.

For more information on the Wang Professional Computer call 021-20101

INFOTRONICS LTD
Business Executive Department

WANG

The Office Automation Computer Company

DESIGN AND INSTALLATION OF DOMESTIC AND INDUSTRIAL SOLAR WATER HEATING SYSTEMS

By I.M. Michaelides, *CEng, MInst E*
Senior Lecturer, Mech. Eng. Dept., H.T.I.

INTRODUCTION

The production of sanitary hot water for domestic use or industrial applications by means of solar energy constitutes one of the most popular and economically feasible applications of flat-plate solar collectors. It is the most viable of all low-temperature solar energy applications because the initial investment is small and the system is used throughout the year. This high use factor results in a larger load factor than any other application. As a rule of thump it can be suggested that solar water heating may be feasible anywhere, if the annual total horizontal irradiation is 1000 kwh/m^2 or more.

However, for the most appropriate and efficient utilisation of solar energy in this field it is necessary to develop and design the appropriate system, select the suitable materials and equipment and size properly the components involved.

In this presentation we shall try to highlight on the factors involved in the development and design of central solar water heating systems intended for domestic or industrial applications, and we shall prpose practical approaches in the sizing of the system components.

For this purpose, the following matters will be treated separately and in conjuction to each other:-

- —hot water demand
- —Solar water heating systems, collection and distribution circuits
- —collector tilting, arrangement, sizing
- —storage

1. HOT WATER DEMAND

It is evident that one of the most important parameters involved in the design of a hot water heating system is the hot water demand over a certain period of time. For the calculation of the daily energy demand (Q, kwh/day) necessary for the generation of sanitary hot water it is necessary to estimate the volumetric daily consunption (C, lt/day), as well as the temperatures of the cold water supply (tc, °C) available from city mains and the distribution temperature (td, °C) of water; then,

$$Q = 1.16 \times 10^{-3} \times C \times (t_d - t_c)$$

In this way the heat required to heat 50 litres of water from 10°C to 45°C is the same as the heat needed to heat 35 litres of water from 10°C to 60°C. However, in a solar installation it is quite important to distribute hot water at as much as low temperature in order to have an increased efficiency in the system. *(see collector characteristics)*

The temperature of use of hot water varies according to the application as follows:-

- —for a wash basin ..... 35°C
- —for a shower ..... 42°C
- —for a kitchen sink ..... 50°C

The average daily consumption of hot water could be evaluated according to the degree of comfort required (low, average, high)

The average daily consumption of hot water could be evaluated according to the degree of comfort required (low, average, high)

Degree of Comfort	Low	Average	High
Average daily consumption per person (lt/day per person)	30	50	75

2. HOT WATER CIRCUITS

The solar installation for the generation of sanitary hot water comprises the following principal circuits:

- — the *collection circuit* which comprises again the solar collectors, the circulator and the storage, and
- — the *distribution circuit* which comprises again the storage and in addition the auxiliary heat source and the piping distributing the hot water to the taps.

The various components are connected together and kept in operation by means of control mechanisms which will be discussed later in this subject.

The system simplified is presented diagramatically in fig. 1.

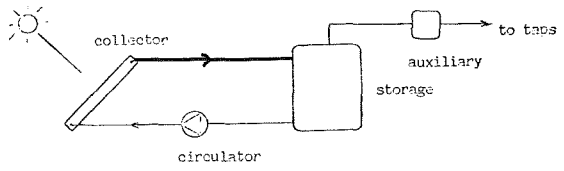

Fig. 1. Schematic diagram of a simplified solar water heating system.

For residential applications the thermosyphon solar water heater could be used efficiently, as shown in fig. 2.

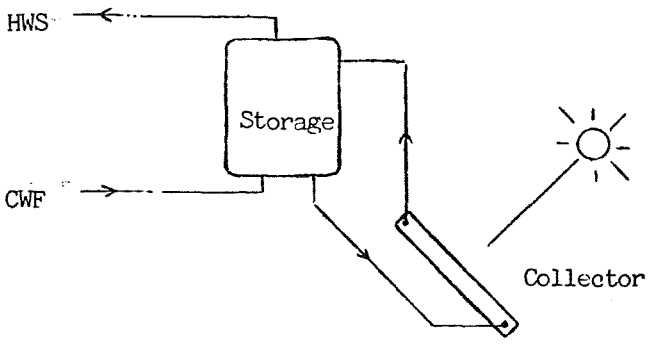

Fig. 2. Thermosyphon solar water heater.

However, this system presents some problems for application in large installations like multi-storey buildings, hotels, etc., and it is for this reason that in this presentation we shall be talking of the forced system.

2.1. COLLECTION CIRCUIT

This is the pure solar circuit in the system and its arrangement and operation will prescribe the efficiency of the system. It is very important to have such a flow in the collector that will keep the temperatures relatively low so as to have an increased collector efficiency.

For this purpose the size of the circulator should be properly decided and its operation suitably controlled.

The water flow should be such that the temperature of the colector will be kept as low as possible in order to have reduced heat losses from the collector; this means that high flow rates are advantageous. However, high volume flow rates need increased pump power consumption. Therefore, an optimum condition should be established. Experiments conducted abroad showed that a flow of about *70 lt/h per m²* of collector is about optimum.

As far as the control of operation of the collection circuit is concerned we shall distinguish between two systems, by the aid of the diagrams of figs. 3 and 4, namely:

—the intermittent pump operation (fig. 3), and
—the continuous pump operation (fig. 4)

Both systems use the defferential control which allows the collectors toheat the water of the storage only when their temperature is greater from the water temperature in the storage.

i. Intermittent pump operation

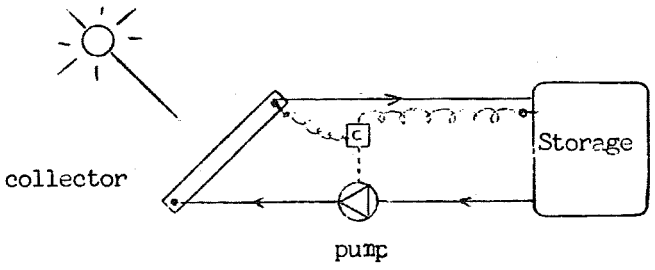

Fig. 3 Intermittent pump operation.

The advantage of this system is the simplicity; two sensors detect the temperatures in the collector and the storage and they set in operation the circulator only when there is a significant temperature difference, usually 5 to 8°C, having thus an intermittent operation of the pump. However, the positioning of the sensor in the collector creates a problem: effectively, it must take a temperature representative of the group of collectors. It is usually placed on the absorber of the last collector in contact with the liquid used.

A second problem exists in setting the system in operation in the morning or when there is a cloudy weather.

According to the volume of water contained in the piping (and which will be cold due to losses) the collector-sensor will be subjected to a series of "hot-cold" sensors and the circulator will suffer from a considerable number of "start-stop". However, for a nice day this problem will exist only twice (morning and evening), but during winter days (cloudy weather) the overall efficiency will be affected.

ii. Continuous pump operation

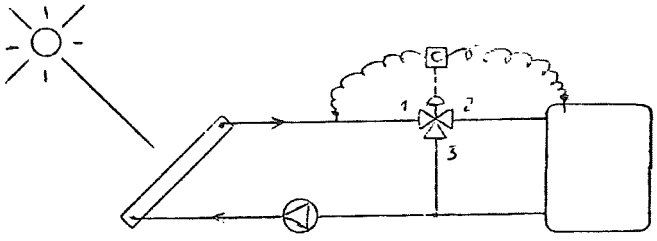

Fig. 4. Continuous pump operation

In this system, the circulator is set in operation in the morning (by means of a photocell or a time switch and the fluid circulates through the collectors. When the temperature of the water contained in the piping coming from the collectors is greater than that of the storage, the 3-way valve allows the flow to the storage, i.e. ports 1 and 2 open, port 3 closed.

The advantages of this system are evident:

a) easy to fix the sensor on the piping;
b) the sensor detects the final temperature resulted from the mixture of water from all the collectors which is thus representative of the system;
c) only one start and one stop of the circulator exist, even in cloudy days, thus the life of the circulator is increased.

2.2 DISTRIBUTION CIRCUIT

In the case of sanitary hot water, the distribution system will be dealt like in a conventional system: try to avoid long piping, have a good insulation, etc. The only difference here is the need for an auxiliary heat source which should be studied in conjuction with the storage.

There are various methods by which auxiliary heat can be supplied to the system:

—electric immersion heater in the storage tank
—hot water heat exchanger in the storage, fed by a boiler
—instantaneous electric heater at the outlet of storage.
—auxiliary heater in series with the storage, etc.

However, there is always a "best" or at least a "more advantageous" way; the best position for the auxiliary heater, which could be either of the instantaneous or the continuous type is in series with the storage and the taps.

This arrangement helps to avoid the heating of the whole quantity of water in the storage, and thus economize auxiliary energy.

This can be achieved by various methods, as illustrated in figures 5, 6 and 7.

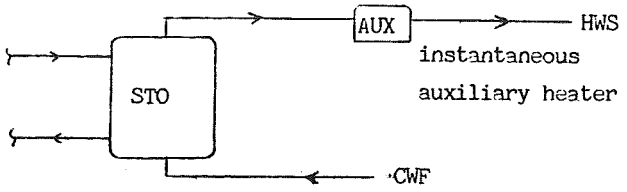

Fig. 5. Instantaneous auxiliary heating

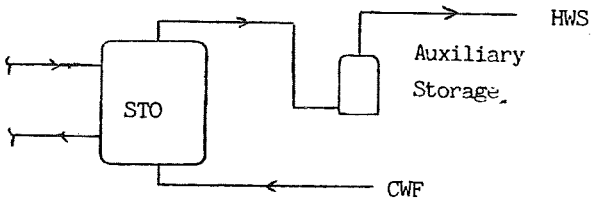

Fig. 6. Auxiliary storage in series with solar storage

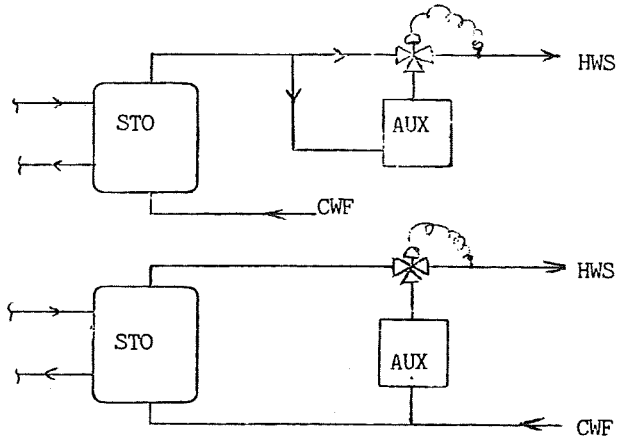

Fig. 7. Auxiliary storage in series/paralles with solar storage.

Using the systems described for the collection and distribution circuits we can develop various systems, like the one illustrated in fig. 8, which presents many advantages and is suitable for application in multistorey-buildings, hotels and for industrial applications.

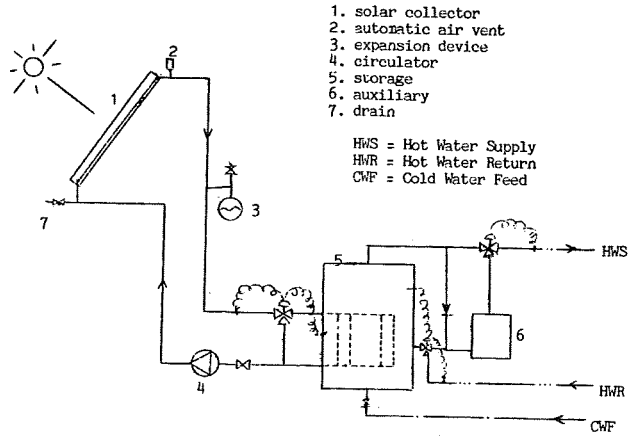

Fig. 8. Schematic diagram of a central solar water heating system

3. ARRANGEMENT OF COLLECTORS

The collectors should be arranged in such a way so as to receive the maximum solar radiation and the connection will be such that a smooth flow of water will be assured. Thus, the problem of panels connection and overshadowing are quite important and should be treated carefully.

3.1. Panels connection

The collector panels in a large installation can be arranged in three ways:

i. in parallel (fig. 9)
i. in series (fig. 10)
iii. mixed parallel/series (fig. 11)

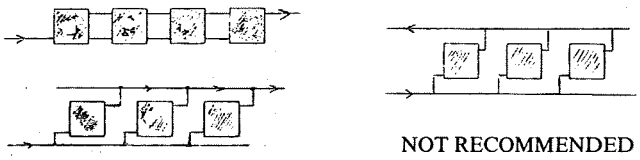

Fig. 9. Arrangement of collector panels in parallel

Fig. 10. Arrangement of collector panels in series

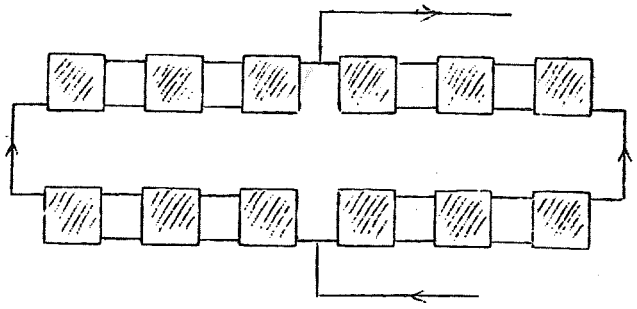

Fig. 11. Mixed arrangement (combined series - parallel)

The connection of collector panels into a "bank" is essentially a problem of plumbing which consists of finding a compromise between the pumping power (which must be as low as possible), the water flow rate (which must be as high as possible to keep the collector temperature low) and the system balancing (limitation of piping and accessories).

The series arrangement does not present any problem of balancing and assures the operation of all panels; it does not require long piping but it implies a high pumping power because the system circulator has to overcome the frictional resistance of all panels.

On the contrary, the parallel arrangement requires a low pumping power but a good balancing is needed to ensure a balanced flow of water through each panel, this requires the provision of valves together with correct pipe sizing.

The pressure drop in the collector panels must always be known for the correct sizing of the pumping system.

The pressure drop in a panel varies greatly according to the type of collector and the flow; there are panels, for example, of $2m^2$ surface area with a P.D. of 10mm w.g. and panels of $1m^2$ having a P.D. of 300mm w.g. for a water flow of 701t/h per m^2 collector. The velocity of water in the circuit should be kept around 1m/s.

In any case, the system total pressure drop should not exceed 1200mm w.g., in order to have a reasonable power consumption of the order of 200W for a water flow of about $15m^3/h$ which is enough for a solar installation having $200m^2$ of collector or even grater.

3.2. Overshadowing

The collector panels should be installed in open air and should be away from any physical obstruction which could prevent solar radiation to reach its absorbing surface. This problem becomes more important when having rows of banks of panels installed the one behind the other, where the distance between the two successive rows must be such that the one row does not overshadow the other.

This distance must be determined from the following parameters:

- — the height of the panel
- — the panel tilt angle
- — the sun altitute, which is different in summer and winter; this angle can be determined using the stereographic sun-path diagram corresponding to the place of application.

Overshadowing must be properly studied because it may reduce the performance of the solar system to an extent that it may tip the balance and render the system uneconomical. The critical time is mid-winter, when the sun is at a low altitude, thus any obstruction would create a longer shadow. Ideally, no shadow should fall on the collector between 8.00 and 16.00 hours (but at least between 9.00 and 15.00 hours).

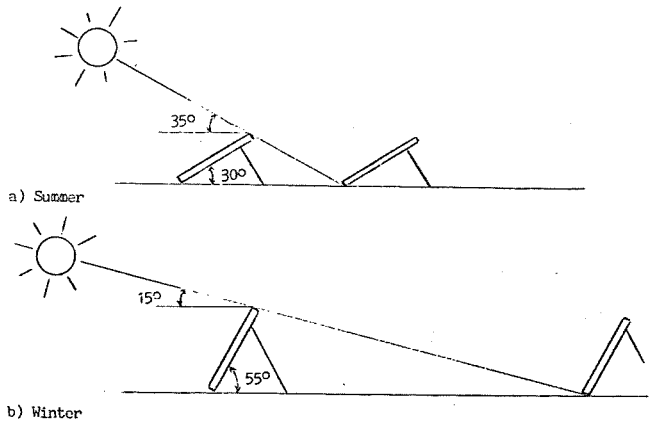

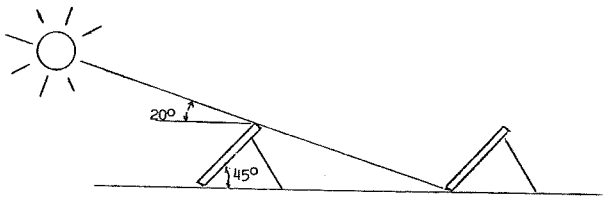

Fig. 12. Arrangement of panel-rows to avoid overshadowing (Cyprus)

3. SYSTEM SIZING

Once the system has been developed, the following questions should be faced when designing a solar water heating system:

a) For a given demand, what size of solar collector and what volume of storage should be used? What type and size of auxiliary?

b) For a given building, if the surface available to accommodate the collectors is limited, how much water could be produced and what would then be the size of the storage and auxiliary?

For the investigation of the above it is necessary to know the solar radiation at the place under consideration; this data should be taken from the nearest meteorological service but it can be calculated in the lack of the latter.

It is equally important to know the efficiency of the collector panel in order to calculate the useful energy which could be collected. The efficiency of the collector is a function of its optical characteristics (absorptivity, reflectance, transmissivity) and its overall heat loss coefficient. In its simplified form, the collector efficiency is given by the expression:

$$n = A - B\ (t_m - t_a)/I$$

where, A is a coefficient corresponding to the collector optical characteristics,

B is the overall heat loss coeffieient, t_m is the collector mean temperature, t_a is the ambient temperature, I is the solar radiation normal to the panel.

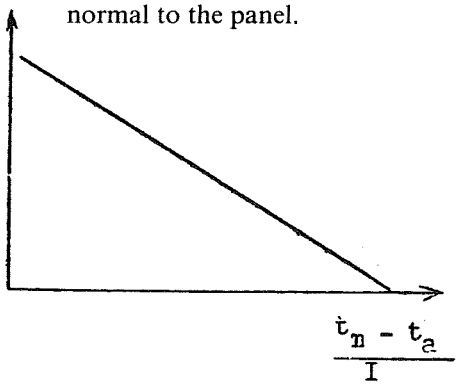

Fig. 13. Collector efficiency curve

For a usual flat-plate solar collector using single glazing and mat-black absorber, insulated with 5-8cm glasswool, the above expresion can be used with a good approximation as follows:

$$n = 0.82 - 8\ (t_m - t_a)/I$$

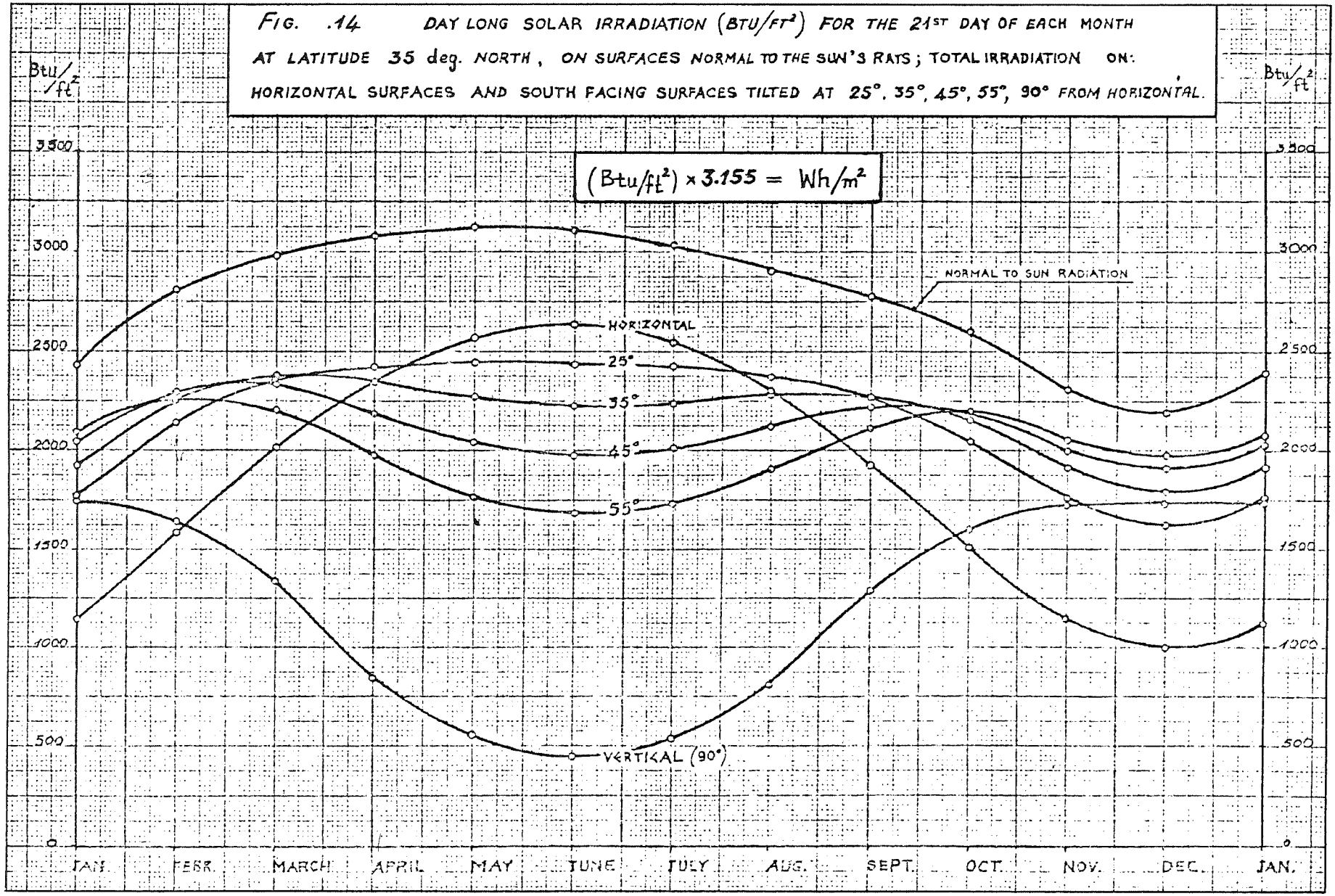
FIG. .14 DAY LONG SOLAR IRRADIATION (BTU/FT²) FOR THE 21ST DAY OF EACH MONTH AT LATITUDE 35 deg. NORTH, ON SURFACES NORMAL TO THE SUN'S RAYS; TOTAL IRRADIATION ON: HORIZONTAL SURFACES AND SOUTH FACING SURFACES TILTED AT 25°, 35°, 45°, 55°, 90° FROM HORIZONTAL.
(Btu/ft²) x 3.155 = Wh/m²
Btu/ft²
3500
3000
2500
2000
1500
1000
500
0
NORMAL TO SUN RADIATION
HORIZONTAL
25°
35°
45°
55°
VERTICAL (90°)
JAN.
FEBR.
MARCH
APRIL
MAY
JUNE
JULY
AUG.
SEPT.
OCT.
NOV.
DEC.
JAN.

3.1. Collector

The collector is the most vital component of the solar installation; its tilting angle will be an important factor for the determination of its size.

The collector should face the noon sun, i.e. south for the northern hemisphere, north for the southern hemisphere. The optimum tilt angle of the collector will be that angle at which the collector will receive the maximum solar radiation throughout the year; one way to determine this is to plot the curves of daylong solar irradiation for various tilt angles throughout the year and select the tilt angle having the maximum solar irradiation for the year. Such a graph was plotted for Cyprus and is presented in fig. 14. For Cyprus, the optimum tilt angle (on a year basis) is around 45° from the horizontal.

As far as the size of the collector is concerned, a techno-economical study should be conducted. For this purpose it is necessary to know the type of auxiliary to be used (oil, electricity, gas), the price of auxiliary energy and the cost for buying and fixing the collector, and of course the efficiency of collector.

The optimum collector size can be established by minimizing the total cost for a number of years (life-time of installation).

Knowing all the above information we can determine the optimum size of the collector needed to satisfy a certain demand, either analytically or graphically. A graphical way of optimizing the collector size is presented in fig. 15.

C=minimum overall cost

S=optimum collector size

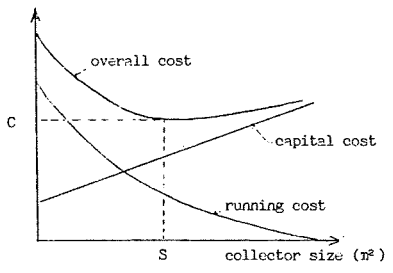

Fig. 15. Optimisation of collector size.

3.2. Storage

The energy collected by the collector is transferred in the storage tank by means of water and is kept there for use when needed. It is therefore important to keep the storage tank well insulated so as to avoid losses to the environment.

For a storage temperature of about 40°C the optimum *U-value* for the storage tank is about *0.28W/m² °C.*

There is an optimal amount of water storage per m² of collector. In a small storage volume the storage temperature will be high: thermal losses from storage will be large, and stored energy can supply heat for only a short time. The cost of large storage volumes is prohibited since the storage capacity of the system will rarely be fully used, resulting in high marginal cost of storage associated with the small load factor; in addition, storage temperature will frequently be too low to be useful. The optimal storage volume per m² of collector is independent of building location, heat demand and insolation. The optimal value ranges from *50 to 75 litres of water per m² of collector,* depending on the quality of the collector.

Knowing the quantity of hot water demand for a certain period, say on day (C, lt/day), and the average temperature of the cold water (t_c °C) it would be possible to determine the average storage temperature (t_s °C) in the tank.

$$t_s = t_c + \frac{E}{1.16 \times C}$$

Where E = daily useful solar energy collected, in Wh/day.

It is also possible to determine the theoretical solar fraction τ which is the ratio of the daily useful solar energy collected over the daily energy demand (D_d) for hot water generation.

$$\tau = \frac{E}{D_d}$$

The solar fraction τ can also be determined using the temperatures of cold water feed (t_c), storage water (t_s) and distribution water (t_d)

$$\tau = \frac{t_s - t_c}{t_d - t_c}$$

Example: C = 1,500 lt/day, S = 30m², V = 2250 litres. If we assume an average daily solar radiation of 6 kwh/m², an average collector efficiency of 30%, then

$$E = 0{,}3 \times 6 = 1.8 \text{ kwh}$$

$$\text{If } t_c = 10°C, \text{ then } t_s = 10 + \frac{1800 \times 30}{1.16 \times 1500} = 41°C$$

Assuming a distribution temperature of 50°C, then solar fraction

$$\tau = \frac{41 - 10}{50 - 10} \times 100\% = 77.5\%$$

or (other method)

$$\tau = \frac{1800 \times 30}{1500 \times 1.16 \times (50-10)} \times 100\% = 77.5\%$$

4. APPROXIMATE SIZING

It is usually necessary to carry out a preliminary design of a solar hot water heating system. For this purpose we shall introduce two auxiliary magnitudes which will interrelate the factors involved in the sizing of the system components, namely, the daily hot water demand (C) in lt/day, the collector surface area (S) in m², and the volume of storage (V) in litres of water.

These are:

i) the storage factor $F = \frac{V}{S}$, in lt/m²

and ii) the storage reserve $R = \frac{V}{C}$, in days.

Usually, R is equal to 1 or 1.5 day, and F is 50 to 75 lt/m².

Example:

If the hot water demand for a building is 1,500 lt/day and the desired storage reserve is 1.5 day, then

$$V = 1{,}500 \times 1.5 = 2{,}250 \text{ litres}$$

With F = 75 lt/m², the collector surface would be

$$S = \frac{2{,}250}{75} = 30 \text{ m}^2$$

REFERENCES

1. I.H.V.E. Guide Manual
2. Duffie & Beckram: SOLAR ENERGY THERMAL PROCESSES
3. Kreider & Kreith: SOLAR HEATING AND COOLING
4. Chateauminois, Mandneau, Roux: CALCUL D'INSTALLATION SOLAIRES A EAU
5. Chauliaguet, Baratsabal, Batellier: L'ENERGIE SOLAIRE DANS LE BATIMENT
6. S.V. Szoklay: SOLAR ENERGY AND BUILDINGS
7. Chittenden, Frankel, Harrison: RENEWABLE ENERGY SOURCES FOR DEVELOPING COUNTRIES

Without Freedom there is no progress but only mechanisation and spiritual death.
Sri-Ram

Study, learn and understand science and virtue but don't show off over it. Of course you wouldn't show off if you truly understand science and virtue.
Dion. Solomos

Don't judge things from their apparent value but from their real value.
Krisnamourti

AN INTRODUCTION TO FIBONACCI SEQUENCES

By George N. Philippou
Lecturer HTI

1. Introduction

Leonardo of Pisa, better known as Leonardo Fibonacci, was probably the greatest European mathematician of the Middle Ages. Born in Pisa, in 1175 A.D., he received his academic education from Moslem tutors in Bougie of Algeria.There he learned the Hindu-Arabic numeration system; he regognized its superiority over the clumsy Roman system which he demonstrated in his widely known book *Liber Abaci* - "Book of the Abacus".

Although Fibonacci's contributions to mathematics were valuable he is today remembered mainly because Edward Lucas, a French mathematician of the 19th century, attached his name to a sequence that arises from a simple problem proposed in his *Liber Abaci.* This is the now famous "Rabbit problem".

Suppose that a pair of adult rabbits is placed inside an enclosure to breed, in the 1st of January. Suppose that rabbits start to bear young two months after their own birth, producing one single male-female pair per month. The problem is to find the number of pairs in the enclosure after one year provided none of the rabbits die.

It is easy to see that the total number of pairs at the first of each month will be:

1, 2, 3, 5. 8,13, 21, 34, 55, 89, 144, 233, each term being the sum of the two immediately preceding terms.

Further we can observe that the sequence of breeding pairs at the first of each month is 1, 1, 2, 3, 5, 8, 13, 21, 34, 55, 89, ... which is of the same form as the previous number sequence. The basic property of such sequences is that each term is equal to the sum of the two preceding terms.

The Fibonacci Sequence is formally defined as

$$F_1 = 1, \quad F_2 = 1 \quad \text{and} \tag{1.1}$$
$$F_{n+2} = F_{n+1} + F_n, \qquad n \geq 1.$$

The terms consisting this sequence i.e.

1, 1, 2, 3, 5, 8, 13, 21, 34, 55, 89, ...

are called Fibonacci numbers.

A serious investigation of this sequence was undertaken only at the beginning of the 19th century. Edward Lucas made a deep study of what we now call "generalized Fibonacci sequence" where the first two terms could be any two natural numbers. The Definition of this sequence is:

$$H_1 = p, \quad H_2 = q \quad \text{and} \tag{1.2}$$
$$H_{n+2} = H_{n+1} + H_n, \qquad n \geq 1.$$

A specific member of this family of sequences found when p=1 and q=3 is now known as "Lucas sequence" and its terms are known as "Lucas numbers". The first few Lucas numbers are:

1, 3, 4, 7, 11, 18, 29, 57, 86, ...

The sequence of Lucas numbers is closely related and shares many common properties with the sequence of Fibonacci numbers.

A list of the first 30 Fibonacci and Lucas numbers is given below.

F_1	1	L_1	1
F_2	1	L_2	3
F_3	2	L_3	4
F_4	3	L_4	7
F_5	5	L_5	11
F_6	8	L_6	18
F_7	13	L_7	29
F_8	21	L_8	47
F_9	34	L_9	76
F_{10}	55	L_{10}	123
F_{11}	89	L_{11}	199
F_{12}	144	L_{12}	322
F_{13}	233	L_{13}	521
F_{14}	377	L_{14}	843
F_{15}	610	L_{15}	1364
F_{16}	987	L_{16}	2207
F_{17}	1597	L_{17}	3571
F_{18}	2584	L_{18}	5778
F_{19}	4181	L_{19}	9349
F_{20}	6755	L_{20}	15127
F_{21}	10946	L_{21}	24476
F_{22}	17711	L_{22}	39603
F_{23}	28657	L_{23}	64079
F_{24}	46368	L_{24}	103682
F_{26}	121393	L_{26}	271443
F_{27}	196418	L_{27}	439204
F_{28}	317811	L_{28}	710647
F_{29}	514229	L_{29}	1149851
F_{30}	832040	L_{30}	1860498

2. Fibonacci in Nature

The interest in Fibonacci number series has recently been increased to justify the publication of a journal with the tittle *The Ficonnacci Quarterly.* These numbers have a way of turning up in unexpected places such as: in golden sections, the spiral arrangement of seeds of sunflowers, multiple reflections of light rays through two face-to-face glass plates, the number of paths that can be taken by a bee crawling over hexagonal cells, in connection with the ideally simplified atoms of a quantity of hydrogen gas, with phyllotaxis, and the list goes on.

Some of those examples will be considered here.

2.1. Number of Reflections

If a beam of light is incident upon two sheets of glass plates, part of the light will be transmitted part will he absorbed and the remainder will be reflected.

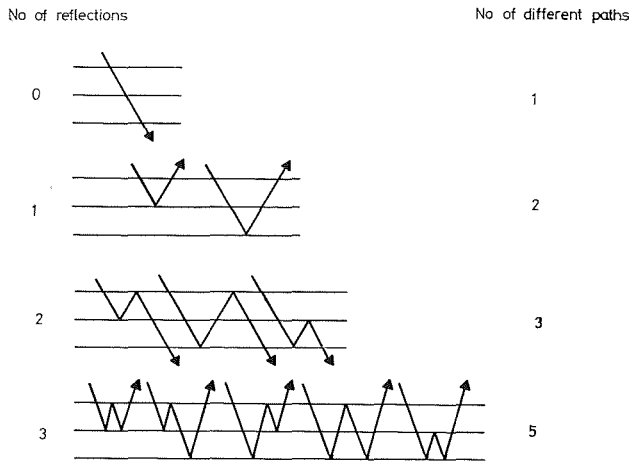

Fig. 1.

In fact there will be multiple reflections. From Fig. 1 it is easily seen that an unreflected ray goes through the plates in only one way. If the ray is reflected once there are two paths, if reflected twice 3 paths and the following table is completed.

Number of reflections	0	1	2	3	4	...	n
Number of parths	1	2	3	5	8	...	F_{n+2}

2.2. The seeds of sunflowers

It has been noticed that the seeds on the face of some varieties of sunflowers appear on spiral arrangements. One can detect two sets of logarithmic spirals one turning clockwise and the other counterclowise.

The number of spirals in the two sets tend to be consecutive Fibonaci numbers. Sunflowers of average size usually have 34 and 55 spirals, but in some cases giant sunflowers have been developed with 89 and 144 spirals respectively.

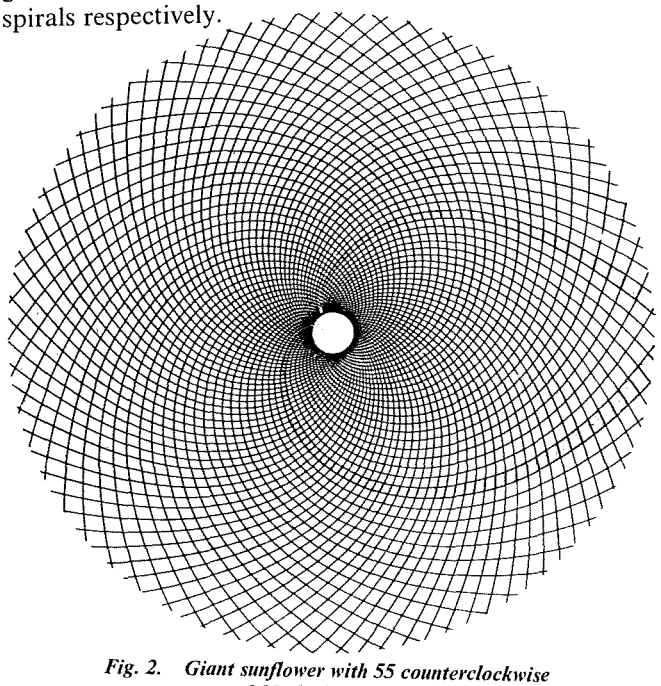

Fig. 2. Giant sunflower with 55 counterclockwise and 89 clockwise spirals

Similarly the seed-bearing scales of a pine cone grow outward is a spiral pattern from the point where it is attached to the branch. The number of spirals in the two sets tend again to be consecutive Fibonacci numbers [1].

2.3. Fibonacci and the Atom

The Fibonacci numbers reappear in connection with the ideally simplified atoms of a quantity of hydrogen gas.

Suppose that the single electron in one of the atoms gains and loses either one or two quanta of energy successively so that it occupies three energy levels say 0, 1 and 2. Assume in addition that:

a) when the gas gains radiant energy all the atoms in state 1 rise to state 2, half the atoms in state 0 rise to state 1 and half to state 2;

b) When the gas loses energy by radiation all the atoms in state 1 fall to state 0, while half of those in state 2 fall to state 1 and half to state 0.

Diagram of Possible Histories of an Atomic Electron

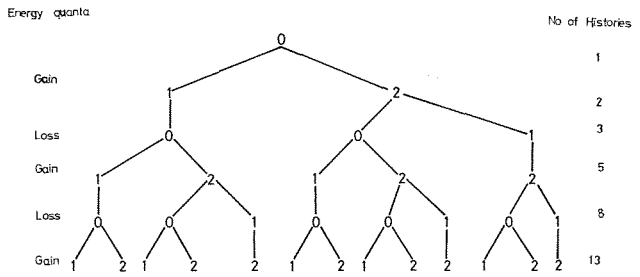

Fig. 3.

From Fig. 3 it is clear that the number of possible different histories of an electron are the numbers of the Fibonacci sequence starting from F_2. Thus after n gain or loss radiations the number of possible different histories of an electron are F_{n+2}.

Further, if we examine the proportion of atoms at each energy state we see that the fractions in each state as time passes are constantly formed of Fibonacci numbers. From the table below it is clear that the proportion of atoms at energy state 1 is

$$\frac{F_n}{F_{n+2}} = 1 - \frac{F_{n+1}}{F_{n+2}}$$

Proportion of Atoms in Each State

Energy Level	0	1	2	3	4	5	...n
0	$\frac{1}{1}$	0	$\frac{2}{3}$	0	$\frac{5}{8}$	0	...
1	0	$\frac{1}{2}$	$\frac{1}{3}$	$\frac{2}{5}$	$\frac{3}{8}$	$\frac{5}{13}$	... $\frac{F_n}{F_{n+2}}$
2	0	$\frac{1}{2}$	0	$\frac{3}{5}$	0	$\frac{8}{13}$	...

2.4. The Golden Ratio

Given a line segnent AB, then by definition the golden section is a point C such that

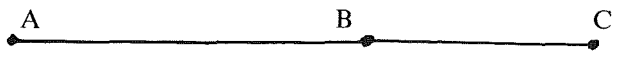

Fig. 4.

$$(2.4.1) \qquad \frac{AB}{AC} = \frac{AC}{CB}$$

and the ratio $X = \frac{AB}{AC}$ is called golden ratio.

Equation (2.4.1) can be written as

$$1 + \frac{CB}{AC} = \frac{AC}{CB} \quad \text{or} \quad 1 + \frac{1}{X} = X$$

and finally

$$(2.4.2) \quad X^2 - X - 1 = 0$$

This equation whose positive root is the golden ratio, is known as "the Fibonacci equation" because the golden ratio X is also the limit of two successive Fibonacci numbers. Indeed if we assume that

$$\lim_{n\to\infty} \frac{F_{n+1}}{F_n} = a$$

(We shall not try to prove that the limit exists here), then

$$\lim_{n\to\infty} \frac{F_{n+1}}{Fn} = \lim_{n\to\infty} \left(1 + \frac{F_{n+1}}{Fn}\right), \text{ or}$$

$$1 + \frac{1}{a} = a$$

and the latter is identical to eqn (2.4.1).

We need not emphasize the aesthetic and psychological appeal of the golden ratio known to appear often throughout classical Greek art and architecture. Another aspect to be stressed is the fact that the Fibonacci sequence, an arithmetic progression, tends to be a geometrical progression as the terms increase, the common ratio being the golden ratio a.

3. Some Properties of Fibonacci Sequences

3.1. The Binet Forms

Solving the Fibonacci equation we have the roots

$$a = \frac{1}{2}(1 + \sqrt{5}) \quad \text{and} \quad b = \frac{1}{2}(1 - \sqrt{5})$$

It is easy to prove, by mathematical induction, that

$$(3.1.1) \qquad a^{n+1} = a^n + a^{n-1} \qquad n \geqslant 0$$

Hence if we let $a^n = un$, then clearly

$$a^0, a^1, a^2, \ldots$$

is a Fibonacci sequence. The same holds for $b^0, b^1, b^2, \ldots$

The following identities are known as Binet Forms and they are very useful

$$(3.1.2) \qquad Fn = \frac{a^n - b^{n-1}}{a - b}, \quad Ln = a^n + b^n$$

To prove them we see that $F_1 = 1, F_2 = 1$ assuming the first to hold for $n = k + 1$ and $n = k$ we have

$$\frac{a^{k+2} - b^{k+2}}{a-b} = \frac{a^{k+1} - b^{k+1}}{a-b} + \frac{a^k - b^k}{a-b}$$

$$= F_{k+1} + F_k = F_{k+2}$$

and the proof is complete by mathematical induction. Many identities involving Fibonacci and Lucas numbers can be proved using the Binet Forms, e.g.

$$(3.1.3) \qquad F_{n-1} + F_{n+1} = L_n$$

$$(3.1.4) \qquad F_n^2 + F_{n+1}^2 = F_{2n+1}$$

Hint: For a proof of (1.1.3.) and (3.1.4.) note that $ab = -1$.

3.2. **The sum of the first n terms** of the generalized Fibomacci sequence is given by

$$(3.2.1) \qquad \sum_{i=1}^{n} Hi = H_{n+2} - q$$

Proof. We observe that $H_3 = H_2 + H_1$,

or $H_1 = H_3 - H_2$

Similarly $H_2 = H_4 - H_3$

$H_3 = H_5 - H_4$

.....

$Hn = H_{n+2} - H_{n+1}$

By adding together we get (3.2.1), since $H_2 = q$. For the Fibonacci sequence and the Lucas sequence the corresponding to (3.2.1) identities are respectively

$$(3.2.2) \qquad \sum_{i=1}^{n} Fi = F_{n+2} - 1$$

$$\sum_{i=1}^{n} L_i = L_{n+2} - 3$$

This identidy may be used as the basis of a pleasant calculation trick: Ask someone to put down any two

starting numbers, then add them to find the third, and write as many terms as he wishes by summing the two precedent to find the next. Then let him draw a line between any two numbers and you can give him the sum of all terms to the line. All you have to do is to substract the second term of the sequence from the second term past the line.

3.3 **The Square of any Fibonacci number differs by 1 from the product of the two numbers on each side** i.e.

(3.3.1.) $F_{n+1}\ F_{n-1} - F_n^2 = (-1)^n$

The corresponding property for Lucas numbers is

(3.3.2.) $L_{n+1}\ L_{n-1} - L_n^2 = 5(-1)^n$

3.4 **For any four consecutive Fibonacci numbers** F_{n-2}, F_{n-1}, F_n, F_{n+1}, **the following formula holds**

(3.4.1.) $F_n^2 - F_{n-1}^2 = F_{n-2}\,F_{n+1}$

The proof is easy by factorizing the difference of squares in the left-hand side.

The corresponding identidy is also true for the generalized Fibonacci sequence and consequently for the Lucas sequence.

3.5. **Divisibility.** It can be observed from the list of Fibonacci numbers that $F_3 = 2$ divides: F_3, F_6, F_9, ...; similary F_8, F_{12}, F_{16}, ... are exactly divided by $F_4 = 3$. It may be proved that F_{pn} is always divided by F_p, {p, n} cN. (For a proof see [¡] p. 37.)

3.6. It has been recently proved that with the trivial exception of 1 the only square Fibonacci number is $F_{12} = 144$ which surprizingly is the square of its subscripe.

It was also proved that 1 and 4 are the only square Lucas numbers.

This list of properties could be extended to fill a book. Interested readers may see references [**2**] [**3**] and for more advanced study the valumes of *The Fibonacci Quarterly.*

4. Fibonacci and Matrices

Let $A = \begin{bmatrix} 1 & 1 \\ 1 & 0 \end{bmatrix}$

then $A^2 = \begin{bmatrix} 1 & 1 \\ 1 & 0 \end{bmatrix}^2 = \begin{bmatrix} 2 & 1 \\ 1 & 1 \end{bmatrix} = \begin{bmatrix} F_3 & F_2 \\ F_2 & F_1 \end{bmatrix}$

and generally by mathematical induction

$$A^n = \begin{bmatrix} F_{n+1} & F_n \\ F_n & F_{n-1} \end{bmatrix}$$

For this reason A is called a matrix generator of the Fibonacci scquence.

By definition the *Characteristic equation* of the matrix A is given by

$$\det\,(A - XI) = \begin{vmatrix} 1-x & 1 \\ 1 & -x \end{vmatrix} = 0$$

which is easily reduced to the Fibonacci equation

$$x^2 - x - 1 = 0$$

Further, since $\det(A^n) = (\det A)^n = (-1)^n$ and

$$\det A^n = \begin{vmatrix} F_{n+1} & F_n \\ F_n & F_{n-1} \end{vmatrix}$$ it follows that

(4.1.1) $F_{n+1}\ F_{n-1} - F_n^2 = (-1)^n$

and this is a proof of the identidy (3.3.1).

Interested readers can prove that the characteristic equation of A^n is

(4.1.2) $X^2 - LnX + (-1)^n = 0$

and the characteristic roots are

$$\frac{L_n + \sqrt{5}\,F_n}{2} \quad \text{and} \quad \frac{L_n - \sqrt{5}\,F_n}{2}$$

Research in this field has being during the last two decades continuous and intensive. The sequence of Fibomacci numbers has been extended and related to many different branches of mathematics and science from Finite Differences, to Probability Distributions, Pascal's Triangles etc.

REFERENCES

1. HOGGAT, V.E. Jr., *Fibonacci & Lucas Numbers,* Hougton Miffin Company, Boston, 1969.
2. HUNTLEY, H.E., *The Divine Proportion,* Dover, New York, 1970.
3. MARTIN, G.,*"Mathematical Circus"*, First Vintage Book Editions New York 1981.

FAULT LEVEL CALCULATIONS AND SHORT CIRCUIT PROTECTION

By A. Kaplanis,
Lecturer HTI

Abstract

Protective devices in Electrical Installations are normally required to withstand the Instantaneous Symmetrical* Fault value currents.

This article attempts to give step by step methods for determining the symmetrical fault (short circuit), current at a given point and thus the breaking capacity of the protective device at that point;

the methods are:-

(a) The ohmic-values-method,
(b) The per-unit values method.

[The percentage values method is similar to the per-unit values method, the various relationships and inter-relationships of which will be outlined herewith].

Introduction

The question of the "breaking capacity" of protective devices offering short circuit protection was recognised both in the 14th Edition of the IEE Regulations, (see IEE Regs. A6 and B82 ii), as well as in the 15th Edition (see 13-7, 434-1 up to 434-4, 435, 436, 473-5 up to 473-8).

Judging by the contents of the above IEE Regulations it will be realised that much more emphasis is given to the subject in the 15th Edition.

The question of Fault Level Calculations and protection against short circuits is very important and should be considered carefully when designing electrical/electromechanical Installations.
[*The writer witnessed, during a test of a certain electrical installation in S.A., the blowing up, explosively, of a protective device of inadequate breaking capacity, causing considerable damage to the installation during a fault*].

It is not the intention to produce any new theory, technique or method on Fault Level Calculations, but rather to collect the various relationships of the different methods named earlier and use them, step by step, in the solution of a case-study with the hope that it will be of benefit to Graduates of HTI and other Electrical Contractors in Cyprus dealing with Fault Level Calculations for Electrical Installations.

Theory:

There are various types of Faults that may occur in a power system; these are:-

Fault of negligible Impedance, (short circuit), between:-

(i) Any phase and Earth
(ii) Any two phases and Earth
(iii) All three phases and Earth
(iv) Any two phases.
(v) All three phases.

In the case of symmetrical faults, i.e. three-phase short circuit with or without earth involvements, these may be considered in terms of one phase only.

Precise calculations of faults in modern complex power networks, with many interconnections and frequent alterations or additions, are very difficult to make and Supply Authorities cannot guarantee that a fault value specified for a given point in the network today say, will not change in six months or a year's time.

For more precise calculations A.C. analysers were used in the past. Nowdays computer programs have been developed.

However, precise calculations are not necessary and simplified methods are used which are quite satisfactory if one assumes the following:-

(a) The voltage at the generator(s) does not change
(b) Generators in parallel have their emfs in phase
(c) Transient reactances of the generators remain unchanged during the fault
(d) The fault is of zero ohms impedance.

If the above assumptions are justified and to most practical cases they are, one can proceed to use the simplified method(s) for Fault Level Calculations.

There are basically two methods in calculating the symmetrical Fault Currents in a system; these are:-

(1) The ohmic Values Method. [If different voltages are involved, the ohmic values of the various elements must be referred to one voltage].
(2) Per-Unit-Values-Method. [When using the P.U. values method it is necessary to refer the relevant quantities to the same Base Apparent Power, S_B].

Some textbooks use the Percentage Impedance Method. This method is in effect the "same" as the P.U. values since, if a transformer has a percentage impedance of say 4.75%, this is the same as 0.0475 per unit. However the various relationships of the Percentage Impedance Method will also be given herewith for comparison.
[If the percentage method is used it will be necessary to convert the percentage quantities involved to the same MVA Rating — usually 100 MVA].

Relevant Equations and relationships used in Fault-Level Calculations:-

1) ***Ohmic-Values-Method.***
Let MVA = Volts x Amps x 10^{-6}.

MVA Fault Value at a point of line Voltage E_l

$$= \sqrt{3}\, E_l \frac{E_l}{\sqrt{3}} \times \frac{1}{Z_{ol}}$$

$$= \frac{E_l^2}{Z_{ol}} \qquad (1)$$

* Symmetrical Fault = balanced Three-Phase conditions. [Electricity Authorities require, as a condition for the supply of Electricity to a consumer, that loads must be balanced in the case of T.P. supply. The maximum unbalance permitted in Cyprus should not exceed 15%.]

(where Z_{o1} is the "source impedance" at that point).

MVA Fault-Value at the same point referred to a different voltage E_2 say, will be:-

$$\text{MVA F.V.} = \frac{E_2^2}{Z_{o2}} \qquad (2)$$

Equating (1) and (2) and transposing we have

$$Z_{o2} = Z_{o1} \times \frac{E_2^2}{E_1^2} \qquad (3)$$

Thus if the ohmic value of impedance at a point is say 0.3Ω at 11KV, then the ohmic value referred to 0.415KV will be, $Z_{o2} = 0.3 \times \frac{0.415^2}{11^2} = 0.427\text{m}\Omega.$

Now $Z_o = R_o + jX_o = \sqrt{R_o^2 + X_o^2}$ Ω

When several impedances are in series then

$$Z_o = \sqrt{(\Sigma R_o)^2 + (\Sigma X_o)^2} \qquad (4)$$

assuming no mutual inductance effects. If resistances and reactances are in parallel then the resultant values of R_o and X_o may be obtained approx. by:

$$\frac{1}{R_{or}} = \frac{1}{R_{o1}} + \frac{1}{R_{o2}} + \ldots \frac{1}{R_{on}},$$

and

$$\frac{1}{X_{or}} = \frac{1}{X_{o1}} + \frac{1}{X_{o2}} + \ldots \frac{1}{X_{on}}$$

assuming no magnetic coupling.

It must be stated here however that if we consider series-parallel group of impedances using R_o and X_o values in eqn (4) an error will be introduced because of the phase difference involved.

The error nevertheless is on the safe side in calculating fault-levels; see worked example.

2) ***Per - Unit - Values - Method***

The definition of the P.U value is:

$$\text{P.U. value of a quantity} = \frac{\text{Actual value of the quantity}}{\text{Base value of that quantity}}$$

Thus the P.U. value of a voltage, $V_{pu} = \frac{V}{V_B}$

Similarly the P.U. values of resistance, reactance, Impedence, and current will be

$$R_{pu} = \frac{R}{R_B}, \quad X_{pu} = \frac{X}{X_B}, \quad Z_{pu} = \frac{Z}{Z_B}$$

and $I_{pu} = \frac{I}{I_b}$ respectively

Now a reminder of what a Base quantity is. Usually it is the nominal or rated quantity. If a transformer has a nominal or rated primary voltage of 250V and a rated secondary voltage of 1000 Volts say then V_B primary = 250V, V_B secondary = 1000V. The Base Apparent Power, $S_B = \sqrt{3}.\ V_B.\ I_B$.

$$I_B = \frac{S_B}{\sqrt{3}\ V_B} \quad \text{and} \quad Z_B \text{ perphase} = \frac{V_B}{\sqrt{3}} \times \frac{1}{I_B}$$

ie $$Z_B = \frac{V_B^2}{S_B} \qquad (5)$$

$$Z_{pu} = \frac{Z}{Z_B}$$

where Z is the actual ohmic value, $= Z_o$

$$Z_{pu} = \frac{Z_o}{Z_B} = \frac{Z_o S_B}{V_B^2} \qquad (6)$$

It is possible to convert P.U. impedances from one Base Apparrent Power S_{B1} to another, S_{B2}.

$$Z_{pu2} = Z_{pu1} \times \frac{S_{B_2}}{S_{B1}} \qquad (7)$$

$$\text{Now } I_{sc} = \frac{V}{Z_o} = \frac{V}{Z_{pu} Z_B} = \frac{V S_B}{Z_{pu} V_B^2} \qquad (8)$$

$$\begin{aligned} \text{Short Circuit Voltamperes, } S_{sc} &= V.I_{sc} \\ &= V_{p.u.} V_B I_{sc} \\ &= V_{p.u.} V_B \frac{V S_B}{Z_{pu} V_B^2} \\ &= \frac{S_B}{Z_{pu}} \qquad (9) \end{aligned}$$

(since $V.V_{pu} = V_B$)

Finally it will be remembered that provided all the P.U. values are referred to the same Base Apparrent power, then when in parallel, their resultant P.U. value is:

$$\frac{1}{Z_{p.u.r}} = \frac{1}{Z_{pu2}} + \frac{1}{Z_{pu2}} + \ldots \frac{1}{Z_{pun}} \qquad (10)$$

Percentage Impedance Method:

The various relationships will be given for com—parison although as mentioned already the Percentage method is similar to the P.U. method.

Let P.C. = Percentage:

$$\text{MVA F.V.} = \frac{\text{MVA Rating x 100}}{Z_{p.c.}} \qquad (11)$$

$$Z_{pc} = \frac{\text{MVA Rating x 100}}{\text{MVA F.V.}}$$

It is possible to refer the percentage impedance at a different MVA Rating.

$$Z_{pc} \text{ at Y MVA rating} = \frac{Y\ .\ Z_{pc} \text{ at C MVA rating}}{\text{C MVA rating}} \qquad (12)$$

Thus if a transformer has a rating of 25 MVA and percentage impedance 10% then at 100MVA rating the percentage impedance will be:

$$Z_{pc}\ (100) = \frac{100 \times 10}{25} = 40\%$$

Since MVA F.V $= \frac{E^2}{Z_o} = \frac{\text{MVA Rating x 100,}}{Z_{pc}}$ then

$$Z_o = \frac{Z_{pc}\ E^2}{\text{MVA Rating x 100}} \qquad (13)$$

or $$Z_{pc} = \frac{Z_o.\ \text{MVA Rating x 100}}{E^2} \qquad (14)$$

Having dealt with the various relationships relevant to Fault-Values one can proceed to solve an example.

Case - Study

In the power distribution network shown in Fig. 1, it is required to find the MVA F.V. at Substation SS_1 as well as at points B, P_1, P_2 and P_3.

Find also the short circuit breaking capacity and S/C P.F. at points P_2 and P_3.

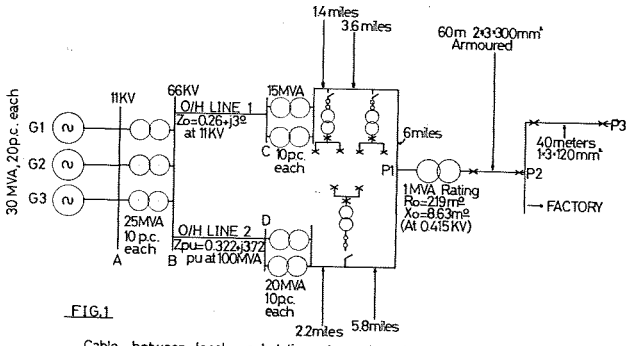

FIG.1

Cable between local substations has impedance of 0.3+j0.115pu at 100MVA

Solution:-

1 Using ohmic values method

Step No.

1. Find Zo at the Power House referred to 11KV.

From Eqn (13), $Z_o = \frac{Z_{pc}\ E^2}{\text{MVA Rating x 100}}$

Thus for *each* generator,

$$Z_o = \frac{20 \times 11^2}{30 \times 100} = 0.8067\ \Omega \text{ at 11 KV.}$$

For the three generators in parallel,

$$Z_o \text{ total} = \frac{0.8067}{3} = 0.2688\ \Omega$$

This is usually reactive ie $Z_o = 0 + j0.2688\ \Omega = X_o$

2. Find MVA F.V. at the Power house, point A.

From Eqn. (1), MVA F.V $= \frac{11^2}{0.2688} = 450$ MVA

3. Find Z_o of the three transformers in parallel, referred to 11 KV.

From Eqn 13,

Z_o for each transf $= \frac{10 \times 11^2}{25 \times 100} = 0.484\ \Omega$

Z_{ot} = Effective Impedance at 11 KV for the transf. in parallel $= \frac{0.484}{3} = 0.1613\ \Omega$ reactive

4. Find total Z_o up to the 66 KV busbar, (referred to 11 KV); this is $0.2688 + 0.1613 = 0.43\ \Omega$

5. Find MVA F.V. at point B (at the 66 KV busbar)

$$= \frac{11^2}{0.43} = 281.3$$

[$E^2 = 11^2$ since $Z_o = 0.43\Omega$ is at 11 KV].

6. Find Z_o of O|H Line 1. $Z_o = 0.26 + J3.\Omega$ given.

7. Find Z_o of each of the 15 MVA Transformers; then find effective Z_o of the two Transformers in parallel.

Z_o of each transformer $= \frac{Z_{pc}E^2}{\text{MVA Rating x 100}}$

$$= \frac{10 \times 11^2}{15 \times 100} = 0.8067\Omega$$

Z_o of two transformers in parallel $= j0.4033\Omega$

8. Find Z_o of O|H Line 2, of $Z_{pc} = 0.322 + j3.72$ p.u. at 100 MVA.

Transforming Eqn 6 we have $Z_o = \frac{Z_{pc}\ V_B^2}{S_B}$

$$Z_o = (0.322 + j3.72) \times \frac{121}{100} = 0.389 + j4.5\ \Omega$$

9. Find Z_o of the 20 MVA transformers in parallel:

$$Z_o = \frac{1}{2} \times \frac{10 \times 121}{20 \times 100} = j0.3025\ \Omega$$

10. Find Z_o of each portion of the cable in ring having $Z_{pc} = 0.3 + j0.115$ pu per mile at 100 MVA.

(a) Portion of 1.4 mile has $Z_{pu} = 0.42 + j0.161$

and $Z_o = (0.42 + j0.161)\frac{121}{100} = 0.51 + j0.1948\ \Omega$ from Eqn 6

(b) Portion 2.6 miles of same cable:-

$Z_{pu} = (0.3 + j0.115)2.6 = 0.78 + j0.3$ pu at 100MVA,

$$Z_o = Z_{pc} \times \frac{V_B^2}{100} = 0.944 + j0.363$$

(c) Portion of 6 miles:-
$Z_{pu} = (0.3 + j0.115)\ 6 = 1.8 + j0.69$ p.u.
$Z_o = 2.18 + j0.835\ \Omega$

(d) Portion of 5.8 miles gives $Z_o = 2.1 + j0.807\ \Omega$

(e) Portion of 2.2 miles gives $Z_o = 0.8 + j0.306\ \Omega$

11. Find Z_o of 1 MVA transformer referred to 11 KV.

From Eqn 3, $Z_{o11KV} = (2.19+j8.63) \times 10^{-3} \times \frac{11^2}{0.4152}$

$= 1.54 + j6.06\ \Omega$

12. Find Z_o of the 2 x 3 x 300 mm² armoured cable 60 metres long, given that $R_o = 6.0\ m\Omega + j.7.5\ m\Omega$ per 100 metres referred to 0.415 KV

$$Z_o = \frac{1}{2}[6.0+j7.5) \times 10^{-3} \times 0.6 \times \frac{11^2}{0.415^2}] = 1.27+j1.58\ \Omega$$

Note: Z_o of 60 Metres of one cable is

$$(0.6 + j7.5) \times \frac{60}{100} \times \frac{11^2}{0.415^2}$$

And Z_o of the two parallel cables = $^1/_2$ of above.

13. Find Z_o of the 40 metres of 1 x 3 x 120 mm² cable referred to 11 KV given that $Z_o = (15.3 + j7.6) \times 10^{-3}\ \Omega$ at 415 volts.

$$Z_o = (15.3+j7.6) \times 10^{-3} \times 0.4 \times \frac{11^2}{0.415^2} = 4.3+j2.136\ \Omega$$

14. Draw an Equivalent circuit of the system —as shown in Fig. 2. which is simplified into that of Fig. 3, where the equivalent impedance of the series parallel group comes to $2.664 + j1.82\ \Omega$ at 11 KV or $Z_{pu} = 1.5 + j22.2$ pu at 100 MVA.

Note:

a) The ohmic values shown are all referred to 11 KV

b) By using relevant equations for P.U. quantities the P.U. values of the various impedances have been calculated and those are also shown (in brackets) in the diagram of Fig. 2.

c) Fig. 3 is yet a more simplified diagram for impedances between the power house and Points P_1, P_2, P_3.

15. Find MVA F.V. of SSI and points P_1, P_2 and P_3, using ohmic values say.

(i) MVA F.V. at Sub-Station SS_1

In case of a fault at SS_1, (Z_3+Z_4) will be in parallel with $Z_5+Z_6+Z_7+Z_8+Z_9+Z_{10}+Z_{11}$

Let $Z_a = Z_3+Z_4 = 0.26+j3.4033\Omega$

Let $Z_b = Z_5+Z_6+....Z_{11} = 7.17+j7.36\Omega$

Resultant impedance of Za, Zb in parallel will be:

$$Z_{or\ v\ at\ SS_2} = \frac{(0.26+j3.4033)\ (7.07+j7.36)}{0.26+j3.4033+7.07+j7.36}$$

$= 0.646+j2.593\ \Omega$ at 11 KV

Z_o total up to SS_1

$= 0.646+j2.593+Z_1+Z_2 = 0.64+j3.23\Omega$
$= 3.091\ \angle 78°$

$$\text{MVA FV at } SS_1 = \frac{E^2}{Z_o} = \frac{11}{3.091} = 39 \text{ MVA FV approx}$$

(ii) Find MVA F.V. at P_1

MVA F.V. at Point P_1 using ohmic values at 11 KV.

In this case $Z_3+Z_4+Z_5+Z_4+Z_7 = Z_X$ say, are in parallel with $Z_8+Z_9+Z_{10}+Z_{11} = Z_y$ say)

$\therefore Z_X = 4+J4.85$ and $Zy = 3.29+j5.91$

$Z_{xy} = \frac{Z_X.Z_y}{Z_X+Z_y}$ comes to $1.853+j2.696\ \Omega$ approx.

Total Impedance up to point P_1

$= Z_{xy} + Z_1 + Z_2 = Zp_1$ say

$= 1.853 + j\ 3.126\ \Omega$ at 11 KV

$Z_{p1} = 3.634\ \angle 59.3°$

$$\text{MVA F.V. at } P_1 = \frac{E^2}{Z_o} = \frac{121}{3.634} = 33.3 \text{ MVA F.V. approx.}$$

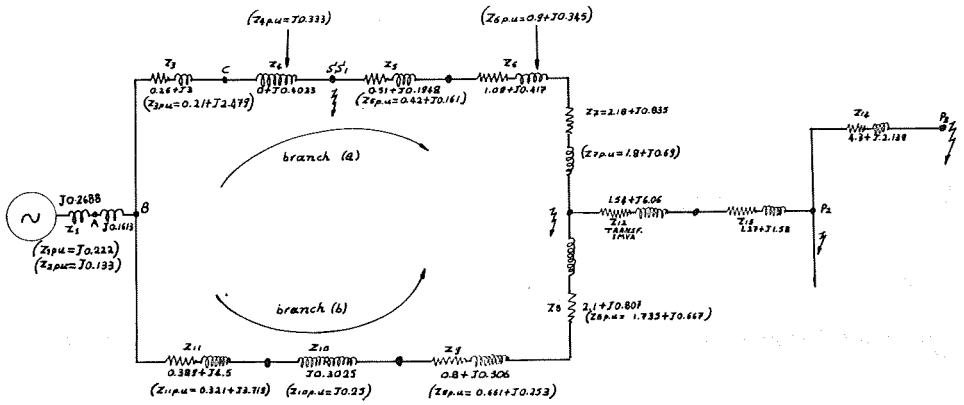

Fig. 2

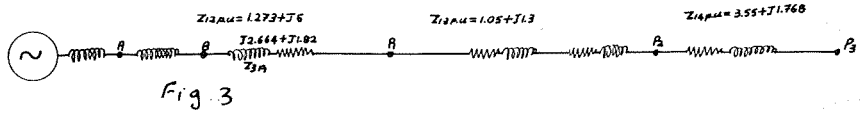

Fig. 3

(III) MVA F.V. AT P_2. Using ohmic values.

Z_o total up to $P_2 = Z_{p1} + Z_{12} + Z_{13}$

$= 4.663 + j10.766 = Z_{p2}$ say at 11KV

$= 11.732 \angle 66.6°$

MVA F.V. at $P_2 = \frac{11^2}{11.732} = 10.31$ MVA F.V.

Short circuit current at point $P_2 = \frac{\text{MVA F.V.}}{\sqrt{3}\, V_L}$

Isc at $P_2 = \frac{10.31 \times 10^6}{1.732 \times 415} = 14.35$ KA

s/c P.F. $= \frac{R_o}{Z_o} = \text{Cos } 66.6^0 = 0.397$

Thus if any protective device is used to offer protection against short circuit at point P_2 (which may be the point of entry to an Industrial Installation such as a Factory say) it must have a S/C breaking capacity in excess of 14.35 KA and S/C P.F of 0.397 in this example.

(IV) Find MVA F.V. at point P_3 (say at a sub-main C.B. or D.F.B. within the Factory complex).

Z_o at P_3 at 11 KV $= Z_{p_2} + Z_{14}$

$= 4.663 + j10.766 + 4.3 + j2.139$

$= 8.963 + j12.9$

$= 15.71 \angle 55^0$ Ω at 11 KV

MVA F.V. at $P_3 = \frac{E^2}{Z_o} = \frac{121}{15.71} = 7.7$ MVA

Isc $= \frac{\text{MVA F.V.}}{\sqrt{3}\, V_L} = \frac{7.7 \times 10^6}{1.732 \times 415} = 10.715$ KA

s/c PF $= \text{Cos } 55° = 0.573$

Thus the device to be installed at point P_3 required to offer short circuit protection, must have a breaking capacity in excess of 10.72 KA and s/c P.F of 0.573 unless IEE Reg. 434.4 regarding lower breaking capacity, applies.

(Some Switchgear manufacturers furnish information regarding R_o and X_o of their protective devices. These values have not been included. The error will be on the safe side however because slightly higher ohmic values will give slightly lower short circuit current. Without these values the s/c breaking capacities of the switchgear will be higher. In addition nomograms are published which use the ohmic values of the various elements, referred to 415V, which can be used for determining the Fault Levels at various points in a distribution system).

If the j-Notation is not preferred, use the relationship $Z_o = \sqrt{(\Sigma R_o)^2 + (\Sigma X_o)^2}$, but an error will occur due to the phase differences incurred when we have impedances in series-parallel. Fortunately the error will be on the safe side — see example.

If then it is preferred to use the above equation to find the MVA F.V. at say P_1 proceed as follows:

(1) Find ΣR_o of upper branch (a) between B and P_1 of fig. 2

$\Sigma R_{o(a)} = R_{01} + R_{02} + \ldots R_{07} = 4.04\ \Omega$ at 11KV

(2) Find ΣR_o of lower branch (b) between B and P_1 of same figure

$\Sigma R_{o\,(b)} = R_{08} + R_{09} + \ldots R_{011} = 3.289\ \Omega$ at 11KV

(3) Find resultant value:

ΣR_o resultant $= \frac{4.04 \times 3.289}{4.04 + 3.289} = 1.813\ \Omega$ at 11KV, between B & P_1

(4) Repeat for X_o's in series - parallel:

Σx_o of upper branch (a) $= X_{01} + X_{02} + \ldots X_{07}$
$= 4.85\ \Omega$ at 11KV

Σx_o of lower branch (b) $= X_{08} + X_{09} + \ldots X_{011}$
$= 5.91\ \Omega$ at 11KV

Resultant ΣX_o between B-P_1 $= \frac{4.85 \times 5.91}{4.85 + 5.91} = 2.66\Omega$

Referring to the equivalent series circuit of fig. 3 the total impedance from source to point P_1 will be:

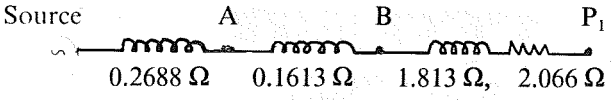

Thus up to point P_1, $\Sigma R_o = 1.813$, $\Sigma X_o = 3.09\ \Omega$

(5) Find Z_o from source upto point P_1,

$Z_{o_{A\text{-}p_1}} = \sqrt{(\Sigma R_o)^2 + (\Sigma X_o)^2} = 3.6\ \Omega$

(6) Find M.V.A. F.V. at point P_1,

MVA F.V. $= \frac{E^2}{Z_o} = \frac{11^2}{3.6} = 33.61$ MVA F.V.

There is a difference (an error) of 0.31 MVA F.V. on the safe side.

[The above equation $\sqrt{(\Sigma R_o)^2 + (\Sigma X_o)^2}$ can be used with no error for resistances R_o and reactances X_o in series, such as from P_1 to P_3 say, if the MVA F.V. at P_1 was known or specified].

If the P.U. values are preferred the relevant relationships given, equations (4) to (9) should be applied.

To find MVA F.V. say at P_1 using the P.U. values, reference to a base apparent power $S_B = 100$ MVA Rating, then:

(1) Let $Z_{x\,pu} = Z_{3pu} + Z_{4pu} + Z_{5pu} + Z_{6pu} + Z_{7pu}$
$= 3.33 + j4_{pu}$

(2) Let $Z_{y\,pu} = Z_{8pu} + Z_{9pu} + Z_{10pu} + Z_{11pu}$
$= 2.71 + j4.9$

(3) Resultant per unit values of Zx pu in parallel with $Z_{y\,pu}$, will be

(4) $Z_{xy\,pu} = \frac{Z_{x\,pu} \times Z_{y\,pu}}{Z_{x\,pu} + Z_{y\,pu}} = \frac{(3.33 + j4)(2.71 + j409)}{6.04 + j8.9}$

$= 1.546 + j2.233$ pu

(5) Z_{pu} total up to $P_1 = Z_{xy\,pu} + Z_{1pu} + Z_{2pu}$
$= 1.546 + j2.62$

Z_{pu} up to $P_1 = 3 \angle 59.5^0$ pu approx.

(6) MVA F.V. $= \frac{S_B}{Z_{pu}} = \frac{100}{3} = 33.33$ MVA F.V.

as in the ohmic-values-method using J-notation.

Conclusion:

The MVA F.V. and symmetrical short circuit Fault currents may be determined using any of the above methods or from nomograms supplied by switchgear manufacturers.

(*Note:* Back-up protection can be used if the short circuit breaking capacity of the switchgear at a given point is of lower breaking capacity, provided the conditions given in IEE Reg. 434-4 are met).

REFERENCES:

(1) IEE Wiring Regulations 14th and 15th Editions.

(2) Standard Handbook for Electrical Engineers by D.E.Fink and W. Beatly.

(3) Higher Electrical Engineering by Shepherd, Morton & Spence.

(4) The Calculation of three Phase Short Circuit Fault Values and the determination of reator sizes. A Reyrolle & Co.

(5) An indroduction to Electric Power Systems by J.A. Harrisson.

(6) Technical Publications by Klockner & Müller, Crabtree, Fereral Electric. etc.

SYMMETRICAL COMPONENTS AND UNBALANCED FAULT CALCULATIONS FOR THREE PHASE NETWORKS

By A. L. Theophanous,
Engineer, Electricity Authority of Cyprus

ABSTRACT

In this article the analysis of a power system under fault conditions is discussed. Short-circuit studies determine the behaviour of the system and provide currents and voltages which are produced in the network after short-circuits.

Fault analysis is a prerequisite step during the process of power system design. Correct design depends on a good understanding of the system behaviour for the complete range of possible system conditions.

An outline of the theory necessary for analysing unbalanced faults is presented, resulting in simplified formulae for determining the magnitude and phase of unbalanced fault currents and voltages.

1.0. INTRODUCTION

During normal balanced operation the power system is treated in terms of a single phase equivalent since the magnitudes of currents and voltages are the same in all three phases. This symmetry, however, is disturbed when a fault occurs, resulting in unbalanced currents and voltages appearing in the network. An exception to this is, of course, the three-phase symmetrical fault, which produces balanced fault currents and voltages. Unbalanced conditions are caused by the short-circuit of any one or two phases to earth or two phases between them. Open-circuited phases will also result in disturbing the network symmetry.

The determination of fault currents and voltages is particularly useful for the following reasons:

(a) The determination of the required short-circuit ratings of power system plant.
(b) The determination of the breaking capacity of planned switchgear and fusegear.
(c) The design and application of protection equipment.
(d) The investigation of unsatisfactory performance of the power system or of power system plant.

Fault analysis of simple power systems is particularly straight forward and requires no complex methods, even for determining unbalanced conditions. The calculation, however, becomes more involved as the interconnection of the power system increases, deviating from the simple radial feeding. It reaches a point when the analysis is only possible if the symmetrical components of the phase currents and voltages are used and various network reduction steps are employed. For very large High Voltage networks, the method becomes cumbersome, and for the past three decades analogue and digital computers are extensively used by Supply Authorities for establishing a detailed system behaviour under all possible fault conditions.

2.0. SIMPLE L.V. FAULT CALCULATIONS

2.1. Introduction

L. V. Systems are characterised by the simple, unidirectional flow of power from the Supply Authority's transformer to the load. This radial feeding allows a simplification of the formulae normally used for fault calculations, symmetrical or unbalanced, without the need to go into the application of the method of symmetrical component analysis, which normally complicates the procedure.

E_R = Red phase-to-neutral voltage supply, referred to the transformer's secondary side when using ohmic values = E.

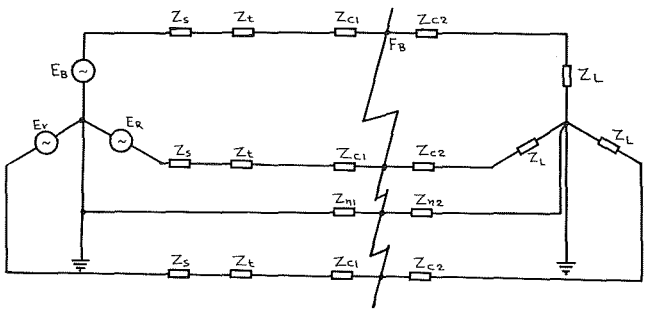

Fig. 2.1. Depicts a typical L.V. radial feeder, with the Supply Authority's system represented as a constant voltage source behind an impedance Z_s and the 11/0.415kV transformer.

E_Y = Yellow phase-to-neutral voltage supply = $E_R \angle 240°$.

E_B = Blue phase-to-neutral voltage supply = $E_R \angle 120°$.

Z_s = Supply Authority's Source Impedance per phase. For a maximum 250 MVA fault level at 11kV, Z_s is j0.4840 Primary Ohms or j0.6889 Secondary mOhms per phase.

Z_t = Impedance of the 11/0.415 kV transformer of the Supply Authority. The sizes of three-phase transformers normally range from 25kVA to 1MVA. A typical impedance for a 315kVA ground mounted transformer is (1.5 + 4.5) % on its own base.

Z_c = Impedance per phase of the Supply Authority's plus consumer's phase conductors. Subscripts 1 and 2 indicate the conductor impedance behind and in front respectively of an assumed fault.
The phase conductor may be composed of any of the following parts: transformer tails, part of the Supply Authority's LV overhead or underground network, aerial and lead-in service, consumer's network.

Z_n = Neutral conductor Impedance in Ohms. Subscripts 1 and 2 indicate the conductor impedance behind and in front respectively of an assumed fault.

Z_e = Earth Impedance. It includes the resistance at the points of earthing the neutral star or conductor, which normally is between 0.4 - 0.8 Ohms.

Z_L = Load Impedance in Ohms per phase.

F = Fault point.

Fig. 2.1. The representation of a typical three-phase L.V. System.

2.2. Three-Phase Fault

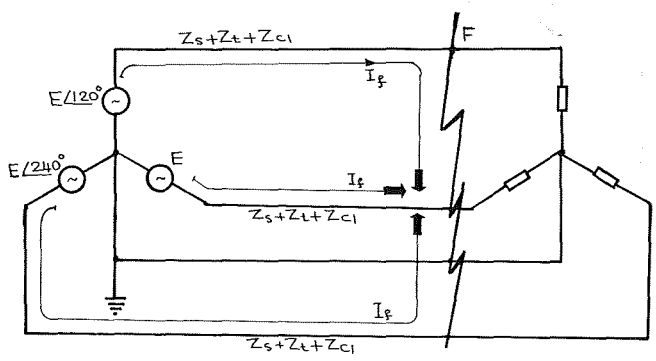

Fig. 2.2. Three-phase to earth fault

$$I_f = \frac{E}{(Z_s + Z_t + Z_{cl})} \text{ Amp.} \qquad (2.1)$$

The parameters are as defined in Section 2.1, Fig. 2.1. A three-phase fault involving the neutral conductor is assumed at F. The same relationship holds even if the neutral conductor and/or the earth are not involved.

2.3. Single-Phase to Neutral Short-Circuit

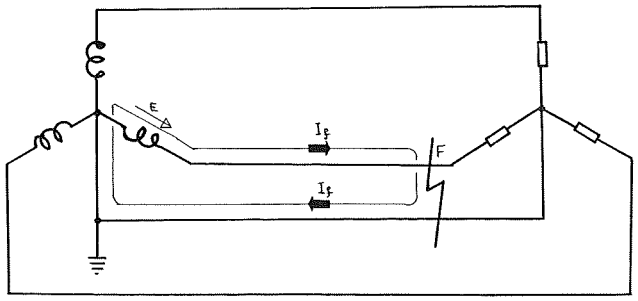

Fig 2.3

If the Source Impedance is neglected, the calculation of the fault current in that case becomes a simple application of Ohms' law. This assumption is valid in most cases, for which the 11kV fault level is above 100MVA and the Supply Authority's transformer does not exceed the 500 kVA size, conditions which are valid in the large majority of applications. In general, it may be said that, the Source Impedance may be neglected when it is much smaller than the sum of the remaining impedances to the fault point.

$$I_f = \frac{E}{(Z_t + Z_{cl} + Z_{nl})} \qquad (2.2)$$

Where E is the 11/0.415kV transformer pre-fault phase to neutral secondary voltage, and the denominator impedances are as defined in Section 2.1, Fig. 2.1.

2.4. Single-Phase to Earth Short-Circuit

By applying similar reasoning as in Section 2.3 the fault current is calculated:

$$I_f = \frac{E}{(Z_t + Z_{cl} + Z_{el})} \qquad (2.3)$$

All parameters have been previously defined.

2.5. Single-Phase to Neutral to Earth Short-Circuit

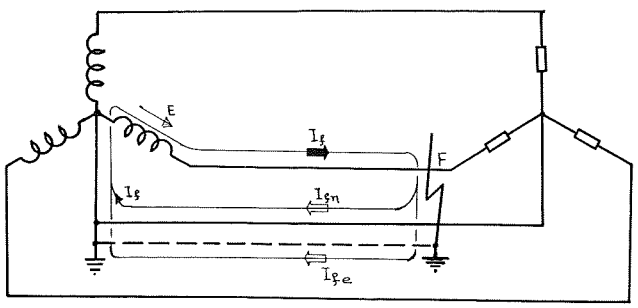

Fig. 2.4 Single-Phase to Earth Short-Circuit

The assumptions remain the same in this case as given in Sections 2.2 and 2.3. The impedance opposing the fault current I_f through the faulted phase is the phase conductor/transformer impedance in series with a parallel combination of the neutral conductor and earth impedances,

i.e. $(Z_t + Z_{cl} + \frac{Z_{nl} Z_{el}}{Z_{nl} + Z_{el}})$.

$$I_f = \frac{E}{(Z_t + Z_{cl} + \frac{Z_{nl} Z_{el}}{Z_{nl} + Z_{el}})} \qquad (2.4)$$

2.6. Phase to Phase Short-Circuit

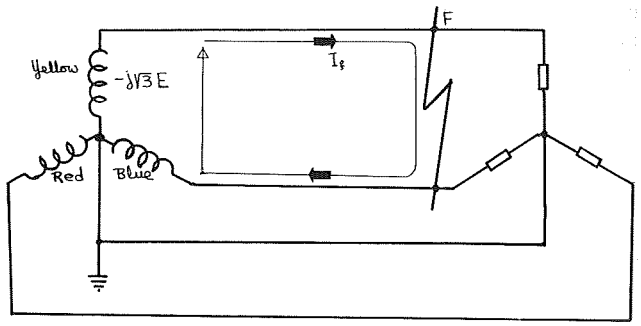

Fig. 2.5. Phase to phase short circuit

The fault current in the case of a phase to phase fault is driven by a line voltage (between two phases) and it is opposed by the sum of the phase conductor impedances to the point of the fault.

$$I_f = \frac{-j\sqrt{3}\,E}{2(Z_t + Z_{cl})} \qquad (2.5)$$

Parameters and assumptions are as described in previous Sections.

The case of phase to phase to earth fault is complicated and it is left for analysis in Section 5.0, using symmetrical components.

3.0 SYMMETRICAL COMPONENT ANALYSIS OF A THREE—PHASE NETWORK

By applying the principle of superposition, any asymmetrical multi-phase vector configuration can be analysed into vectors belonging to as many symmetrical systems as there are phases. In this way, an asymmetrical three-phase vector configuration can be split up in three symmetrical systems, known as positive, negative and zero sequence. The vectors may either represent current or voltage in an electrical system.

(a) Positive Sequence Component: It consists of three vectors equal in magnitude, displaced from each other by 120° and having the same phase sequence as the balance system i.e. Red, Yellow, Blue, clockwise, rotating in an anti-clockwise sense (Subscript 1 i.e. I_1, or V_1).

(b) Negative Sequence Component: It consists of three vectors equal in magnitude, displaced from each other by 120° and having opposite phase sequence to the balanced system i.e. Red, Blue, Yellow, clockwise, also rotating in an anti-clockwise sense (Subscript 2, i.e. I_2 or V_2).

(c) Zero Sequence Component: It consists of three vectors equal in magnitude, in phase with each other and rotating in an anti-clockwise direction (Subscript O, i.e. I_o or V_o).

For the mathematical analysis of any unbalanced three-phase set of vectors, the following relationships can be used, taking as reference vector the red phase:—

$$I_1 = {}^1/_3(I_R + aI_Y + a^2I_B) \qquad V_1 = {}^1/_3(V_R + aV_Y + a^2V_B)$$

$$I_2 = {}^1/_3(I_R + a^2I_Y + aI_B) \qquad V_2 = {}^1/_3(V_R + a^2V_Y + aV_B) \qquad (3.1)$$

$$I_o = {}^1/_3(I_R + I_Y + I_B) \qquad V_o = {}^1/_3(V_R + V_Y + V_B)$$

$$I_R = I_1 + I_2 + I_o \qquad V_R = V_1 + V_2 + V_o$$

$$I_Y = a^2 I_1 + a I_2 + I_o \qquad V_Y = a^2 V_1 + a V_2 + V_o \quad (3.2)$$

$$I_B = a I_1 + a^2 I_2 + I_o \qquad V_B = a V_1 + a^2 V_2 + V_o$$

Where 'a' is the vector operator $e^{j120°} (= -\frac{1}{2} + j\frac{\sqrt{3}}{2})$, which rotates the vector on which it operates by 120° in the anti-clockwise direction.

Subscripts: R = Red phase, Y = Yellow phase, B = Blue phase,
1 = Positive sequence, 2 = Negative sequence,
o = Zero sequence.

Any complicated three-phase network can be represented by a single line diagram. Such a network may be reduced to a single source in series with an equivalent impedance by applying Thévenin's theorem. The driving voltage is the e.m.f. of the source, expressed in terms of a phase-to-neutral voltage E. It is convenient to demonstrate and analyse the system by reducing the network to an equivalent as described above. This, however, does not preclude the possibility of carrying out the calculations with the actual system or an equivalent after a small number of star-delta transformations.

When an unbalanced fault occurs, the phase impedances are no longer identical. The method of symmetrical components permits the use of three balanced networks composed of the same branches as the original one, but with distinct parameters.

Any network, therefore, can be considered as composed by three distinct networks, a positive sequence, a negative sequence and a zero sequence network which are connected at the point of the fault according to the type of fault and as described below. The only sequence network with a driving voltage is the positive sequence one.

All power system equipment are characterised by parameters reflecting all three component networks.

The positive sequence parameters are those used for analysing balanced conditions.

For rotating plant, the negative sequence parameters are different to the positive sequence parameters.

The zero sequence parameters are the most difficult to accurately specify and the winding connection of transformers plays a significant part in the continuation of the zero sequence network.

These networks are demonstrated in Fig. 3.1 for a simple equivalent system.

The representation and impedance values of power system plant are described in detail in Section 4.0.

Fig. 3.1. demonstrates the method for connecting the sequence networks at the point of fault and after reducing the power system network to the Thévenin's equivalent.

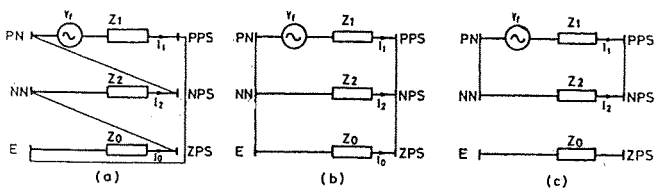

(a) Single-phase-to-earth fault (b) Phase-phase-to-earth fault (c) Phase-phase fault.

Fig. 3.1 Sequence network connections for various types of faults.

Normally, it is not sufficient to calculate the fault conditions at the fault point but a current and voltage distribution in a system due to a fault is required. After the calculation of the three sequence network overall conditions, branch currents and voltages for each sequence network may be evaluated. The sequence components may then be combined for each branch to provide the phase currents and voltages.

A simple example demonstrating this procedure is given in Section 6.0, the results of which are summarised in Fig. 6.1.

An important factor which must be taken into consideration when calculating branch currents and voltages resulting from unbalanced faults is the phase-shift caused by Y - Δ transformers. For the purpose of calculating the sequence components the phase-shifts are neglected.

The phase shifts must be taken however into consideration prior to converting the sequence to phase vectors bearing in mind that a Dyll transformer rotates the positive sequence vectors of the Y-side by -30° as for balanced conditions, and the negative sequence by 30°. The zero sequence vectors are not present.

In conclusion, the steps followed for the calculation of fault currents/voltages and fault current distribution in parts of the network are briefly given below:

1. Establish the sequence networks, either by reducing the single line diagram to a source in series with the equivalent impedance as viewed from the point of the fault, or by examining the complete/partly reduced network.
2. Connect the three networks according to the type of short-circuit as shown in Fig. 3.1, at the point of the fault.
3. Calculate the sequence currents/voltages by the straightforward application of Kirchhoff's and Ohm's laws.
4. Transfer the sequence quantities into phase quantities by using the relationships (3.2). Care must be taken when considering fault current distribution behind delta-star transformers to take into account the resulting phase-shift.

4.0 POWER SYSTEM REPRESENTATION

4.1 Introduction

The first steps towards the solution of any power system problem are the derivation of a suitable model and the selection of appropriate parameters for each of the elements of the model. The complexity of the model and the choice of the parameters will depend on the application.

4.2 Synchronous Generator Representation

The generator is represented as a constant voltage behind the machine reactance, transient or subtransient. These reactances are variations of the positive sequence reactance, whereas the negative and zero sequence reactances have a unique value. All machine impedances can in general be regarded as pure inductive reactances. The negative sequence impedance is of roughly the same value as the positive-sequence subtransient reactance. The zero sequence reactance tends to vary from one machine to another but in general it is less than the negative sequence reactance.

The flow of earth fault currents through the generator windings will greatly depend on the earthing of the star point of the generator. Normally generators are high resistance earthed. A very convenient form of this type of earthing is through a distribution transformer. In this case, the selected value of the secondary resistor is such, as to counter-act capacitive surges.

The choice between the transient or subtransient reactance of the machine will depend on the requirements of the application. It should be born in mind that the subtransient short-circuit time-constant is in the region of 0.02 - 0.05 secs, whilst the transient is about 0.75 secs for a 60MW turbine generator; (the transient short-circuit time-constant reduces with the size of the set). In particular, when a fault study is made for *circuit-breaker rating* determination, the values of fault current are distinguished in:

1. *Momentary:* The value of the short-circuit current occuring in the 1st cycle (0.02 secs) after fault incidence.
2. *Interrupting:* The value of short-circuit current at breaker contact parting time, which occurs 3 - 8 cycles (0.06 - 0.16 secs) after fault incidence; (what is normally termed as *breaking capacity* of the circuit-breaker).

To determine momentary fault currents it is required to use the machine subtransient (x_d^{11}) reactance, while interrupting current calculations make use of transient (x_d^{1}) values. This is verified by considering the elapsing time of transient and subtransient currents.

The transient reactance must be used for *relay setting* purposes.

4.3 Overhead Lines and Cables

The phase-sequence circuits for an overhead line or underground cable are in general represented by the nomical π-equivalent circuit.

The value of the zero sequence impedance depends on the medium of the return path for the zero-sequence currents (i.e. the body of the earth and the earth wires or cable sheaths). This impedance is usually two-to-three times greater than the positive sequence impedance.

The values of these parameters are dependent on the conductor size and type, tower configuration for overhead lines, cable core formation and other less significant factors.

4.4 Transformer Representation

The positive sequence circuits of transformers for fault study purposes neglect the iron losses and include basically the leakage reactance and in some occasions the copper resistance. By far the most convenient units to adopt for the transformer reactance, as well as the rest of the network, is in the per unit system. The definition of base voltages for the various voltage levels of the power system is significantly influenced by the transformer nominal voltage ratios.

The negative sequence circuits of transformers are, of course, identical to the positive equivalent.

The zero sequence circuit, however, presents difficulties regarding a uniform representation, which depend on the winding connection and the method of earthing. Fig. 4.1 depicts the equivalent circuits of commonly used transformers.

The zero sequence impedance value is, in general, considered to be equal to the positive sequence one. This is not, strictly speaking, correct for single bank three phase transformers. The difference is, however, small and in general it is ignored.

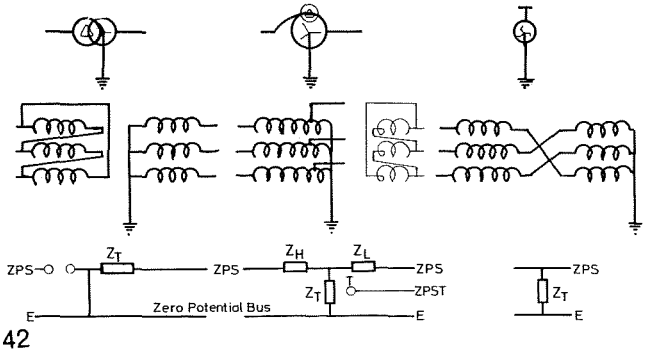

5.0 L.V. FAULT CALCULATIONS USING THE SYMMETRICAL COMPONENT ANALYSIS

5.1 Introduction

When the complexity of the network is beyond the simple radial system analysed by inspection in Section 2.0, then it becomes impossible to determine fault currents and voltages due to unbalanced faults, without using the symmetrical component transformation.

In this Section fault currents will be calculated using the method of symmetrical components and the simple system of Fig. 2.1. The parameters are the same as those used in Section 2.1, with the exception of Z_s which is not now neglected.

A simple system was preferred for two reasons:

(a) Such a system is the one most commonly met in L.V. applications.

(b) It is easier to demonstrate the rather complex symmetrical component analysis. A high voltage transmission/ distribution system is examined in Section 6.0.

5.2 Single-Phase to Neutral Short-Circuit

Figures 2.1 and 2.3 refer. A Red phase to Neutral fault is considered. The way of connecting the three symmetrical component networks in shown in Fig. 3.1(a). It may be observed that for a single phase to neutral (and/or earth) fault the three sequence currents are equal and the phase fault current is equal to their sum, i.e. $I_1 = I_2 = I_o$, $I_f = I_R = 3I_1$. These may be verified by considering relationships (3.1.) and substituting $I_Y = I_B = 0$, $V_R = V_n$.

$$Z_{clo} \approx Z_{cl} + 3Z_{nl}$$

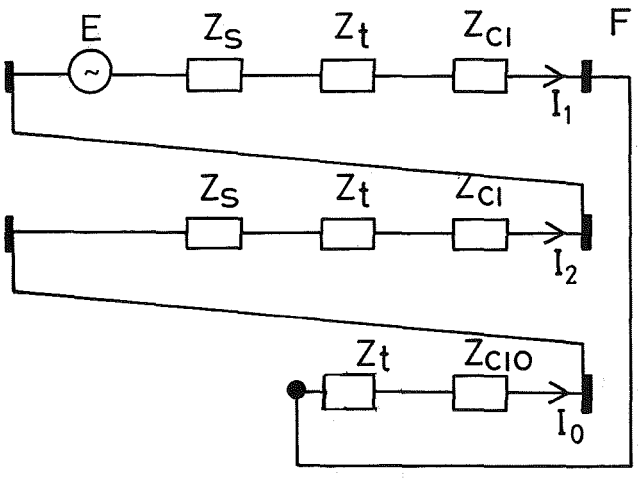

Fig. 5.1 Phase sequence network for a single-phase to neutral short-circuit.

$$I_1 = E/(2Z_s + 3Z_t + 2Z_{cl} + Z_{clo})$$
$$= E/(2Z_s + 3Z_t + 3Z_{cl} + 3Z_{nl})$$
$$I_f = E/(^2/_3 Z_s + (Z_t + Z_{cl} + Z_{nl})) \qquad (5.1)$$

By comparing equations (5.1) and (2.2), it is observed that they would be identical if $Z_s = 0$ in (5.1).

5.3 Phase to Phase Short-Circuit

Figures 2.1 and 2.5 refer.

The way of connecting the three symmetrical component networks is shown in Fig. 3.1(c). It may be observed that for a phase to phase short-circuit, $I_2 = -I_1$, $I_o = 0$, $V_1 = V_2$, $I_f = I_Y = -j\sqrt{3}I_1$. These may be verified by considering relationships (3.1), (3.2) and substituting $I_R = 0$, I_B, $= -I_Y$, $V_B = V_Y$, for a Yellow-Blue phase short-circuit.

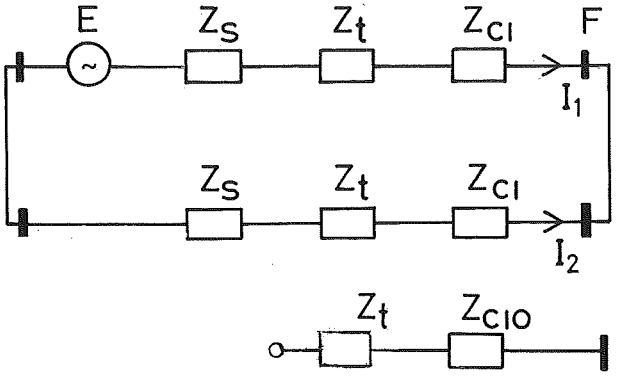

Fig. 5.2 Phase sequence network for a phase-phase short-circuit.

$$I_1 = E/2(Z_s + Z_t + Z_{cl}) \quad \text{and}$$

$$I_f = I_Y = \frac{-j\sqrt{3}E}{(Z_s + Z_t + Z_{cl})\,2} \qquad (5.2)$$

By comparing equations (5.2) and (2.5), it is observed that they would be identical if $Z_s = 0$ in (5.2).

5.4 Phase to Phase to Neutral to Earth Short-Circuit

Figure 2.1 refers. A Yellow-Blue-Neutral-Earth short-circuit is considered. The way of connecting the three symmetrical component networks is shown in Fig. 3.1(b). It may be observed that for this type of fault $I_1 + I_2 + I_o = 0$, $V_1 = V_2 = V_o$, $V_R = 3V_1$. They may be verified by considering relationships (3.1), (3.2) and substituting $I_R = 0$, $V_B = V_Y = 0$.

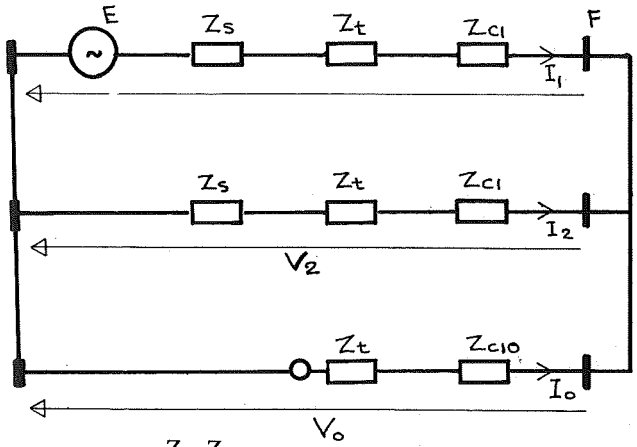

$$Z_{c10} \approx Z_{cl} + 3.\frac{Z_{nl}\,Z_{el}}{Z_{nl} + Z_{el}}$$

Fig. 5.3 Phase sequence network for a phase-phase-neutral-earth short-circuit

$V_1 = E - (Z_s + Z_t + Z_{cl})I_1$ or $I_1 = (E - V_1)/(Z_s + Z_t + Z_{cl})$

$V_2 = -(Z_s + Z_t + Z_{cl})I_2$ or $I_2 = -V_2/(Z_s + Z_t + Z_{cl})$

$V_0 = -(Z_t + Z_{c10})I_0$ or $I_0 = -V_0/(Z_t + Z_{c10})$

$I_R = 0 = I_1 + I_2 + I_0$ or

$(E - V_1)/(Z_s + Z_t + Z_{cl}) - V_1/(Z_s + Z_t + Z_{cl}) - V_1/(Z_t + Z_{c10}) = 0$ or

$V_R = 3(Z_t + Z_{c10})E/(2Z_{c10} + Z_s + 3Z_t + Z_{cl})$. Therefore

$I_1 = (2Z_t + Z_{c10} + Z_s + Z_{cl})E/((3Z_t + 2Z_{c10} + Z_s + Z_{c_l})(Z_s + Z_t + Z_{cl}))$

$I_2 = -(Z_t + Z_{c10})E/((3Z_t + 2Z_{c10} + Z_s + Z_{cl})(Z_s + Z_t + Z_{cl}))$

$I_0 = -(Z_s + Z_t + Z_{c10})E/((3Z_t + 2Z_{c10} + Z_s + Z_{cl})(Z_t + Z_{c10}))$

The fault current through the Yellow phase is

$I_f = I_Y = a^2I_1 + aI_2 + I_0 =$ (see equation (3.2))

$$= \frac{E((a^2(2Z_t + Z_{c10} + Z_s + Z_{cl}) - a(Z_t + Z_{c10}))/(Z_s + Z_t + Z_{cl}) - 1}{(2Z_{c10} + 3Z_t + Z_s + Z_{cl})} \text{ or}$$

$$I_f = \frac{j\sqrt{3}(a(Z_s + Z_t + Z_{cl}) - (Z_t + Z_{c10}))}{(Z_s + Z_t + Z_{cl})(2Z_{c10} + 3Z_t + Z_s + Z_{cl})}$$

$I_f^1 = I_B = aI_1 + a^2I_2 + I_0$

$$= \frac{j\sqrt{3}((Z_t + Z_{c_{10}} - a^2(Z_s + Z_t + Z_{cl}))}{(Z_s + Z_t + Z_{cl})(2Z_{c10} + 3Z_t + Z_s + Z_{cl})}$$

Substituting for Z_{c10} the above relationship becomes,

$$I_f = \frac{j\sqrt{E(a(Z_s + Z_t + Z_{cl}) - (Z_t + Z_{cl} + \frac{3Z_{nl}\,Z_{el}}{Z_{nl} + Z_{el}}))}}{(Z_s + Z_t + Z_{cl})(Z_s + 3(Z_t + Z_{cl} + \frac{2Z_{nl}\,Z_{el}}{Z_{nl} + Z_{nl}})} \qquad (5.3)$$

6.0 AN EXAMPLE OF POWER SYSTEM FAULT ANALYSIS

6.1 An Introduction

The methods described in Section 5.0 are demonstrated with the aid of an example, providing detailed calculations for analysing various types of faults on a simple network (Fig. 6.1).

Consider the simple system shown in Fig. 6.1 consisting of a 60 MW generator, a 75 MVA 11.8/145 kV generator transformer, a 132 kV overhead transmission line and 132/11 kV distribution substation.

In this example fault currents will be calculated resulting from various types of faults on the 11 kV side of the 45 MVA Step-Down transformer.

6.2 Parameters

All parameters are based on the equipment rating. To work on the p.u. system, the parameters must be transferred to a common 100 MVA base and the voltage bases of 10.7 kV, 132 kV and 11 KV.

6.2.1 *Positive sequence parameters*

Generator

$X_d^{11} = j11.1\%$ (75 MVA, 11.8 kV)

$$X_d^{11} = j0.111 \times \frac{100}{75} \times \frac{(145)^2}{(132)^2} = j0.179 \text{ p.u.}$$

Generator Transformer

$X_{tg} = j12.5\%$ (75 MVA, 11.8/145 kV)

$$X_{tg} = j0.125 \times \frac{100}{75} \times \frac{(145)^2}{(132)^2} = j0.201 \text{ p.u.}$$

Transmission Line

$Z_L = 60 \times (0.2544 + j0.6708)\ \Omega$

$$Z_L = 60 \times (0.2544 + j0.6708) \times \frac{100}{132^2}$$

$= (0.0860 + j0.231)$ p.u.

Neglecting the resistance in order to simplify the calculations,

$X_L = j0.231$ p.u.

Step-Down Transformer

$X_t = j12.5\%$

$X_t = j0.125 \times \frac{100}{45} = j0.278$ p.u.

6.2.2 ***Negative sequence parameters***

Generator

$X_2 = j10\%$

$X_2 = 0.1 \times \frac{100}{75} \times \frac{(145)^2}{(132)^2} = j0.161$

The remaining negative sequence parameters are identical to the positive sequence reactances given in 6.2.1.

6.2.3 ***Zero sequence parameters***

Generator

$X_o = j5\%$

$X_o = j0.05 \times \frac{100}{75} \times \frac{(145)^2}{(132)^2} = j0.080$

Step-Down Transformer

$X_{to} = X_t = j0.278$ p.u.

Generator Transformer

$X_{tgo} = X_{tg} = j0.201$ p.u.

Transmission Line

Since $\frac{Z_o}{Z_1} = 2.5$, $X_{Lo} = j2.5 \times 0.231 = j0.578$ p.u.

6.3 **Sequence Networks**

6.3.1 ***Positive sequence network***

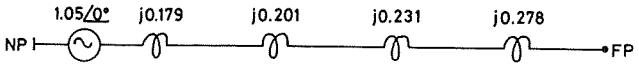

6.3.2 ***Negative sequence network***

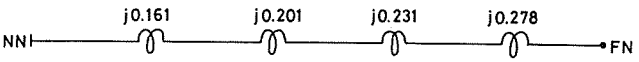

6.3.3 ***Zero sequence network***

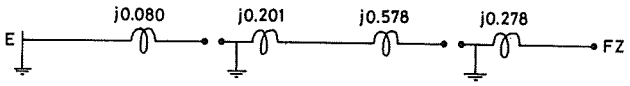

6.4 **Fault Calculations**

6.4.1 ***Three-phase short-circuit fault at F.***

a) Current through the 11kV winding of the Step-Down transformer

$$I_{RD} = \frac{1.05}{j(0.179 + 0.201 + 0.231 + 0.278)} = -j1.181 \text{ p.u.}$$

$$= 1.181 \text{ p.u.} \angle -90° = 1.18 \times \frac{100000A}{\sqrt{3} \times 11} \angle -90°$$

$$= 6199A \angle -90°$$

$$I_{YD} = 6199A \angle -90° - 120° = 6199A \angle 150°$$

$$I_{BD} = 6199A \angle 150° - 120° = 6199A \angle 30°$$

b) Current through the 132kV windings of the Step-Down tansformer

$$I_{RW} = 6199 \times \frac{11}{132\sqrt{3}} A \angle -90°$$

$$I_{YW} = 6199 \times \frac{11}{132\sqrt{3}} A \angle -150°$$

$$I_{BW} = 6199 \times \frac{11}{132\sqrt{3}} A \angle 30°$$

c) Current through the 132kV transmission line

$$I_{RL} = I_{RW} - I_{BW} = 6199 \times \frac{11}{132\sqrt{3}} (e^{-j90°} - e^{j30°})$$

$$= 6199 \times \frac{11}{132} A \angle -120°$$

$$I_{YL} = I_{YW} - I_{RW} = 6199 \times \frac{11}{132\sqrt{3}} (e^{j150°} - e^{-j90°})$$

$$= 6199 \times \frac{11}{132} A \angle -120°$$

$$I_{BL} = I_{BW} - I_{YW} = 6199 \times \frac{11}{132\sqrt{3}} (e^{j30°} - e^{j150°})$$

$$= 6199 \times \frac{11}{132} A \angle 0°$$

d) Current through the 11.8kV windings of the generator transformer

$$I_{RT} = 6199 \times \frac{11}{132} \times \frac{145}{\sqrt{3} \times 11.8} A \angle -120°$$

$$I_{YT} = 6199 \times \frac{11}{132} \times \frac{145}{\sqrt{3} \times 11.8} A \angle 120°$$

$$I_{BT} = 6199 \times \frac{11}{132} \times \frac{145}{\sqrt{3} \times 11.8} A \angle 0°$$

e) Current through the stator windings

$$I_{RG} = I_{RT} - I_{BT} = 6199 \times \frac{11}{132\sqrt{3}} \times \frac{145}{11.8} (e^{-j120} - 1)$$

$$= 6199 \times \frac{11}{132} \times \frac{145}{11.8} \angle -150°$$

$$I_{YG} = I_{YT} - I_{RT} = 6199 \times \frac{11}{132\sqrt{3}} \times \frac{145}{11.8} (e^{j120} - e^{-j120})$$

$$= 6199 \times \frac{11}{132} \times \frac{145}{11.8} \angle 90°$$

$$I_{BG} = I_{BT} - I_{YT} = 6199 \times \frac{11}{132\sqrt{3}} \times \frac{145}{11.8} (1 - e^{j120})$$

$$= 6199 \times \frac{11}{132} \times \frac{145}{11.8} \angle -30°$$

A summary of the above is given in Fig. 6.1.

6.4.2 **Single-phase-to-earth fault at F. (Red phase fault)**

$I_1 = I_2 = I_0$

$I_f = I_R = I_1 + I_2 + I_0 = 3I_1$

Where I_f = current through the fault arc.

$$I_f = \frac{3E}{Z_{total}},$$

$$= \frac{3 \times 1.05}{j(0.179+0.201+0.231+0.278)+j(0.161+0.201+0.231+0.278)+j0.278}$$

$$= 1.546 \angle -90° \text{ p.u.} = 1.546 \times \frac{10}{\sqrt{3} \times 11} A \angle -90° = 8113A \angle -90°$$

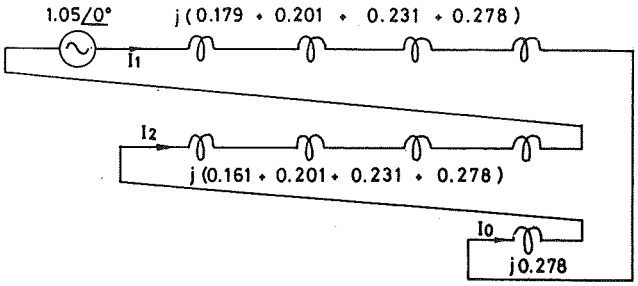

a) Current through 11kV windings of the Step-Down transformer

$I_{RD} = I_f = 8113A \angle -90°$

$I_{YD} = I_{BD} = 0$

$I_{nD} = I_{RD} + I_{YD} + I_{BD} = 8113A \angle -90°$

$I_1 = I_2 = I_0 = 2704 \angle -90°$

Where I_n = Current through the neutral connection to earth.

b) Current through the 132kV windings of the Step-Down transformer.

$$I_{RW} = 8113 \times \frac{11A}{132\sqrt{3}} \angle -90° = 390 \angle -90°$$

$I_{YW} = I_{BW} = 0$

$$I_{1W} = {}^1/_3 (I_{RW} + aI_{YW} + a^2 I_{BW}) = \frac{390A}{3} \angle -90°$$

$$I_{2W} = {}^1/_3 (I_{RW} + a^2 I_{YW} + a^2 I_{BW}) = \frac{390A}{3} \angle -90°$$

$$I_{0W} = {}^1/_3 (I_{RW} + I_{YW} + I_{BW}) = \frac{390A}{3} \angle -90°$$

6.4.3 *Phase-to-Phase-to-earth fault at F (Blue-to-Yellow-to-earth)*

$I_1 + I_2 + I_0 = 0$

$I_f = I_Y + I_B$

$I_R = 0$

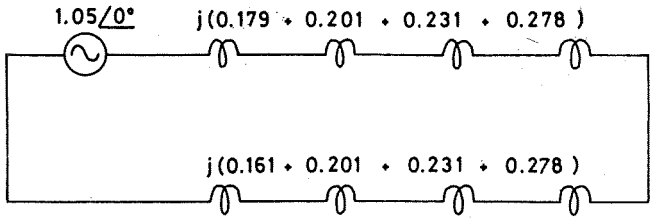

a) Current through 11kV windings of the Step-Down transformer

$$I_1 = \frac{1.05 \angle 0°}{j(0.179+0.201+0.231+0.278) + \frac{j(0.161+0.201+0.231+0.278) \times 0.278}{0.161+0.201+0.231+0.278+0.278}}$$

$= 0.955 \text{ p.u.} \angle -90° = 5012A \angle -90°$

$j0.871 I_2 = j0.278 I_0$

$$-j0.955 + \frac{0.278}{0.871} I_0 + I_0 = 0$$

$$I_0 = \frac{j0.955}{1.319} = j0.724 \text{ p.u.} = 0.724 \text{ p.u.} \angle 90° = 3800A \angle 90°$$

$$I_2 = j\frac{0.278}{0.871} \times 0.724 = 0.231 \text{ p.u.} \angle 90° = 0.231 \text{ p.u.} \angle 90°$$

$= 1212A \angle 90°$

Therefore,

$I_{RD} = 0$

$I_{YD} = 7846 \text{ A} \angle 133°$

$I_{BD} = 7846 \text{ A} \angle 47°$

$I_{nD} = 3I_0 = 11400 \text{ A} \angle 90°$

b) Current through the 132kV windings of the Step-Down transformer

$I_{RW} = 0$

$$I_{YW} = 7846 \times \frac{11A}{132\sqrt{3}} \angle 133°$$

$$I_{BW} = 7846 \times \frac{11A}{132\sqrt{3}} \angle 47°$$

c) Current through the 132kV transmission line

$I_{RL} = 0 - 377 \angle 47° = 377A \angle 227°$

$I_{YL} = 377 \angle 133° - 0 = 377A \angle 133°$

$I_{BL} = 377A \angle 47° - 377A \angle 133° = 519A \angle 0°$

$I_{1L} = 418A \angle -120°$

$I_{2L} = 101A \angle 120°$

$I_{0L} = 0$

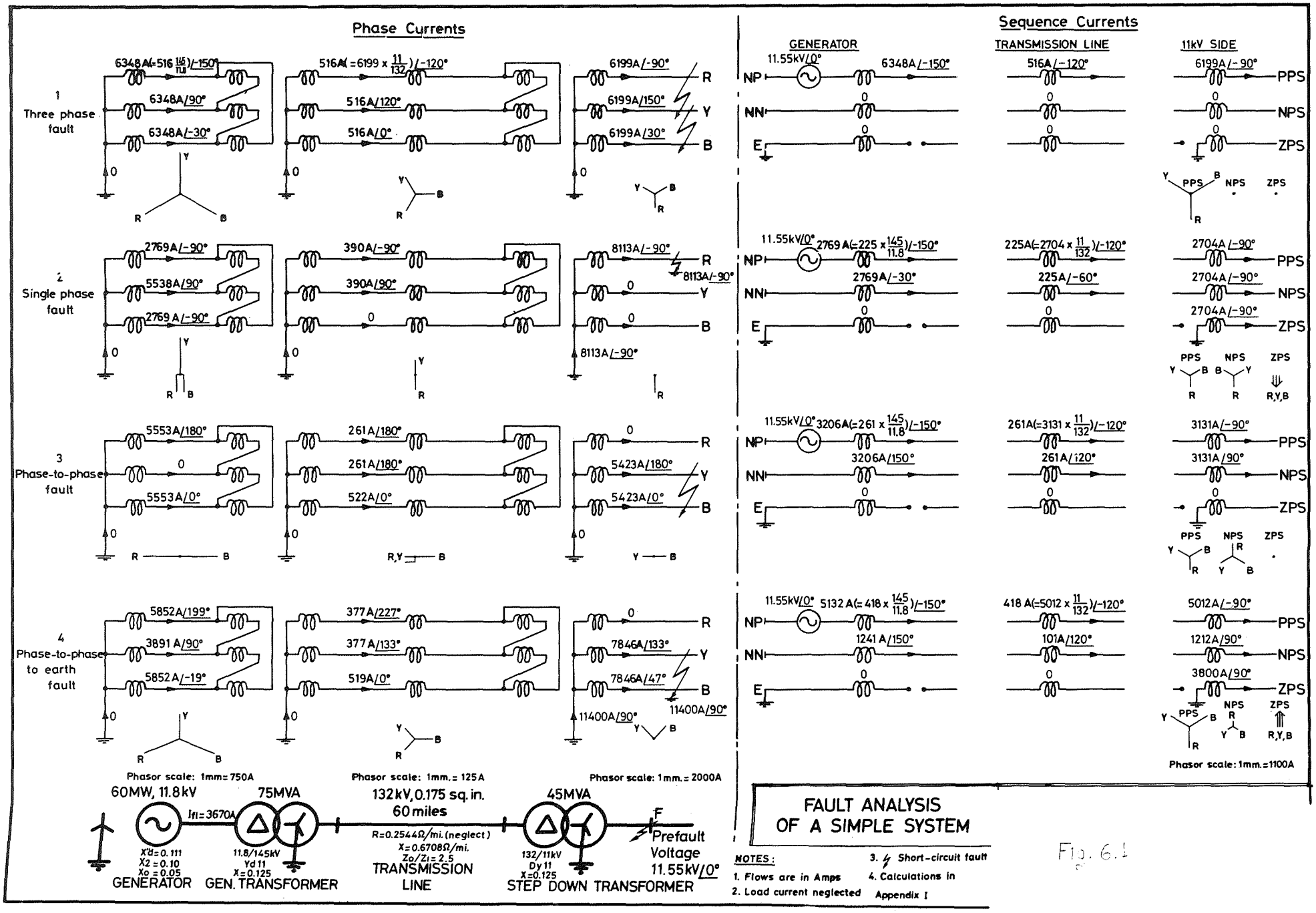

FAULT ANALYSIS OF A SIMPLE SYSTEM

NOTES:
1. Flows are in Amps
2. Load current neglected
3. ϟ Short-circuit fault
4. Calculations in Appendix I

Fig. 6.1

7.0 CONCLUSIONS

Fault calculations have always been a routine step during High Voltage power system design. After the recent changes in the I.E.E. Wiring Regulations, (15th Edition), similar calculations appear to be justifiably required, in extensive detail, even for Low Voltage applications. In the case of unbalanced faults the calculating procedure is unfortunately cumbersome unless some simplifications are assumed. In this article a brief introduction to short-circuit studies was presented, with particular emphasis on simple system applications.

Recent advances in the production of digital computers and with the wide availability of microcomputers, hand calculations, as described here, for complex systems may soon be phased out. Nearly all electrical utilities now have computer programs which perform such calculations at very short notice and with minimal preparation. Even in those cases, however, a thorough understanding of the methods used by the computer program to produce the results, avoids the risk of misinterpreting them. Terms which may appear as mathematical concepts, such as negative or zero sequence currents are now used as physical quantities by relays, derived by means of appropriate filters.

8.0 REFERENCES

8.1 Electricity Council (1981). *Power System Protection.* Vol. 1, Peter Peregrinus.

8.2 Clarke, E. (1950). *Circuit Analysis of A.C. Power Systems.* John Wiley and Sons.

8.3 Wagner, C.F., and R.D. Evans (1933). *Symmetrical Components.*

8.4 G.E.C., Measurements (1975). Protective Relays Application Guide.

INTERCHANGEABILITY

By C. K. Tavrou
Lecturer H.T.I.

Has anyone ever thought why all spare parts we buy for our car, washing machine, or industrial machine fit correctly? Maybe yes, but in most cases if at any time a spare part does not fit where it should, the buyer will not accept it as a natural event, on the contrary he will angrily complain. Why should it be unacceptable that some of those millions of components manufactured may not fit with each other? In some cases cars of over fifteen years old are expected to have spare parts. The argument here is not only why should different parts fit with each other perfectly, but the fact that these parts have been propably produced at two different factories and maybe a number of years later. This is what this article is about to explain, why components can be made to fit perfectly.

Mechanical components will be used as examples, but the principles are the same for all types of components.

The very first important point to be noted is that exact dimensions are non-existant. No one can say that a component can be manufactured at a length of 11mm and not 11.000001mm. To overcome the problem of not being able to manufacture exact dimensions, limits are used within which a manufactured length will be acceptable, e.g. 11 ± 0.2mm.

When two components are to fit into each other, then dimensions may allow them to fit with one of two ways, clearance or interference. Two components are said to fit with clearance if relative movement between them is possible, and two components are said to fit with interference if the opposite occurs. In the second case some force will be required to fit the two components into each other. If a shaft and a hole are taken as example, one may say that they will fit with clearance if the hole is larger than the shaft and with interteference if the hole is smaller. The specification of dimensions on a drawing may become a little more complicated if it is considered that the dimensions of the hole and shaft are given with their tolerances.

Fig. 1

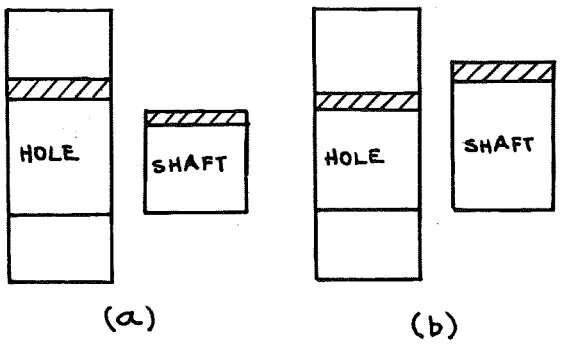

In order to have toleranced dimensions and yet achieve the required fit the components are made as shown schematically in fig. 1. In the case of the clearance fit, the tolerances and dimensions of the components are specified suitably, so that if they are made within their respective tolerance, the fit is succeeded. Similarly the interference fit can also be achieved. Therefore, using this method, it may be seen that, two components do not need to be manufactured "exactly" to one dimension in order to give the required fit.

An argument may arise against the above method since two different pairs of components may have two different degrees of clearance or interference had these been within the tolerances but at different dimensions. This is an inherent characteristic of this method and the designer has to decide on allowable variation of the clearance or interference. This is where interchangeability of components is based. The limits of the fit are decided by taking into consideration the aplication of the fit. Therefore, the problem of manufacturing components at "exact" dimensions, which is very costly, has been converted into a pure design problem.

The relationship between the components tolerances and the tolerance of the clearance or interference is shown in fig. 2 and given by equations (i) and (ii).

Fig. 2

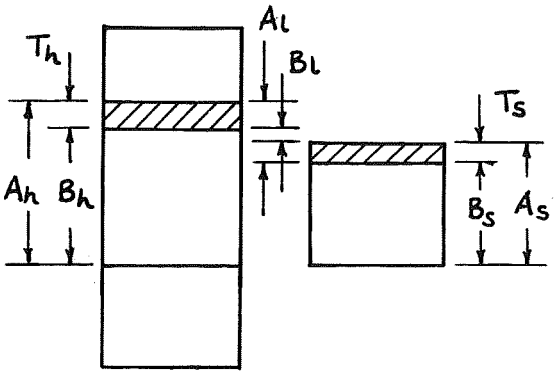

$$Al = Ah - Bs \quad \text{... (i)}$$

and $$Bl = Bh - As \quad \text{... (ii)}$$

where Al = High limit of clearance

Bl = Low limit of clearnance

Ah = High limit of hole

Bh = Low limit of hole

As = High limit of shaft

Bs = Low limit of shaft

In order to make it easier for the designer to decide on the tolerances to be used, there are standard tables for Limits and Fits which recommend the size difference and tolerances of the two parts to give the require fit.

An example will be used to illustrate clearly how easy it is for the manufacturer to achieve fitting between any two components even if millions are produced.

A shaft and a hole with diameter approximately equal to 15mm are to fit with clearance. The shaft's tolerance limits can be selected from standard tables and be $15 \begin{smallmatrix} +0.03 \\ +0.01 \end{smallmatrix}$ mm and the hole to be $15 \begin{smallmatrix} -0.01 \\ -0.02 \end{smallmatrix}$ mm.

A gauge can be used which can be set to two dimensions ie. 15.03 and 15.01mm as shown in fig 3a. As the components are manufactured, they are tested with this instrument and as long they pass through the GO Side and do not pass through the NOT GO Side, then, they are accepted. In the same way a gauge is made for the holes, shown in fig 3b. This makes the production and testing process faster, easier and more reliable.

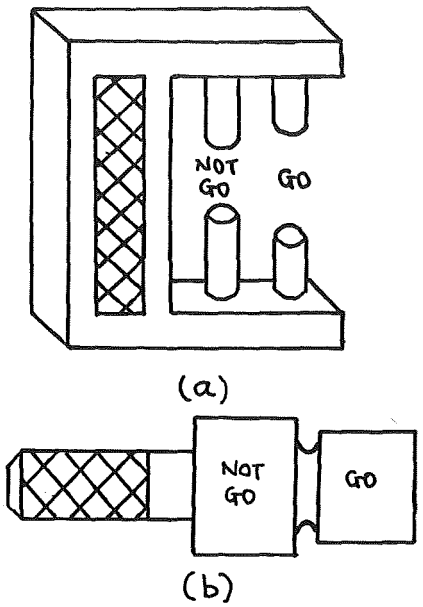

Fig. 3

If it is assumed that one thousand shafts and holes are manufactured within their respective limits, then, any one couple of shaft and hole will "fit without fail". This is what is called "interchangeability".

Happiness is to do your duty well. The more difficult your duty the more happiness you will have.

N. Kazantzakis

It's not our fluent speech and good words that count but our good deeds to help others.

Sri-Ram

We were born to love and not to hate our fellow man.

Dante

There is no sacred war. Unavoidable, perhaps, but never sacred.

P. Kanellopoulos

THE STUDY OF HEAVY-ION DAMAGE IN PURE COPPER

By Dr. A. Y. Stathopoulos,*
Lecturer at H.T.I.

ABSTRACT

TEM has been used to study the small vacancy clusters (8 Å ⩽ diameter ⩽ 90 Å) created in pure copper by 30 keV ions. Quantitative investigations show that cluster visibility depends on the imaging conditions such as the orientation of the foil, the magnitude of the diffraction vector **g** and the deviation parameter **w**. The main conclusion is that reliable and accurate determinations of the geometry, density, size and depth distribution of the defect clusters require a combination of micrographs taken under a series of strong-beam diffraction conditions or a combination of strong - and weak-beam conditions. Failure to do this can result in significant errors, particularly in determining the number density where a combination of micrographs is required to identify the layer boundary loops, which represent⩾ 20% of the loop population at any given diffraction condition.

The damage consisted entirely of Frank loops equally distributed on the four {111} planes. The degree of dissociation on neighbouring planes of many of these loops was found to be a function of foil orientation being greater in <111> than in <011> foils. A defect yield of 0.50 ± 0.01 was obtained with Cu^+ ions and 0.60 ± 0.01 with W^+ ions, whereas the cascade efficiency was 0.35 ± 0.02 with Cu^+ ions but increased by a factor of two with Q^+ ions owing to the increase in vacancy supersaturation. Larger loops were found on the edge-on than the inclined planes with both types of ions. This is explained in terms of a model which allows more efficient collapse and growth on the edge-on planes because of elongation of the average cascade along the ion beam direction.

Introduction

Collision cascades are one of the most important displacement mechanisms in metals irradiated with fast neutrons in a reactor environment. They are formed by energetic lattice atoms having energies > 10 keV which are displaced initially by fast neutrons. These primary knock-on (p.k.o.) atoms undergo subsequent collisions with lattice atoms and create small regions of damage containing a high concentration of interstitial and vacancy point defects. This damage process can be simulated by irradiation with heavy ions in an accelerator which results in cascades being produced at depths of a few hundred Angströms from the surface of the specimen. The damage created by heavy ions in f.c.c. and b.c.c. metals has been extensively studied (for a review see Eyre (1973) and Wilkens (1975)). The main feature of the damage is that the vacancy-rich centres of the cascades are observed to collapse to form vacancy clusters; interstitial clustering is not observed and it is presumed that the interstitials either form sub-microscopic clusters or are lost to the adjacent foil surface. Considerable emphasis has been placed on determining the defect yield, defined as the fraction of incident ions which give rise to visible loops, the cluster geometry and the size distribution of the clusters; from the latter the cascade efficiency, defined as the fraction of the calculated number of vacancies which survive in loop form, is obtained. The measurement of these provides considerable insight into the damage processes in the cascade (Merkle 1966, 1969).

One of the most widely studied f.c.c. metals is copper. Wilson (1971), Wilson and Hirsch (1972) and Häussermann (1972) all studied heavy-ion irradiation of copper at room temperature, whilst Schindler (1974) and English et al (1976) studied the effect of irradiation at elevated temperatures. The majority of the work concerned the damage produced by 30 keV Cu^+ ions and the main conclusions were that vacancy clusters in the size range 10 -90 Å were formed from collision cascades, with defect yields of 0.35. The geometry of the defect clusters was analysed using the so-called l-analysis and the results showed the clusters to be mainly Frank faulted loops. Wilson and Hirsch first studied the fine structure of some of the images formed in $\mathbf{g} = 200$ (where **g** is the reflection vector) and interpreted it as arising from the dissociation of the Frank loop on neighbouring {111} planes towards a stacking fault tetrahedron (s.f.t.). This was confirmed in silver and copper by Jenkins (1974) using the weak-beam technique.

However, the existing evidence is incomplete and inaccurate. For example, only faulted loops on two of the four possible planes were observed and no account was taken of the fact that loop visibility depends critically on loop depth in the foil in determining the defect density, or that the ratio between image size and cluster diameter was not well understood. Recently, considerable progress has been made in understanding the contrast from small clusters close to the foil surface (Eyre, Maher and Perrin 1977 a, b, Saldin, Sbathopoulos and Whelan 1978, 1979, Holmes, Eyre, English and Perrin 1979, Katerbau 1976, Hirsch 1978, Ohr 1976, 1978). It is now possible from the experimental micrographs to identify size with reasonable precision, to determine accurately the distribution of clusters on the various planes, and to distinguish between Frank loops and s.f.t. In a study of the effect of alloying on the formation of vacancy loops from cascades in copper and copper alloys (Stathopoulos 1977) it was found necessary to establish methods, based on the recent theoretical work, of analysing the damage formed by 30 keV Cu^+ and W^+ ions) An experimental procedure was developed for comprehensively analysing relative loop numbers on all four {111} planes as well as accurately measuring the defect yield, cluster size and depth distributions and cascade efficiency) Several new features of both the analysis and the results on pure copper will be presented here). In a subsequent paper (Stathopoulos, English, Eyre and Hirsch 1981) the results from the alloys will be presented and compared with those obtained in pure copper.

2. Experimental Procedure

30 keV Cu^+ and W^+ ions have been used to irradiate single crystal specimens of 5N pure copper to a dose of 2×10^{11} ions/cm^2. The material was supplied by Johnson Matthey Ltd. and the single crystals were grown using a Bridgman furnace. The specimen normals had off-axis (O.A.) [011] orientations ~3° from the [023] pole. The foils were electro-polished in an electrolyte containing 1:2 nitric acid in methanol with an applied voltage of ~4V at -42°C and then irradiated at room temperature in the Harwell Lintott separator with the incident beam perpendicular to the foil surface.

---

* The author's article "Damage in the Cation Sublattice of a- AL_2O3 Irradiated in the HVEM" which appeared in last year's edition of the 'H.T.I. Review' has subsequently been accepted without change and published in the "Philosophical Magazine" scientific journal (Phil. Mag. A, Vol. 47, No. 3, 381 - 394).

The irradiated specimens were examined in a JEM 100B or a Siemens 102 electron microscope. A systematic range of diffraction conditions were used at selected orientations in the stereographic triangle to assess the number density and geometry as well as size and spatial distribution of the defect clusters produced. The size distributions were measured from micrographs with a total magnification of x 3 x 10^5 with the aid of an eyepiece with a graticule. For the depth distribution of the damage inside the foil, the stereo-technique (Diepers and Diehl 1965) was employed. The parallax of each Cu^+ ion defect cluster, with respect to sharply defined circular islands of gold (10—15 Å diameter) evaporated onto the surface immediately after irradiation, was measured directly from x 12 x 10^4 stereomicrograph pairs using a Hilger-Watts type SB185 mirror stereoscope with a x 4 binocular.

3. Image Analysis and Results from Cu^+ ion Irradiated copper

In this image the results from the study of Cu^+ ion damage are presented. The image analysis methods employed for the precise determination of the defect cluster geometry, number density, depth distribution and size distribution are also des cribed. Frequently, in the literature, different imaging conditions have been used for quantitative analysis of the damage structures and where appropriate these will be compared and the optimum conditions specified.

3.1 *The geometry of defects in pure copper*

In agreement with the results of previous workers only vacancy clusters were identified. In pure copper the likely geometry of the vacancy clusters is as follows. Faulted a^83 <111> Frank loops on α, β, γ or δ planes in the usual Thompson tetrahedron notation (Thompson 1953), Frank loops dissociating towards stacking fault tetrahedra (s.f.t.),

Fig. 1

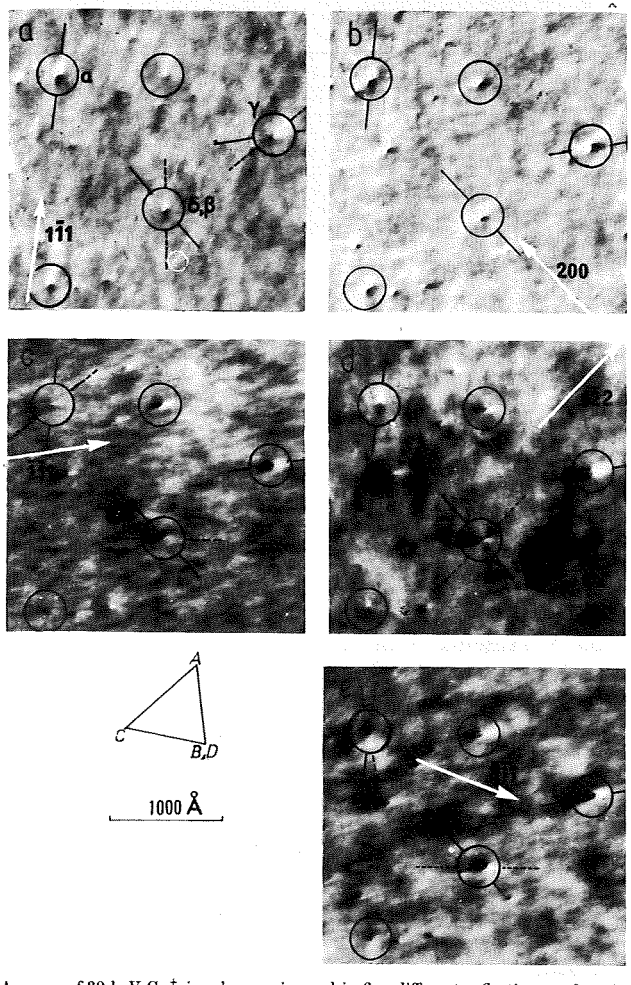

An area of 30 keV Cu^+ ion damage imaged in five different reflections under s.b. dynamical conditions. Full lines indicate $\mathbf{b}_p$ ($\mathbf{b}$ projected onto the image plane) directions and dashed lines indicate I-vector directions.

Fig. 2

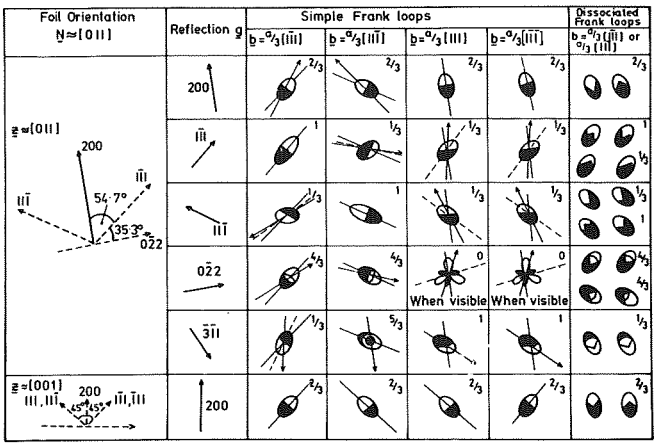

Schematic of image behaviour of simple and dissociated Frank loops as observed experimentally under s.b. conditions. ——— $\mathbf{b}_p$, – – – I observed, ——— I theoretical (Ohr 1976, Saldin *et al.* 1979). Wherever I obs. is not shown, I obs. is parallel to $\mathbf{b}_p$. Wherever only $\mathbf{b}_p$ is shown, all three vectors coincide. The numbers beside each image represent $|\mathbf{g} \cdot \mathbf{b}|$ values.

completes s.f.t., and perfect $a/2$ <011> loops. For an [011] foil two of the four possible Frank loop Burgers vectors $\mathbf{b}$ are close to the plane of the foil, $a/3$ [1$\bar{1}$1] and $a/3$ [11$\bar{1}$], referred to in this paper as edge-on, and two are inclined at ~35°C to the foil normal, $a/3$ [111] and $a/3$ [1$\bar{1}\bar{1}$], referred to as inclined. In all previous work on foils with an [011] normal only edge-on faulted loops had been identified and Wilson (1971) assumed the inclined faulted loops to be out of contrast. In this section we first consider the identification of Frank loops, and the method of differentiating between the four possible Burgers vectors.

The experimental procedure adopted was to compare the image behaviour of the same defect in several different strongly excited reflections. In fig. 1 the irradiation-produced defects are shown imaged in five low-order gs about [011]. It is clearly possible to identify images from individual defects in the different gs and from the geometry and streaking directions a cataloque of image types was made. Figure 2 summarizes schematically the image types observed and classifies the defects as being either simple Frank loops on one of the four possible {111} planes or dissociated Frank loops on edge-on planes. The assignment of $\mathbf{b}$-vectors was made from $|\mathbf{g}\cdot\mathbf{b}|$ product criteria, the value of which is given on the figure for each image. In the case of simple Frank loops a comparison of the experimental images will those computed for an isotropic crystal (Saldin *et al.* 1979) for all gs except $\mathbf{g} = \bar{3}1\bar{1}$ confirmed the identification of $\mathbf{b}$-vectors; a few minor differences were found in the detailed shape of the interface line and the more elongated shape of the edge-on loop image (when $|\mathbf{g} \cdot \mathbf{b}| = 1$) observed experimentally. The image behaviour shown in the last column corresponds to examples of dissociated loops with $\mathbf{b}$ in the plane of the foil; the greater the dissociation the closer the streaking is aligned to the $\mathbf{g}$-vector direction and, for full dissociation, the contrast is that of the tetrahedron (Saldin *et al.* 1979). Lastly, concerning the simple Frank loops, the images show marked deviations of the $\mathbf{I}$-vector (the vector joining the centre of the black to the centre of the white lobe) between the predictions of isotropic calculations and what is observed experimentally.

At [011] the Burgers vectors of the two possible inclined loops project onto the same direction and thus cannot be distinguished. However, $a/3$ [111] and $a/3$ [1$\bar{1}\bar{1}$] were distinguished from each other by progressively tilting the specimen along the 200-band towards the [001] pole where a^83 [111] projects along [220] and $a/3$ [1$\bar{1}\bar{1}$] projects along [2$\bar{2}$0].

as shown in the bottom row of fig. 2. A second advantage of tilting is that the projected shape change and relative streaking directions enable inclined Frank loops and small s.f.t. to be distinguished (Saldin *et al.* 1979).

The weak-beam technique (Cockayne, Ray and Whelan 1969) was applied in an attempt to obtain information on loop geometry. In fig. 3 the same area of damage is shown imaged in $\pm \mathbf{g} = 0\bar{2}2$ with $s \approx 2 \times 10^{-2}$ Å^{-1} together with a $\mathbf{g} = 200$, $s \approx 0$, D.F. micrograph: (s is the excitation error of the operating reflection). The circles help position the same defects on each micrograph and loops α, β, γ and δ are as identified on strong-beam micrographs. Unlike the dynamical case, no simple pattern is obvious because there is a variety of complicated images varying in size, shape and intensity even for loops on the same plane. There is little correlation in the intensity and fine structure of the images in strong-beam and weak-beam. Also, comparison of the two $\pm$ g w.b. micrographs reveals that many of the loops give interchangeable images of 'white dots' going into 'double arcs', and vice versa. This behaviour, however, is not consistent with **b** and cannot be attributed to inside-outside contrast. The inclined loops show contrast comparable to that from edge-on loops although they would be invisible under strong $0\bar{2}2$ type conditions. Thus weak-beam conditions were not found to be useful in determining the geometry of these irradiation produced defects, in agreement with Perrin and Eyre (1973) and Häussermann, Katerbau, Rühle and Wilkens (1973).

Table 1. Geometry analysis of vacancy defects in pure copper irradiated with 30keV Cu^+ ions in a given area.

Burgers vector (b)	Number of loops	Percentage of total
$(^1/_2)[1\bar{1}1]$	185	23.8 ± 1.4
$(^1/_2)[11\bar{1}]$	150	19.3 ± 1.4
$(^1/_2)[111]$	168	21.6 ± 1.4
$(^1/_2)[1\bar{1}\bar{1}]$	157	20.1 ± 1.4
Unknown†	118	15.2 ± 1.4
$a/3\langle 111\rangle$		
Perfect loops	None	None
Tetrahedra	none	None

† 'Unknown' refers to defects identified as Frank loops which could not be confidently assigned a **b**-vector.

The results of the analysis as obtained using strong-beam images are shown in Table 1. No perfect loops or complete s.f.t. were identified and the numbers of Frank loops were approximately equally divided between the four possible Burgers vectors. There was still, however, a population of defects, marked 'unknown', which were identified as Frank loops but could not be assigned a Burgers vector unambiguously. Furthermore, 63% of the edge-on loops have dissociated, but in strong beam no dissociated inclined loops were identified, although the presence of images from inclined loops in $\mathbf{g} = 0\bar{2}2$ weak beam, where $\mathbf{g} \cdot \mathbf{b} = 0$, may be due to dissociation.

3.2. *Defect yield determination*

An accurate measurement of the defect yield is important in determining the efficiency with which vacancies are retained in loop form. It is essential to identify all the defects in an area of interest, and it was found necessary in this work to investigate the optimum combination of diffraction conditions to achieve this.

3.2.1. *Defect yield as a function of diffraction conditions*

Examination of the visibility of a given image in $\mathbf{g} = 200$, $\bar{1}\bar{1}1$, $1\bar{1}1$ and $0\bar{2}2$ shows that it is a function of imaging reflection. Apart from loop disappearance through $\mathbf{g} \cdot \mathbf{b} = 0$ (images mostly invisible in practice), loops with $\mathbf{g} \cdot \mathbf{b} \neq 0$ also appear or disappear when going from one reflection to another. Defect visibility was also found to be a function of orientation. This was studied by imaging the same area in $\mathbf{g} = 200$ at three orientations:

Fig. 3

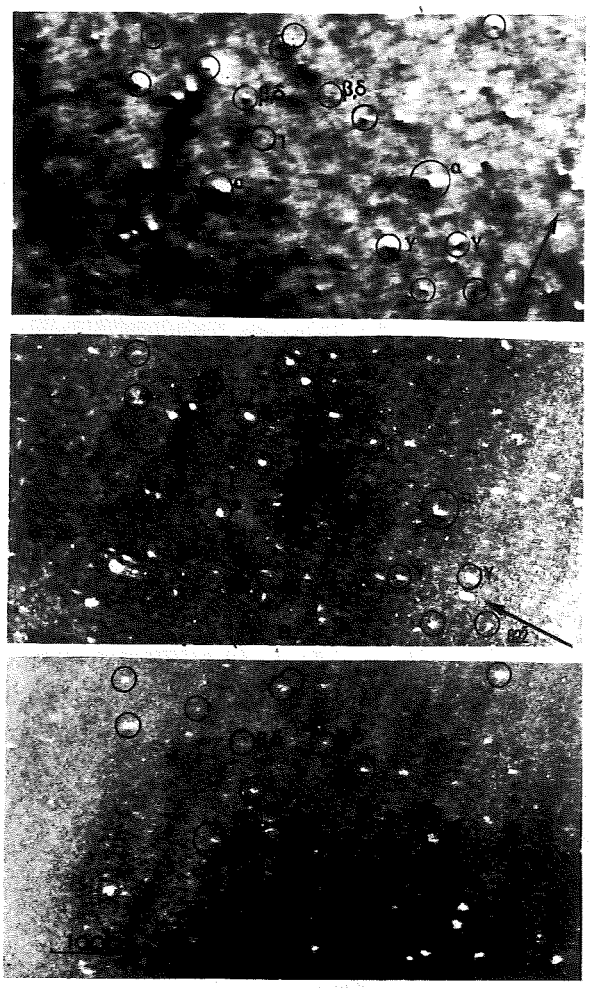

Comparison of s.b. with w.b. $\pm$ g pair; (*a*) $\mathbf{g} = 200$, s.b.; (*b*) $\mathbf{g} = 02\bar{2}$, w. b., $s \approx 2 \times 10^{-2}$ Å^{-1}; (*c*) $\mathbf{g} = 0\bar{2}2$, w.b., $s \approx 2 \times 10^{-2}$ Å^{-1}.

Table 2. Defect yields when tilting along 200-band.

Orientation	Defects counted in 79 1000 Å identical area squares	Yields
[011]	616	0.39 ± 0.01
[023]	573	0.36 ± 0.01
[013]	593	0.38 ± 0.01

Table 3. Presence of defect images identified in the same area as table 2 at different orientations.

Combination of orientations	Number of common defects	Total number of defects
[011], [023], [013]	437	616
[011], [023]	437 + 55	present
[011], [013]	437 + 55	at [011]
[111] only	437 + 69	
[023], [013]	437 + 50	156 extra
[023] only	437 + 43	identified
[013] only	437 + **63**	on titling

[011], [023] and [013]. Table 2 gives the results of defect yield determination from three different dynamical micrographs, and it shows that similar total numbers of defects were present at each orientation. However, when the images swere studied individually it was found that at each orientation there was a proportion of new images appearing while others went out of contrast. Table 3 shows the detailed results obtained from identifying all the defects in a given area. From the micrographs obtained at [023] and [013] an extra 156 clusters were identified. Thus the total yield became 0.49 ± 0.01, an increase of 26% over the value of 0.39 ± 0.01 obtained from the analysis of the [011] micrograph.

The question of whether or not the method of tilting in strong beam helped to identify all the defects in the foil was investigated further by studying a series of w.b. ± **g** = 0$\bar{2}$2 conditions with four different values of ς close to 2 x 10^{-2} Å^{-1} together with an s.b. micrograph. Details were given by Stathopoulos (1977) and the quantitative results showed that the yield depended on the imaging conditions with a decrease of betw een 14 to 23% in the total number of loops present on each w.b. micrograph compared with s.b. However, the w.b. micrographs contained collectively a number of extra loop images (see fig. 3, no. 1 images) otherwise absent under s.b. **g** = 200 at [011]. When these extra defects were added onto those counted in s.b., the total yield increased to 0.50 ± 0.22, in agreement with the value obtained by the method of tilting in s.b.

A more dramatic decrease in the number of observable defects occurred when the same area was imaged under $\omega \simeq 0.8$ conditions (w = s.ξ **g**, where ξ **g** is the extinction distance of the operating **g**). Direct comparison of the numbers of observable defects for a certain area revealed 52% fewer loops than under $\omega \simeq 0$ at the same [011] orientation, and ~ 54% of the total number of loops identified commonly in the $\omega \simeq 0.8$ than $\omega \simeq 0.0$. conditions was found at [023] and [013]. A detailed classification by **b** vector of the loops gave the results tabulated in Table 4, which indicate that a loss of images occurred irrespective of loop plane, but a more severe loss of inclined and unknown loops occurred on going to $\omega \simeq 0.8$. Stereomeasurements demonstrated that loops absent under $\omega \simeq 0.8$ came from all depths inside the region of damage. The kinematical micrograph therefore gives a biased view of the damage distribution and is unsuitable for studies of this nature.

Table 4. Approximate loop population per **b**-vector under $\omega \approx 0.8$ at [111] and $\omega = 0.0$ conditions in a given area.

Burgers vector (b)	Distribution of loops in $w \approx 00$ (number/percentage)	Distribution of loops in $w \simeq 0{\cdot}8$ (number/percentage)	Number/perentage of loop images which disappear in going from $w \simeq 0{\cdot}8$ $w = 0{\cdot}8$
$(^1/_3)a[1\bar{1}1]$	115/22	68/28	47/41
$(^1/_3)a[11\bar{1}]$	91/17	60/24	31/34
$(^1/_3)a[111]$ and $(^1/_3)a[\bar{1}\bar{1}1]$	233/46	95/38	138/59
Unknown	82/15	25/10	57/70
Total	521/100	248/10	273/52

3.3. *Depth distribution of 30 keV Cu^+ ion damage*

Kinematical conditions giving rise to 'black spot' contrast have been preferably used in the past for stereomeasurements (see, for example, Rühle Wilkens and Essman 1965, and Rühle 1967). In the present case, because of the loss of a large number of clusters under such conditions, steropairs were taken under dynamical conditions in a wide-angle tilt on both sides of the [011] pole. Each parallax measurement was repeated six times and an average value was taken for each defect given a most probable error of ± 3 Å. No appreciable

Fig. 4

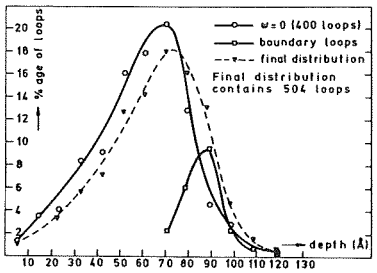

Depth distribution of 30 keV Cu^+ ion damage. The depth position of L1 → L2 boundary for $w \approx 0$ centres at about 84 Å. The $w \approx 0$ and the final depth distributions are separately normalized with respect to the total number of loops in each case. The curve belonging to the boundary loops is normalized with respect to the total number in the final distribution.

oxide or contamination layer between the gold and the specimen surface was detected. The microscope magnification was known accurately to within ± 2% as determined by the method of Hirsch, Howie, Nicholson, Pashley and Whelan (1965). 'Z focusing' of the image by adjusting the specimen position rather than the objective-lens current by adjusting the specimen position rather than the objective-lens current enabled in-focus micrographs of identical magnification to be obtained at all orientations. The tilt angle was determined to within ± 0.2° from the Kikuchi lines appearing on the diffraction patterns; this gives an error in the depth measurements of less than 1% for the tilt angle of 22° used. Thus, the total error associated with each measurement was ± 10%.

The depth distribution from 400 defects is shown in fig. 4. The defects were found to lie within 120 Å of the foil surface with the peak occurring at ~70 Å. Further stereomicroscopy was performed in order to incorporate the extra loops observed at titled orientations. The stereo-pairs used were obtained from the series of micrographs at different poles in the following combination of orientations: [011]/[032], [023]/[011], [012]/[023], [012]/[011], [013]/[011], [013]/[023], [013]/[012] and [001]/[023]. The position of the extra loops was measured from their relative elevation with respect to previously measured clusters. This led to the additional distribution for the boundary loops shown in fig. 4. These defects lie in depths between 70 Å and 95 Å, i.e. at the first to the second layer (L_1 to L_2) boundary. The total depth distribution of combining those with the$w \simeq 0$ spectrum gives a final distribution with a peak at ~ 75 Å which extends to a depth of 120 Å from the foil surface.

3.4 *Size distribution of the defects*

3.4.1. *Size measuring procedure*

Measurement of the size distribution of the loops is needed in order to determine the efficiency of point-defect retention in each cascade. Dynamical images were employed in this work to avoid the loss of images under kinematical conditions (see § 3..2). It is important to know the relationship between image width and loop diameter under the $w \simeq 0$ conditions. For Frank loops $\lesssim$ 90 Å in copper it has been demonstrated by computer simulation of the images of 30 Å diameter edge-on and inclined loops that the width of the black-white interface for layer 1 loops is equal to the projected loop diameter; Saldin *et al.* (1979) illustrated this for the case of an edge-on loop in **g** = 1$\bar{1}$1, but the result is independent of loop inclination and **g**(details were given by Stathopoulos (1977)). This width stays constant throughout L1 and for the black or white dot images observed at the L1⇌L2. A 1:1 correspondence between width and projected diameter for the smaller loops examined in this work was also verified by computer simulation of a < 20 Å diameter loop (D. K. Saldin 1980, private communication). Loop diameters were therefore measured directly on micrographs taken in **g** = 200 near the

[011] orientation. As discussd in §3.2. invisibility problems were encountered for loops ≲20 Å at theL1⇌L2 boundary, and these loops were measured on micrographs obtained with the same **g** but at different tilts between [011] and [001]. The choice **g** and beam orientation were such that similar images were used for both edge-on and inclined loops ($|\mathbf{g} \cdot \mathbf{b}| = 2/3$ in all cases for $\mathbf{g} = 200$) with a well-defined interface line which coincides with the loop diameter in the image plane; for dissociated Frank loops the longest edge visible was measured which is sharply defined at [011]. No defects smaller than ~8 Å were identified, and it is considered that an average error of ± 5 Å was involved in each measurement.

3.4.2. *The total distribution and relative sizes of Frank loops on the various planes*

Figure 5 shows the separate size spectra for the loops on planes α, γ, β and δ and the set of Frank loops which could not be unambiguously classified. The total distribution obtained by adding up all the clusters is also shown. No loop images larger 90 Å were observed and the total size spectrum peaks between 10 and 20 Å with a mean diameter of 22.·7±0.·3 Å. Almost all the loops with diameters ⩾ 50 Å lie on the two edge-on planes, and although all the distributions peak at the same diameter, the inclined loop mean diameters are substantially smaller than the edge-on ones, i.e 25·7 ± 0·6 as against 30·6 ± 0·9 Å. The distributions are normalized to show the yield result of the loops being equally distributed in numbers between the edge-on and inclined planes.

It was necessary to determine whether the above size differences between edge-on and inclined loops were real or due to an imaging effect. The same area imaged near [011] was also imaged at the [001] orientation where all the {111} planes are inclined at the same angle. The corresponding size distributions for the edge-on set and the inclined set of loops

Fig. 5

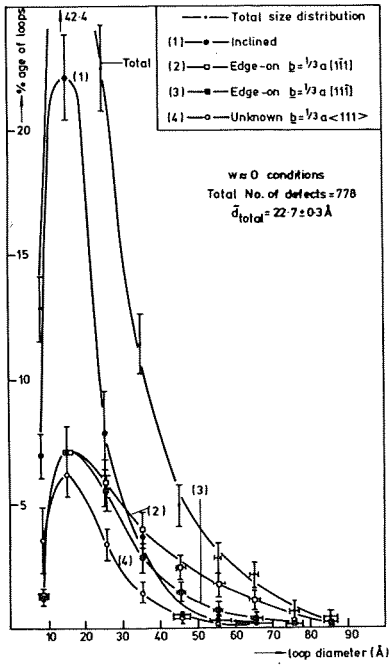

Size distributions of Frank loops in pure copper irradiated with 30 keV Cu^+ ions. Each separate spectrum is normalized in numbers with respect to the total distribution.

at the two orientations are shown in fig. 6. From these it can be concluded that the substantial differences between the distribution of edge-one (at [011]) and inclined loops (at [011]) distributions are still present. The peak positions of the two distributions cannot be compared with those in fig. 5 because only loops in constrast at both orientations were sized here. It is concluded that the inclined loops have genuinely smaller sizes than the edge-on loops.

3.4.3. *Variation of loop size distributions with depth in the foil*

Loop size distributions in different depth intervals were constructed from the clusters used in the depth distribution measurements in order to see whether there was any colleration of cluster size with depth. Three distributions for loops lying in three different depth zones, chosen from the beginning, middle and end of the damage ranges, are presented separately as histograms and also compared in the form of smooth curves in fig. 7. Within the experimental errors it can be concluded that similar sizes of loops occur at all depths with the same frequency. Although there is some tendency towards smaller sizes of loops away from the foil reflected in the absolute values of the mean diameters, this is not significant when the large standard errors attached are taken into account.

Fig. 6

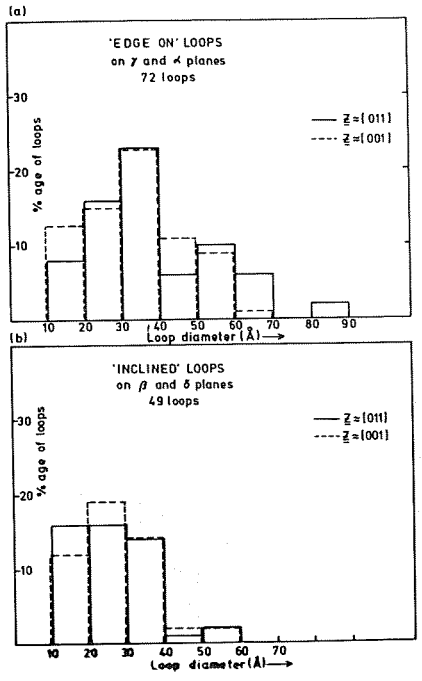

The effect of inclination on Frank loop sizes: (*a*) edge-on loops at $\mathbf{z} \approx [011]$ and $\mathbf{z} \approx [001]$; (*b*) inclined loops at $\mathbf{z} \approx [011]$ and $\mathbf{z} \approx [001]$.

Fig. 7

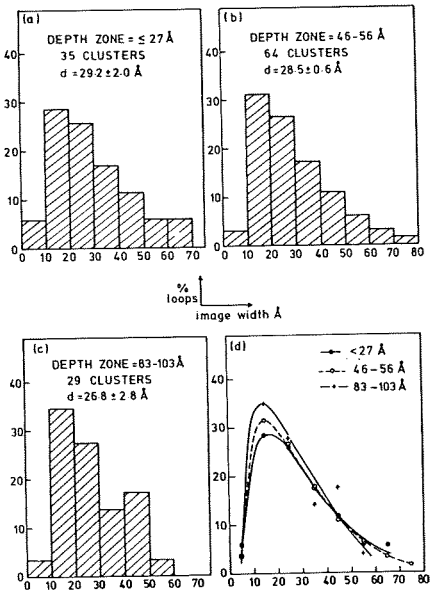

Size distributions at various depths in the foil.

4. 30 keV W^+ ion damage in copper — comparison wit Cu^+ ion damage

In order to study the effects of using an ion of heavier mass than the self-ion, irradiations were carried out under identical beam and foil orientation conditions using W^+ ions. Figure 8 shows directly comparable micrographs of the damage structures as produced by Cu^+ and W^+ ions. Although there are fewer dissociated Frank loops it is immediately obvious that a large number of loops is produced with W^+ ions. In fact, a defect yield of $0{\cdot}60 \pm 0{\cdot}01$ was measured for $^+$ ions, which is an increase of 20% on that obtained with Cu^+. No perfect loops were found with W^+ ions. The size distributions of the W^+ ion clusters are shown in fig. 9 for the edge-on, inclined and 'unknown' Frank loops as a fraction of the total size distribution. The total mean diameter is $31{\cdot}7 \pm 0{\cdot}4$Å,

Fig. 8

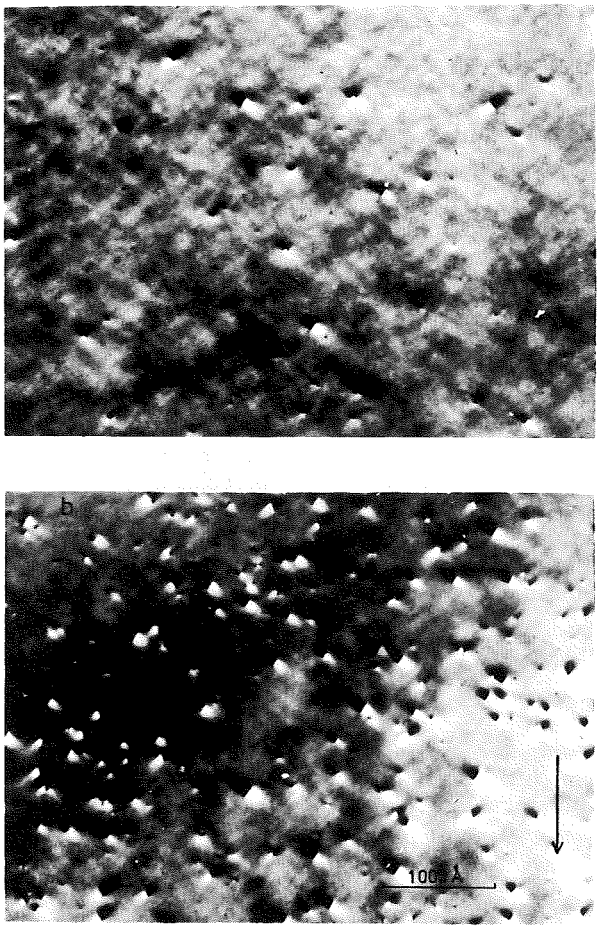

Damage as a function of ion mass (dose 2×10^{14}, $E = 30$ keV) in pure copper. (*a*) Cu^+ ions; (*b*) W^+ ions.

compared with $22.7 \pm 0{\cdot}3$Å for $^+$ ions. The peak diameter is ~ 15 Å for both cases, although only 27% of the loops are <20 Å in the former case compared with 50% in the latter. Figure 10 compares the size and number distributions of the loops on the various {111} planes for the two ion irradiations. The following are the main differences between the two cases.

(i) More edge-on loops than inclined loops were identified after W^+ ion-irradiations, whereas the clusters were equally distributed on edge-on and inclined planes in the Cu^+ ion irradiation.

(ii) The main increases with W^+ ions in the sizes of loops occurred on the edge-on planes with the sizes of inclined loops remaining basically the same.

(iii) There were slightly more and larger loops with $\mathbf{b} = a/3[11\bar{1}]$ than with $\mathbf{b} = a/3\,[111]$ in the Cu^+ ion case; this relative difference in*d* between the two edge-on sets of loops was also found in the W^+ ion case, but the difference in relative numbers was even larger.

Fig. 9

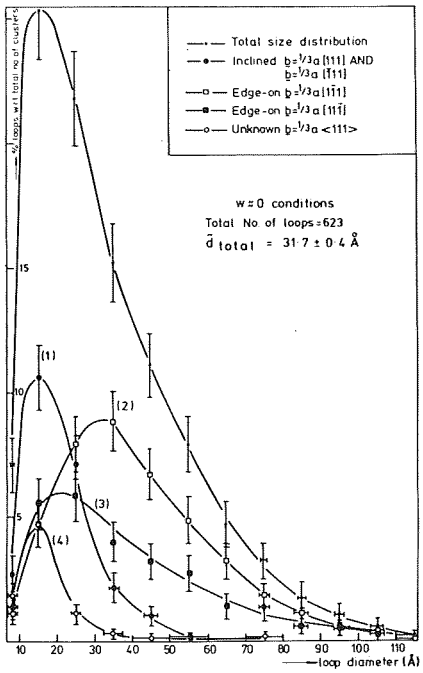

Size distributions of Frank loops in pure copper irradiated with 30 keV W^+ ions.

Fig. 10

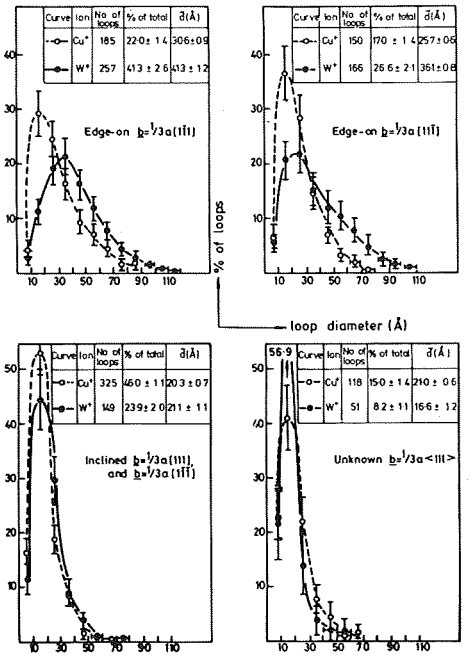

A comparison of the size and number distributions of loops on the various {111} planes for Cu^+ and W^+ ion irradiations.

5. Discussion

The information presented in §§ 3 and 4 has established both a procedure for precisely characterizing the damage structure in heavy-ion irradiated pure copper and quantitative results on vacancy clusters produced by cascade collapse of the vacancy-rich centres of cascades produced by both Cu^+ and W^+ ions. In this section we will discuss firstly the imaging conditions required to obtain accurate results, and secondly several features of the irradiation produced damage structures.

5.1 *Imaging procedures*

From the detailed depth distribution it can be seen that the differences in observed loop number density under different imaaging conditions were due simply to the presence of defects close to and inside the transition layer between L1 and L2. It was shown that an accurate defect yield could only be derived from a comparison of micrographs taken under different imaging conditions; in this work these extra defects were identified from strong-beam micrographs taken with $\mathbf{g} = 200$ at different orientations between [011] and [001] or from a combination of weak-beam micrographs, taken in $\pm$ 022 with different values of s, and one = strong-beam micrographhall at the [011] orientation. In the former case tilting the foil causes the transition layer centre to move from ~ 84 Å to ~ 66 Å, while in weak beam the defects extend over two transition layers at about 50 and 100 Å, above and below (due to the smaller effective extinction length) the $\mathbf{g} = 200$, $w = 0$ transition layer. Thus in both cases it was possible to sample the whole irradiated volume, and this is supported by the agreement between the two values obtained of the defect yield.

Micrographs taken under kinematical conditions have frequently been used for sizing defect populations and for stereo-pairs used in determining the depth distributions. It was shown in § 3.2 that this can lead to errors because of the invisibility under these conditions of half the number of loops, with preferential disappearance of the inclined Frank loop images. This is due to the combinationn of two effects. Firstly, the transition zone at ~ 66 Å, for $w \sim 0.8$, is now very close to the peak in the distribution, and secondly the visibility of the loops throughout the layer depends on w in a periodic way (Saldin *et al.* 1979).

The last point of interest arising from the use of strong-beam imaging is the behaviour of the **l** vector of the black-white images. The experimental results for both edge-on and inclined loops disagree with the prediction of the isotropic calculations. A number of investigations (see, for example, Rühle, 1967, McIntyre, Brown and Eades 1970) have also observed the tendency of **l** for edge-on FRank loops to align with the Burgers vector, and Yoffe (1970) and Ohr (1979) have shown that this is due to the anisotropy of the lattice; the latter's computed edge-on $|\mathbf{g}\cdot\mathbf{b}| = 1$ image exhibits the elongation along $\mathbf{b}_g$ which was observed here. We have demonstrated that for inclined Frank loops at [**011**] the **l** vector behaviour is a function of $|\mathbf{g}\cdot\mathbf{b}|$. For $\mathbf{g}\cdot\mathbf{b}| = 1$, **l** lies close to that predicted by isotropic calculations (Saldin *et al.* 1979), Ohr 1976), but for $\mathbf{g}\cdot\mathbf{b}| = 1/3$, **l** lies parallel to **g** and thusconsiderable care is required to distinguish between small inclined loops and stacking fault tetrahedra in anisotropic

1900 The image contrast under w.b. conditions was too complicated to be understood from simple geometric arguments, unlike the case for defects> 100 Å (Jenkins 1974). Images with $\mathbf{g}\cdot\mathbf{b} = 0$ were visible and this may be due to contrast from the Shockley partials as many of the loops were dissociated. Also identical images in strong beam of various loops on the same plane present a variety of different images in weak beam, suggesting that there is also some dependence of image profile on depth in the foil. This is consistent with the expected layer structure for $w = 2 \times 10^{-2}$ Å^{-1} over the damage layer of ~ 120 Å. The estimated beam divergence of 2.2×10^{-3} rad was insufficient to smear out the near-surface oscillations (Holmes, Cockayne and Ray 1974, Melander and Sandström 1974). Thus, in conclusion, it is felt that the weak-beam technique is not particularly useful in analysing the geometry, or nature by inside-outside contrast, of small (< 90 Å) loops lying close to the surface. Indeed, we have shown that provided the correct sequence of images is taken by analysing dynamical micrographs, the Burgers vectors, degree of dissociation, size and depth parameters of the entire defect population could be determined reliably.

5.2. *Cascade collapse after Cu^+ and W^+ ion irradiation*

In this section the results on cascade collapse will be discussed and compared with both earlier work and the theoretical cascade parameters.

5.2.1. *Defect yield and cascade efficiency*

Before discussing the effect of ion mass on the cascade collapse, it is interesting to compare our present results with those obtained by Häussermann (1972) with 30keV Cu^+ and Au^+ ions implanted at a similar foil orientation, [011]: from Table 5 (*a*) it can be seen that there is very good agreement between the results of W^+ and Au^+ irradiation, in keeping with their similar masses. However, the yield obtained by Häussermann for Cu^+ ions is significantly lower than the present result. This is probably due to the increasing importance of transition layer defects and the problems they represent in analysis.

Turning to the effect of ion mass, it can be seen from Table 5 (*a*) and 5 (b) that although the W^+ ions produce smaller cascades with fourfold increase in energy density, the calculated number of vacancies is not appreciably greater. It is the increase in vacancy supersaturation which is thought to be largely responsible for the increase in the number of cascades collapsing to form visible clusters, and the resultant increase in the defect yield from 0.5 to 0.6 on going to W^+ ions. The major effect of the smaller W^+ cascades seems to be on the cascade efficiency, which increases by a factor of two. Although no simple explanation can be offered for this, two comments can be made. Firstly, the separation between vacancies and interstitials is more efficient in the W^+ ion cascade because of the smaller volume of the vacancy zone in the core, which means a smaller overlap with the knocked-out interstitials and less recombination taking place than in the Cu^+ ion case. In this respect Wilkens (1975) has pointed out the likely importance of the ratio of replacement collision sequence length l_i and cascade radius R_c on the total recombination. With increasing l_i/R_c, interstitials are more effectively separated, and thus the amount of recombination is reduced. Since l_i is a constant between the two irradiations, the smaller R_c in the W^+ ion cascades leads to a larger number of the vacancies surviving. Secondly, because of the closer on average

Table 5. Damage parameters in pure copper (5N). $\bar{N}_v$ = average number of vacancies per loop. $\bar{N}_v$ experimental was calculated assuming that the loop of mean area is circular and taking the cross-sectional area of a vacancy to be $(\sqrt{3})\ a^2/4$, where a is the lattice parameter. $\bar{N}_v$ where a is the lattice parameter. $\bar{N}_v$ theoretical is obtained using the NRT model (Norgett, Robinson and Torrens 1972) assuming a displacement energy $E_d = 30$ eV.

(a)

Ion	Atomic mass	Defect yield	$\bar{N}_v$ experimental (theoretical)	Cascade efficiency	Source
Cu^+	65	0.5 ± 0.01	$100 \pm 4.5(282)$	0.36 ± 0.02	This study
Cu^+	65	0.35	—	—	Häussermann (1972)
W^+	184	0.60 ± 0.01	$215 \pm 6.6(302)$	0.71 ± 0.02	This study
Au^+	197	0.6	250(305)	0.82	Häussermann (1972)

(b)

Ion	Energy	$\langle x\rangle_D$(Å)	$\sqrt{(\langle\Delta x^2\rangle_\Delta)}$(Å)	$\sqrt{\langle y^2\rangle}$D(Å)	θo(eV/atom)
Cu^+ (calculated)	30 keV	67	42	32·1	0·20
Cu^+ (experimental)	30 keV	64·4±0·3			
W^+	30 keV	42·5	25·8	17·2	0·80

$\langle x\rangle_D$=mean damage depth, $\sqrt{(\langle Dx^2\rangle_D)}$=half-width of damage depth distribution, $\sqrt{\langle y^2\rangle}_D$=half with damage distribution perpendicular to the beam. θo =max. energy per atom in the cascade, calculated as indicated by Sigmund (1974).

distance of the vacancies from the cluster nucleus and the probability of spike effects, the vacancy capture cross-section and diffusion path length to the loop nucleus will be higher in the W^+ ion case. Both factors will lead to a more efficient loop growth process.

It is interesting to compare these results with recent observations in b.c.c. metals by Jenkins, English and Eyre (1978) and English (1979). Here, in both α-Fe and molybde—num, an increase in vacancy concentration dramatically increases the defect yield whilst the cascade efficiency is not as markedly affected, suggesting that the energy in the cascade might be a more critical factor governing cascade collapse than for f.c.c. metals.

5.2.2. *The distribution of damage on the various {111} planes*

One of the most interesting results presented in § 4 was that in off-axis [111] foils the edge-on Frank loops were on average larger than the inclined Frank loops. From observations at the [111] pole it was possible to show that this was not an imaging effext. In this section we consider whether or not this difference in size can be explained by surface interaction or whether it is due to the collapse mechanism itself.

Jäger and Wilkens (1975) have considered the influence of the surface on the unfaulting of $a/2$[110] loops in b.c.c. metals and demonstrated that the surface interaction was sufficient to cause the inclined faulted loops to preferentially unfault to inclined perfect loops as against edge-on loops. The very high stacking fault energies of b.c.c. metals mean that all the faulted loops unfault to perfect loops. In the present case, in view of the low stacking fault f.c.c. metal (40 erg/em^2) and the marked tendency of the Frank loops to dissociate towards s.f.t., this mechanism is clearly less important. Their calcu-lations have shown that the probability of aunfaulting increases with loop size, and it could be argued that in the present case the larger loops on the inclined planes have unfaulted and been lost to the surface. This, however, seems unlikely as in such a case some edge-on loops would be expected to unfault to $a/$[011] perfect loops which would be retained in the foil; but in fact no perfect loops have been found on any plane. Also the probability of unfaulting would be greater for loops close to the surface and this would result in a surface denuded zone; no such region denuded of loops was found. Thus, in conclusion it appears that the low stacking fault energy of copper favours dissociation rather than unfaulting. In a subsequent paper (Stathopoulos *et al.* 1981) it will be shown that this difference in size also occurs in alloys with an s.f.e. of 5 erg/cm^2, where unfaulting to perfect loops is even less probable.

We next consider whether or not the explanation for the orientation dependence of loop sizes lies in the detailed shape of the cascade and the geometry of the crystal lattice. The WSS theory (Winterbon, Sigmund and Saunders 1970, and Westmoreland and Sigmund 1970), predicts that the average cascade is elongated along the ion beam direction, and from table 5 (*a*) the elongation is expected to be greater for W^+ ions than for Cu^+ ions. In addition, Lindhard (1965) has presented a qualitative analysis to show that in a crystalline structure the WSS theory underestimates this elongation because of the correlation between collission in a regular lattice. This elongation will have implifications on the subsequent nucleation and growth of visible loops. For the case of O.A. [011] foils the edge-on $(1\bar{1}1)$ and $(11\bar{1})$ planes will be parallel to the major axis of the cascade, and the growth of a nucleus on these planes may be enhanced preferentially as the vacancies will on average be closer to the cluster nucleus and thus have a greater probability of participating in cluster growth. The difference in size between the two sets is larger in the W^+ ion irradiation, which is consistent with the argument as this difference might be expected to increase as the cascade becomes more enlogated. The above model implies that loop sizes will depend on specimen orientation with respect to the ion beam. This was confirmed by irradiating on O.A. $[1\bar{1}1]$foil; the loops formed on the three similarly inclined (~70°) planes with an average size of ~25·0 Å per plane, a size intermediate between the mean edge-on loop size of 28·4 Å and the inclined loop size of 20·3 Å for [011] foils; flat-on loops with $b = a/3$[111] were not observed, even when the specimen was titled to [011]. In O.A. [011] foils with both Cu^+ and W^+ ions one set of edge-on loops, $a/3$[111], was consistently larger than the other edge-on set $a/3$[111]. The difference in orientation with respect to the foil normal of the two loop planes, 6·3°, respectively, may be sufficient for the effects of cascade shape to be apparent.

For the case of the Cu^+ ions into O.A. [011] foils the experimental results show that cascade collapse occurs with equal probability on all four {111} planes. However, in the W^+ ion irradiation more edge-on loops were found. This may be either because the increase in elongation of the cascade leads to a greater percentage of inclined loops with diameters less than the visibility limit, or alternatively the nucleation of more edge-on loops.

5.2.3. *Depth distribution of 30 keV Cu^+* ion damage

A comparison is made in table 5 (*b*) between the experimental depth distribution of the vacancy clusters and the damage depth distribution calculated from the WSS theory for an amorphous tarhet. It can be seen that there is good correspondence between the mean damage depth and the mean depth of the clusters in the experimental distribution, although the width of the experimental distribution is slightly smalle r than predicted. The shapes of the two distributions also show differences, with the peak of the experimental distribution lying further into the foil than the peak of the theoretical damage distribution, $\langle x_D\rangle$. The mean cluster depth lies between the two peaks. This is probably due to the difference in the energy loss processes in a lattice as against an amorphous solid.

The only other depth distribution for 30 keV Cu^+ ions into off-axis [011] foils is from the work of Wilson (1971). There the damage clusters were distributed over a depth of 100 Å with a mean depth of 30-40 Å. The probable reasons for the discrepancy with the present distribution are that Wilson had a smaller sample size, only included clusters > 30 Å diameter, and did not identify between layer defects which for his chosen reflection, $\mathbf{g} = 1\bar{1}1$, coincided with the mean damage depth.

The observation that there was no marked dependence of loop sizes on depth suggests both that there is no preferential loss of large loops near the surface, and that the efficiency of vacancy survival in the collapsed cascades is not sensitive to depth over the damage range of ~ 120 Å. A similar result was found by Norris (1969) for 80-150 keV Au^+ and Ni^+ ion irradiation of gold (defect sizes 100 Å), while Häussermann noted a small diameter decrease from 60 to 45 Å after 70 keV Au^+ ion irradiation of an <001> aluminium foil where the damage region extended to 420 Å.

§ 6. Summary of results.

The principal conclusion of this work is that in order to characterize accurately by TEM the small vacancy clusters (8 Å ⩽ diameter ⩽ 90 Å) formed in pure copper after irradiation with 30 keV heavy ions, it is necessary to select carefully the imaging conditions and involve a series of diffraction vectors at different orientations. Failure to do this result in significant errors particularly in the damage yield. By comparing micrographs of the same area taken in a number of gs near [011], and in $\mathbf{g} = 200$, $w \simeq 0$, at several orientations between [011] and [001] the following points were established.

(i) The vacancy cores of cascades collapsed to form Frank loops on both the edge-on and inclined planes and both simple and dissociated edge-on loops were observed. It was also found that the ratio of edge-on to inclined loops depended on ion mass.

(ii) The true defect yield for Cu ion radiation was found to be $0{\cdot}50 \pm 0{\cdot}01$.

(iii) Defect depth distributions for all the defects identified after Cu^+ ion irradiation established that the extra defects seen at tilted orientations arose from clusters lying within the transition zone at [011]. The mean cluster depth (64·4 ± 0·3 Å) and shape of the distribution are in agreement with the WSS theory. No significant variation was found of cluster size with depth in the foil.

(iv) The defect sizes were larger after W^+ than after Cu^+ irradiation, $d = 31{\cdot}7 \pm 0{\cdot}4$ Å and $22{\cdot}7 \pm .{\cdot}3$ Å, respectively, and this can be explained on the basis of the higher vacancy supersaturation, the smaller recombination and higher capture cross-section for vacancies that can be associated with the average W^+ ion cascade and cluster nucleus.

(v) The relative distribution in sizes of Frank loops on the {111} planes depends on the foil orientation: the edge-on loops in O.A. [011] foils are larger than those produced on inclined planes, although in numbers they are approximately equal. Approximately equal sizes were obtained on the three steeply inclined {111} planes in O.A. [$\bar{1}11$]foils. The inclined loops have similar sizes with both W^+ and Cu^+ ions, but the edge-onn loops are larger in size in the former case. These results could be explained in terms of a model that involves preferentail loop growth on the edge-on planes because of the elongated shape of the damaged zones parallel to these planes.

The method developed for analysis the defects also served as a basis for the analysis of the clusters formed after irradiating a range of copper binary alloys (Stathopoulos *et al.* 1981) with 30 keV Cu^+ and W^+ ions.

REFERENCES

Cockayne, D. J. H., Ray, I.L.F., and Whelan, M. J., 1969, *Phil. Mag.*, **20,** 1265.

Diepers, H., and Diehl, J., 1965, *Phys, Stat. Sol.*,**16,** K109.

English, C. A., 1981

English, C. A., Eyre, B. L., and Summers, J., 1976,*Phil. Mag.*, **34,** 603.

Eyre, B. L., 1973, *J. Phys.* F, **3,** 422.

Eyre, B. L., Maher, D. M., and Perrin, R. C, 1977 A, *J. Phys.* F, **7,** 1359; 1977 b, *Ibid.*,**7,** 1371.

Häussermann, F. 1972, *Phil. Mag.*, **25,** 537.

Häussermann, F., Katerbau, K. H., Ruhle, M., and Wilkens, M. 1973, *J. Microsc.*, **98,** 135.

Hirsch, P. B., 1978, *Electron Diffraction 1927 1977,* edited by P. J. Johnson, J. B. Pendry and C. J. Humphreys, Inst. Phys. Conf. Ser. No. 41 (London, Bristol: The Institute of Physics), p. 2.

Hirsch, P. B., Howie, A., Nicholson, R. B., Passhley, D. W., and Whelan, M. J. 1965, *Electron Microscopy of Thin Crystals* (London: Butterworths).

Holmes, S. M., Cockayne, D. J. H., and Ray, I. L. F., 1974, *Proceedings of the 8th International Congress Electron Microscopy,* Canberra, Vol. **1,** p. 290

Holmes, S. M., Eyre, B. L., English, C. A., and Perrin, R. C., 1979, *J. Phys.* F. **9,** 2307.

Jäger, W., and Wilkens, M., 1975, *Phys. Stat. Sol.* (a), **32,** 89.

Jenkins, M. L., 1974, *Phil. Mag.*, **29,** 813.

Jenkins, M. L., English, C. A., and Eyre, B. L., 1978, *Phil. Mag.* A, **38,** 97.

Katerbau, K. H., 1976, *Phys. Stat. Sol.* (a), **38,** 463.

Lindhard, J., 1965, *Mat.-fys. Meddr.*, **34,** No. 14.

McIntyre, K. G., Brown, L. M., and Eades, J. A., 1970, *Phil. Mag.*, **21,** 853.

Melander, A., and Sandström, R., 1974, *Phys. Sol.* (a), **22,** 587.

Merkle, K. L., 1966, *Phys. Stat. Sol.*, **18,** 173; 1969, *Radiation Damage in Reactor Materials,* Vol. 1(Vienna: IAEA), p. 159.

Norgett, M. J., Robinson, M. T., and Torrens, I. M., 1972, Harwell Report AERE-TP494.

Norris, D. I. R., 1969, *Phil. Mag.*, **19,** 527.

Ohr, S. M., 1975 *Fundamental Aspects of Radiation Damage in Metals,* edited by M. T. Robinson and F. W. Young, Jr. (USERDA, CONF.-751006-P1., p. 650; 1976, *Phys. Stat. Sol.* (a), **38,** 553; 1979, *Phys. Stat. Sol.* (a), **56,** 527.

Perrin, R. C., and Eyre, B. L., 1973, *J. Microsc.*, **98,** 200.

Rühle, M., 1967, *Phys. Sol.*, **19,** 263.

Rühle, M., Wilkens, M., and Essmann, U., 1965,*Phys. Stat. Sol.*, **11,** 819.

Saldin, D. K., Stathopoulos, A. Y., and Whelan, M. J., 1978, *Electron Diffraction 1927-1977,* edited by P. J. Dobson, J. B. Pendry and C. J. Humphreys, Inst. Phys. Conf. Ser. No. 41 (London, Bristol: The Institute of Physics), p. 50; 1979. *Phil. Trans. R. Soc.*, **292,** 513.

Schindler, R., 1974, Diplomarbei, Universität Stuttgart.

Sigmund, P. 1974, *Appl. Phys. Lett.*, **25,**169.

Stathopoulos, A. Y., 1977, D. Phil. Thesis, University of Oxford.

Stathopoulos, A. Y., English, C. A., Eyre, B. L., and Hirsch, P. B., 1981, *Phil. Mag.* A, **44,** 309.

Thompson, N., 1953, *Proc. Phys. Soc.* B, **66,** 481.

Westmoreland, J. E., and Sigmund, P., 1970, *Radiat. Effects,* **6,** 187.

Wilkens, M. 1975, *Fundamental Aspects of Radiation Damage in Metals,* edited by M. T. Robinson and F. W. Young, Jr. (USERDA, CONF—751006-P1), p. 98.

Wilson, M., 1971, *Phil. Mag., 24, 1023.*

Wilson, M., and Hirsch, P. B., 1972, Phil. Mag., **25,** 983.

Winterbon, K. B., Sigmund, P., and Saunders, J. B., 1970, *Mat-fys. Meddr.*, **37,** No. 14.

Yoffe, H. E., 1970, *Phil. Mag.*, **21,** 833.

H.T.I. CALENDAR OF ACTIVITIES -
Academic Year 1982 - 83

D. Charalambidou
Lecturer H.T.I.

SEPTEMBER

• The 1982-83 academic year commenced on September 13th. Four hundred and sixty-two (462) students were enrolled on regular courses including seventeen (17) students from overseas.

. The polyvalent course for Medical Technicians began with five (5) students from various Middle East and African countries and three (3) Cypriots.

• The X-Ray course admitted seven (7) overseas students and one (1) Cypriot.

• The Hospital Laboratory course began with nine (9) overseas students and two(2) Cypriots.

• The academic and social life of H.T.I. was enhanced by the efforts to devote every other Wednesday to cultural, social and sports activities alternating with Cultural Electives.

• Cultural Electives were compulsory for all first year students and lectures ran fortnightly throughout the academic year. Subjects requested by the students were ART - CYPRIOT STUDIES - MODERN GREEK LIT - PSYCHOLOGY - SOCIOLOGY and SPORTS & ATHLETICS.

• The Astronomy Club organises its first lecture. Mr. A. Achillides, H.T.I. Senior Lecturer, talks on "Theories on U.F.O." on September 16th.

OCTOBER

• The Photography Club organises its first lecture. Mr. J. Ionas, H.T.I. lab assistant, talks on "How to use the camera and its accessories" on October 6th.

• The Christian Society Club organises a debate on "Faith", co-ordinator, Mr. M. Poullaïdes, H.T.I lecturer on 6th October.

• On October 11th a lecture was held at the H.T.I Lecture Theatre by Dr. Walther L. Fisher, University of Erlangen-Nurnberg on "Today's Natural Science and Goethe".

• The H.T.I. Film Club shows "The Long Riders' on October 14 at the H.T.I. Lecture Theatre Room at 7.00 p.m.

• Dr. Stavros Constantinou gives a lecture on "Computer Aided Design and Implementation Aspects of Buildings and theirMechanical and Electrical Services" on October 20th.

• Mr. G. Lanitis gives a lecture on "Introduction to Photography" on 20th October.

• Mr. A. Achillides, H.T.I. Senior Lecturer, gives a lecture on "The Creation of the Univesre" organised by the H.T.I.Astronomy Club on 27th October.

• Dr. Walther L. Fisher, University of Erlangen-Nurnberg gives talks on (a) Educational Mathematics, (b) Foundations of Geometry, (c) Theory of Tolerance Spaces, (d) Mathematical Linguistcs, (e) Mathematics and Art.

NOVEMBER

• On November 3rd there was a lecture on "Psycho-Spiritual Development" by Dada Tabhavanandra AVT at the Lecture Theatre.

• UNESCO DAY was celebrated this year at Asinou. Students and staff visited the tiny Byzantine Church of Panayia Phorviotissa at Asinou where the Nikitari priest briefed them on the the historical and cultural background of the church and its famous frescoes.

Students and staff admired the ikons and frescoes of the church and volunteered to clear and tidy up the surrounding grounds of the church. After work and long walks in the wood they lunched at the nearby restaurants and departed for Nicosia in the late afternoon.

• On November 17th there was a lecture on "Thalassaemia" by Mr. M. Aggastiniotis, a paediatrician, at the Lecture Theatre.

The greater part of the first two weeks in November was taken up by the Mid-semester exams.

DECEMBER

• On December 1st there was a talk by Mr. Nikos Phalas, the president of the co-ordinating committee of Karpasia, on "Karpasia - Enclaved" at the Lecture Theatre.

• The Christian Society gives a lecture on "The New Creation" by Mr. Christos Shiakalis.

The annual staff-student Christmas party took place on December 23rd in the Students' Canteen. Snacks and drinks were served. Song and dancing followed till late afternoon.

• On 15th December The Christian Society organises a lecture on "Truth or Lie" by Mr. J. Photiades.

• The Photography Club organises a Lecture on "Printing" by Mr. J. Angelis, H.T.I. lab-assistant.

• The Association of H.T.I. Graduates held their annual Christmas Dinner at the Ledra Hotel.

JANUARY

A hectic time for both students and staff as the first semester exams approach.

FEBRUARY

• Exams are over to the relief of everyone. The routine of lectures and Cultural Electives is resumed again.

• On Wednesday 16th Dr. N. Pavlides, president of the Blood Donation Committee, gave a lecture on "Blood Donation".

• Mr. Sotiris Rallis was elected president of the Student Union.

MARCH

• On March 9th the Photo Club organises a debate on "Photography for Exhibitions".

The second part of the month is marked with tension and fever because of the Mid-semester exams.

APRIL

• On April 6th Dr. Ludovit Molnor, professor on Computer Science of the Electrotecnical Faculty of the Bratislava Technical University, gave a lecture on "Artificial Intelligence" at the Lecture Theatre.

MAY

• SPORTS DAY was May 4th. The finals of various sports activities of this academic year were held on Sports Day. The activities included Football Depts - Chess - Table Tennis - Tennis - Volleyball Depts -Cross Country - Basketball Depts - Badminton -Softball Depts - Seven-A—Side Depts.

On May 18th the trophies and medals were awarded to the winners.

• On May, 24th the Film Club showed two video films "Granida No. 3" and "Thraneo No. 8" in the Lecture Theatre at 7.30 p.m.

JUNE

• Final-Year students took their exams 23rd May - 3 June.

• Second and First Year students had their exams 6 June - 17th June.

The annual Graduation Ceremony will be held on 8 July.

Happiness is Freedom and Freedom is the power of the psyche.

Thoukidides

I would rather be good, kind and just even if people think of me to the contrary, than being called good, just and kind when I am bad.

Saadi

SKF The largest manufacturer of ball and roller bearings

S K F is an international group with factories in twenty countries, and international sales network and its own service organisation spread around the world.
S K F bearings are made in 8.000 basic types and sizes and many thousands of variants ranging from 3mm to several metres in outside diameter and from a weight of 0.036 grammes to more than 6,000 Kg. There are S K F bearings which can run at a speed of 400,000 r.p.m. and others which at low speed canm carry loads of more than 2,000 tons.
S K F research efforts stretch from theory right through applied mathematics by computer to manufacturing process and product development. To illustrate the degree of accuracy required we may cite the example of any one medium sized bearing where ball diametres must not deviate more than 0.00002in., and where errors in spherity in one particular ball must not exceed 0.00001in.

MUCH MORE THAN BEARINGS

BALL BEARINGS

ROLLER BEARINGS

CASTINGS

MACHINE TOOLS

TOOLS

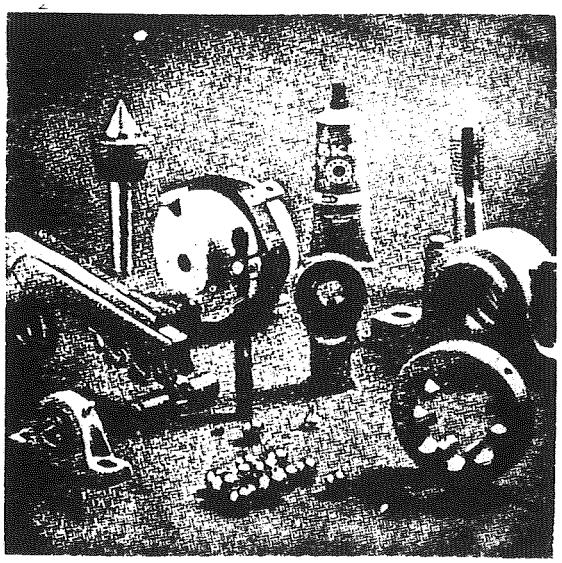

TEXTILE MACHINERY

COMPONENTS

PLANETARY ROLLER

SCREWS

FLUIDICS

SKF

SKF Best possible service to customers

Research and development in the SKF group is applied in three directions. The first is the development of production development, the second is the development of new products and the third is a continuous process of developing the traditional products ranges to changing market requirements.
SKF faces strong competition in all the most important industrial countries. It is, however, true to say that SKF is foremost in the field of roller bearing engineering, in addition to being the most important exporter of ball and roller bearings.
SKF has attained this pre-eminent position for several reasons. One of them being that SKF was the first bearing firm to undertake systematic theoretical and experimental research in ball and roller bearing engineering.

SOLE AGENTS:
SWEDISH LEVANT TRADING (CYPRUS) LTD.
P. O. Box 1252 - Tel. 43833 - NICOSIA-CYPRUS

Χρόνια πολλά
και υγεία για όλους!
ΒΙΟΜΗΧΑΝΙΚΗ ΜΕΤΑΛΛΟΥΡΓΙΚΗ Α.Ε.
ΤΚ 174 ΑΓΙΟΣ ΘΩΜΑΣ (051) 69222 & ΛΕΥΚΩΣΙΑ ΤΗΛ (021) 48243